COMPUTATIONAL AND EXPERIMENTAL ANALYSIS OF THE EFFECTIVENESS OF ARGON RESERVOIR

by

Mallik R. Ahmed

Bachelor of Science
Bangladesh Institute of Technology, 1992

Submitted in Partial Fulfillment of the

Requirements for the Degree of Master of Science in the

College of Engineering & Information Technology

Department of Mechanical Engineering

University of South Carolina

2003

Department of Mechanical Engineering Director of Thesis	Department of Mechanical Engineering Second Reader

Dean of the Graduate School

Acknowledgements

I would like to convey my sincere gratefulness to my advisor, Dr. Jamil A. Khan, for his appreciable encouragement, constant support and endless help throughout the research. His guidance helped me to learn details in the field of argon-air diffusion, buoyancy driven flow and exposure of gas in a chamber to complete this work. I also learnt a lot on fluid mechanics, heat transfer, and modeling of computational fluid dynamics from him.

I would like to thank Dr. Curtis Rhodes for his overall suggestions and help in modeling and simulating the computational works of this research. Thanks are also due to Thomas Tisdale, Anthony Fernandez, and Corey Linen who continually helped me in the research experimental works. Gary Dowdey and Burt Ward, staffs of the machine shop of our department, did a great job to fabricate the experimental set up and extended their hands during the exponential works whenever we needed. So, thanks are also for them.

I am grateful to Westinghouse Savannah River Company (WSRC) for its financial support to conduct the research. I am especially grateful to Dr. William Brizes who throughout the research provided valuable inputs and encouragement to get effective outcome.

Thanks to Mir Zahedul Huq Khandkar, Wei Jiang and Sanjida Tamanna for their help and support. Finally, I remember the encouragement and immeasurable sacrifice of my wife for this work and would like to thank her a lot. Also, I am always grateful to my parents who remotely bless me for the ultimate success.

Abstract

Experimental and computational studies were performed to evaluate the effectiveness of an Argon Reservoir (AR). The AR is designed to prevent the ingress of air into the extraction furnace during the insertion and removal of the extraction basket, which contains Tritium Producing Burnable Absorber Rods. Computational computer code studies were performed to evaluate the AR design concept. The computer code was validated and verified by experimental testing using a $1/5^{th}$ scale model of the extraction furnace and extraction furnace module. Computational studies were performed using commercial computational Fluid Dynamics software FLUENT and FIDAP.

Based on the results of this study it was concluded that the Argon reservoir would be very effective in keeping air and moisture from infiltrating into the furnace module if the reservoir was continuously supplied with make-up argon. Another observation relative to the AR is that AR would require a significant amount of make-up argon due to diffusion and convection losses. This was especially true during the initial filling of the AR.

After the initial computational studies with the AR were completed, a furnace module without the argon reservoir was studied. These studies demonstrated that during the withdrawal of the extraction basket, if make-up argon was injected into the furnace module, then less than 1% oxygen (less than 3% air) would infiltrate into the furnace module. The rate of optimum make-up argon required was determined to be equal to or slightly greater than the volume withdrawal rate. Similarly, during the insertion process, it was determined that the infiltrated oxygen level was less than 1% without make-up argon. Although the amount of infiltrated oxygen was slightly more without the argon reservoir, the infiltrated amount was found to meet the design requirements for the furnace module. As a result, it can be concluded that the furnace module will operate well below the design requirement (~3% of O_2 infiltration) as long as make-up argon is supplied to the furnace module during the withdrawal of the basket.

Table of Contents

List of Tables

List of Figures

Chapter 1: Research Description

1.1 Introduction

The production furnace for the Commercial Light Water Reactor Tritium Extraction Facility at the Westinghouse Savannah River Company (WSRC) requires an inert atmosphere be maintained during the insertion and removal of the extraction basket containing Tritium Producing Burnable Absorber Rods (TPBARs). Introduction of air and/or humidity into the furnace module is undesirable since tritium will exchange with water. A blanket of Argon gas provides the inert atmosphere. First it was thought that an argon reservoir (AR) could be placed above the sliding gate of the furnace module to prevent atmospheric air from entering the furnace module, retort and extraction basket during the insertion and removal of the extraction basket. Therefore, initially the effectiveness of the AR has been investigated. To determine the effectiveness of the argon reservoir (AR) it was required to develop a computational model of the furnace components to evaluate potential ingress of air into the furnace module. The developed code predictions had to be validated with measurements from a physical model. The physical model (experiments) consisted of a $1/5^{th}$ scale model of the furnace module and extraction basket. Several parametric studies were performed. During the removal and insertion of the basket, the air transport mechanism was found to be influenced by the temperature difference between the room air and module, withdrawal and insertion rate of the extraction basket, the argon make-up rate, and the HVAC flow rate across the top of the module. Therefore, in order to evaluate the effectiveness of the AR, these factors

were to be considered. For the present study CFD analyses were performed with the help of commercial software FLUENT and FIDAP.

FLUENT uses a finite volume based algorithm and is capable of solving the governing equations of conservation of mass, momentum, and energy and species transport. Whereas, FIDAP uses a finite-element based algorithm. FIDAP is also capable of solving the governing equations describing conservation of mass, momentum, and energy and species transport. An added feature of FIDAP is that it can solve moving object problems. This added feature was especially useful in simulating the motion of the extraction basket.

During the first phase of the investigation when the experimental set-up was still being designed and fabricated, detailed computational studies were performed. In the course of this investigation, based on the numerical results, it was thought to investigate the possibility of not having an Argon Reservoir. Accordingly, the experimental scale model design was modified in such a way that the withdrawal and insertion of the basket with the Argon Reservoir (AR), as well as without reservoir could be simulated. A significant portion of the investigation evaluated the feasibility of not having an Argon Reservoir. The following report includes results from both of these cases, and recommendations are based on the findings.

1.2 Objectives

The objective of the project was to perform computational fluid dynamics (CFD) analysis, and perform necessary experimental validation of the CFD models. These studies were performed to evaluate the effectiveness of the Argon Reservoir (AR), as well as study the feasibility of meeting the design requirements for limiting the ingress of air if the AR

was eliminated. As mentioned in the introduction section, the purpose of the Argon Reservoir was to prevent room air and moisture from entering the furnace module, retort and extraction basket during the insertion and withdrawal of the extraction basket. Therefore, computational experiments were performed to determine the infiltration of room air/moisture with the AR, and without the AR under various operating conditions. The computational and experimental investigation was performed in several stages. This was done to better understand the physics of the problem by isolating each of the driving mechanisms.

1.3 Literature Review

A thorough search of literature did not revealed any research paper closely related to this work, however a number of papers on argon-air diffusion, buoyancy driven flow, and exposure of a gas in air were studied in details. Below is a list partial literature detailing with research in diffusion of argon, and buoyancy driven flows.

Heung [1995] tested a tritium transport vessel using depleted uranium in the laboratory using deuterium and protium. The vessel contained 0.5 kg of depleted uranium and could hold up to 18 grams of tritium. The conditions for activation, tritium loading and unloading were defined. They focused on evaluation of some safety aspects such as air-ingress, tritium diffusion, temperature and pressure potentials. When the uranium was fully hydrided, air ingress did not cause any temperature surge, however when the uranium was dehydrided, it created a temperature peak of 200 degrees Celsius. Accumulation of non-reactive gases such as argon and moisture in the air blocked further air ingress. It was found that only a flow-through type of air ingress could damage the vessel.

Chen et al. [1995] carried out the experiments of argon diffusion dynamics for biotite at 700-1000 degrees Celsius and 0.5-2.0 GPa and the diffusion coefficient and activation energy using different models were calculated. The results indicated that the pressure, P, has no effect on argon diffusion and its effect is opposite to that of temperature. The results also showed that with the increase of P, the activation energy increases and diffusion coefficient decreases. It was found that in low T and high P conditions, the argon diffusion from the environment to the system could occur and incur the appearance of the external argon in minerals.

Murphy [1995] presented the calculated values of the viscosity, thermal conductivity and electrical conductivity of air and mixtures of air and argon, air and nitrogen, and air and oxygen at high temperatures. Combined ordinary, pressure, and thermal diffusion coefficients were also presented for the gas mixtures. The calculations, which assume local thermodynamic equilibrium, were performed for atmospheric pressure plasmas in the temperature range from 300 to 30,000 K. More reliable values of the transport coefficients were found.

Partridge and Mukhopadhyay [2000] reported an investigation in which a novel dynamic gas-permeability tester built for the automotive industry was used to measure the permeability characteristics of uncoated airbag fabrics by using air, argon, and helium at 100 kPa pressure. The gas velocity, the exponent of the pressure-velocity curve, and the fabric bulge height were the parameters to analyze the performance of the airbag fabrics. Experimental data clearly indicated that with helium the fastest gas velocity could be obtained. However, at a certain fabric cover factor, every gas reached a limiting velocity. The exponent values appeared to be influenced by the amount of fabric deformation and the physical characteristics of the gases.

Fumizawa [1993] ,both numerically and experimentally, investigated the flow and mass transfer behavior of a laminar argon jet with circular cross-section discharging into stagnant air. The SIMPLE method and two numerical schemes- PLDS and QUICK- were used in the TEAM code modified by adding the binary diffusion equation. Tthe experiments were performed at room temperature and atmospheric pressure. As regards the centerline argon mass fraction, results indicated that the numerical analyses by PLDS and QUICK were in good compliance with the experimental results.

Egoshi et al. [1997] performed experiments to measure mass fluxes in binary distillation of the nitrogen-oxygen and argon-oxygen systems in a wetted-wall column under total reflux conditions for a wide range of turbulent flows. They observed that diffusion fluxes of each component in binary distillation were proportional to their concentration driving forces, whereas the observed mass fluxes were not. Finally they proposed a new correlation for vapor phase diffusion fluxes in the nitrogen-oxygen and argon-oxygen systems.

Gunes [2002] presented a low-dimensional dynamical models for transitional buoyancy-driven flow in differentially heated enclosures. He solved full governing partial differential equations with the associated boundary conditions by a spectral element method. Using the most energetic empirical eigenfunctions for the velocity and temperature fields as basis functions and applying Galerkin's method, he obtained low-order models consisting of few non-linear ordinary differential equations. For all cases, which were close to the design conditions, the low-order model (LOM) predictions were in excellent agreement with the predictions of the full model. Far from design conditions, the LOMs captured some important characteristic properties of the full model solutions.

Dragojlovic et al. [2001] explained that under-relaxation in an iterative CFD solver is

guided by fuzzy logic to achieve automatic convergence with minimum CPU time. Two turbulent problems based on a kappa-epsilon (κ–ε) model were solved here. They included buoyancy driven flow in a rectangular cavity and mixed convection over a backward facing step. The SIMPLER algorithm with simple substitution was used to solve the incompressible Newtonian conservation equations. It was found that the fuzzy control algorithm with the optimal membership functions significantly reduced the CPU time needed to solve the problem compared to the highest relaxation factors without causing divergence.

Davidson [1993], taking advantage of shared behavior of swirling flow and buoyancy-driven flow, investigated the structure of steady-state solutions of the governing equations. It was found that, Batchelor regions apart, the steady state for each type of flow must consist of a quiescent stratified core, bounded by high-speed wall jets. Then a general, if approximate, method for finding these steady-state flow fields was given which employs a momentum-integral technique for handling the boundary layers. Starting with swirling flow, an energy minimization technique was used to show that stable solutions of arbitrary net azimuthal vorticity exist. The analogy with buoyancy-driven flow, however, suggests that these solutions are all of a degenerate, stratified form.

Kazmierczak and Chinoda [1992] numerically investigated the problem of laminar buoyancy-driven flow in a square cavity driven by a warm vertical wall with a uniform surface temperature changing periodically while the opposite cold wall was maintained at a constant temperature. Solutions were obtained for different cases which illustrate the effects of the oscillating surface temperature on the fluid flow and the heat transfer through the enclosure. Resulting streamlines indicate that a weak secondary flow cell intermittently appears and then disappears in the upper corner of the enclosure near the

hot driving wall, rotating in a direction opposite to the main flow. The effect of the periodically changing wall temperature was felt only partially into the enclosure and, overall, the time-averaged heat transfer across the enclosure was rather insensitive to the time-dependent boundary condition.

Shahraki [2002] presented fluid dynamic and thermal fields for numerical simulations of laminar, steady, two-dimensional buoyancy-driven flows in an annulus between two vertically eccentric pipes using the penalty finite element method. Varying Rayleigh numbers between 10(3) and 10(5) and radius ratio of 2.6, and with various eccentricities, simulations were accomplished with the usual Boussinesq approximation. However, a modified Boussinesq approximation with temperature-dependent viscosity and thermal conductivity was used in order to demonstrate the effects of temperature-dependent physical properties for natural convection in a concentric annulus. The varying viscosity had the most effect on the fluid velocity, while the effects of varying thermal conductivity were most noticeable in the temperature profiles and local Nusselt numbers.

Moshkin [2002] simulated the flow and heat transfer in a two-layer system of an immiscible incompressible fluid using finite-difference approximation of the Navier-Stokes equations under the Boussinesq-fluid assumption. The numerical model was validated with a benchmark solution, which is buoyancy-driven flow in a square cavity with differently heated vertical sides. The results of the two-dimensional numerical simulation were compared with the experimental data of the hydrodynamics and heat exchange within a horizontal two-layer medium consisting of two immiscible liquids of different densities and viscosities. Agreement was observed between numerical and experimental results.

Papanicolaou and Belessiotis [2002] numerically studied the transient state of natural convection in a vertical cylindrical enclosure for water at high Rayleigh numbers, extending into values characteristic of the turbulent flow regime. For this purpose, several two-equation turbulence models were used. Cylindrical vertical surface was at a constant heat flux while the horizontal bounding surfaces were adiabatic and the development of stratification was studied. A quasi-steady state was achieved after the fluid followed an oscillating pattern where secondary flows alternately appeared and vanished. These patterns affected the development of stratification in the vessel, Low-Reynolds k-epsilon models predicted eventually a relaminarization at large times while high-Re form of the k-epsilon model obtained sustained or very slowly decaying turbulence instead.

Khanafer and Vafai [2000] focused on obtaining an accurate representation of effective boundary conditions at the open side of two- and three-dimensional open-ended structures. This study reduced the more complicated open-ended boundary conditions to a closed-ended domain and resulted in substantial savings in CPU and memory usage. Galerkin weighted residual method of finite-element formulation was used in the numerical procedure. The results presented in this work constituted an innovative way to describe correctly the boundary conditions at the open side of an open-ended boundary.

Li et al. [1996] numerically studied the temporal formation of the buoyancy-driven flow structures in a bottom heated, shadow, cylindrical fluid layer was. The unsteady three-dimensional Navier-Stokes and energy equations were discretized by the power law scheme and solved by the fully implicit Marker-and-Cell method. Computations were carried out for the pressurized argon and water layers for various Rayleigh numbers and heating rates of the layer. In the pressurized argon layer at a slightly supercritical Rayleigh number with, a steady straight roll pattern was formed when the heating rate

was very low after a long transient stage. When the heating rate was raised, a very different structure like U-rolls was formed at steady state.

Khan and Yao [1993] presented a numerical solution comparing steady natural convection of water and air in a two dimensional, partially divided, rectangular enclosure. Rayleigh numbers investigated range from 10(6) to 10(8), and the opening ratios studied are 0, 1/4, 1/6, and 1/8 respectively. The average Nusselt number obtained for water was only 2 approximately 5% larger than that for air at the same conditions. The exchange flow rate for water was found to be 10, approximately 20% larger than that for air. It was observed that for the opened partition the average Nusselt number was 13, approximately 24% larger than that for unopened partition. Also it was found that an opening in the partition reduced the exchange volume flow rates by 5.68 approximately 15.2% for water and 1 approximately 11.4% for air depending on the Rayleigh number and the opening ratio.

Fiegley et al. [2002] worked on improving the use of mixing factors for dilution ventilation design. General equation at steady state, Q= K*G/C where K is the safety factor which arises due to several factors, one of which is imperfect mixing. Different inlets, exits and source locations were studied and some of them were validated by experimental results. Unlike orthodox design approaches, this work suggests that air monitoring data often can be used to calculate dilution flow rate requirements, which can be reduced by enhancing room mixing with fans or alternating air inlet configuration.

Bennett et al. [2000] mainly compares mathematical models- completely mixed- (CM-1), CM-2, and uniform diffusivity (UD)- for exposure assessment with Computational Fluid Dynamics (CFD) simulation. Room air flow, concentration fields, and the breathing zone concentration of a stationary worker were studied for both constant and time varying

source. For both constant and time varying emission sources , exposure estimates depended on receptor and source location. For the constant source case, ventilation rate was inconsequential to CM-1 model error. UD model was close to CFD results at near source breathing zone; although, CM-1 model underestimated this zone, it shows good compliance at zone away from the source. At near source breathing zone, CM-2 model results, compliance is between CM-1 and UD.

Sherman [1992] discussed and used the tracer gas techniques- Continuity Equation, Tracer Decay, Long Term Integral and Constant Concentration Technique- for measuring ventilation in a single zone. He discussed all mathematical models and also analyzed those. Depending on the quantity desired, the stability of the air flows and the experimental limitations, various choices can be made. The choice of method to use in a given situation will depend on the practical details of the experimental as well as the reason for measuring the air change in the first place.

Furtaw et al. [1996] concentrated on the models to find the concentration of pollutants near the source and compared this with Completely Mixed model. His research is based on experiments to focus source-proximate-effect (SPE). Results indicated that at normal indoor air flow rates, measured concentration near the source was 1.5 to 2.0 time higher than that predicted by completely mixed model. The proposed SPE model simulates actual measured concentration more realistically than does single compartment model.

Nicas [1996] discussed well mixed and two zone model and their errors in estimating exposure intensity in an imperfectly mixed room. He also discussed ventilation efficiency for imperfectly mixed room. The paper is fully based on mathematical modeling. He analyzed the drawbacks of completely mixed model, two zone model and uniform

diffusivity model and then suggested some ways and modeled some equation to improve those models to get much accurate concentration field in different zone in room.

Waters and Simons [1987] examined the theory of multi-zone air-movement model in order to improve strategies for the deviation of inter zonal air flows from tracer decay measurements. Analyzing the decay curves he tried to measured flow rate in a multi cell building. A detailed examination of the forward solution, in which tracer gas concentration was predicted from known flow rates, was carried out. Proposals were made for seeding strategy, and for computational procedures.

Fiegley et al. [2002] presented a comparison between concentration estimates from simple models and that from CFD simulations. Using different configurations of air inlets, exits and source locations author compared concentrations of breathing zone in a workroom from CFD results. Parameters of the CM-1, CM-2 and UD model were estimated from CFD results and then calculated concentrations from these results were compared with that of CFD results. Results proved that CM-1 model underestimate near source concentration, while CM-2 model was better there. UD model performed poorly on average in poorly in both near and far fields.

Nicas and Jayjock [2002] compared between exposure assessment by air monitoring and that by mathematical model where he defended mathematical models under some conditions.

Dunham et al. [2001] compared qualitative exposure models with several other exposure models. The compared hazard ranking calculated from three exposure assessment models with actual exposure data of three weeks. Results showed that overall the models appeared to be predictive of exposures. Finally he made a comment that the

models can be useful tools to help make decisions on exposures level in a work room that can cause illness to employees.

Lee et al. [26] investigated the effect of the type of air inlet velocity boundary condition in simulating the dispersion of indoor contaminants by CFD. Author used uniform velocity and profile velocity (measured from experimental data) boundary conditions to compare the results. Distribution of tracer gas concentration using the profile inlet velocity showed better agreement qualitatively and quantitatively with experimentally measured chamber concentration.

Chapter 2 : Experimental Study

2.1 Experimental Facility

A 1/5th scale model of the furnace module was constructed for the experimental investigation. Figure 2.1 shows the schematic of the furnace module without the AR. The model furnace module was constructed out of Lexan® and the Argon reservoir was constructed from stainless steel sheet. Tables 2.1 and 2.2 show the comparison of the dimensions of the experimental model with the production furnace module.

Table 2.1: Comparison of the dimensions of the experimental facility with the production furnace.

	Furnace Module			Extraction Basket			Retort		Volume (ft^3)				Module Lid Opening
	Length	Width	Height	Outer Diameter	X-Area(ft^2)	Height	Outer Diameter	Height	Basket	Reservoir	Retort	Module	Diameter
Production	19'-9"	6'-6"	26'-7"	12.75"	0.887	16'-8"	20"	260"	14.5	49	280	3600	2.5'
Model	54"	17"	64"	2.5"	0.034	40"	4"	52"	0.116	0.48	0.5	30	6.0"

Table 2.2: Comparison of basket speed and make-up volume flow rates for the experimental model and the production unit.

Basket Withdrawal Rate	Module (ft/m)	0.38	0.50	1.00	1.50	2.00
	Production (ft/m)	1.90	2.50	5.00	7.50	10.00
Module Filling Rate	Mod. (cfh)	0.75	1.00	2.00	3.00	4.00
	Production (cfm)	1.56	2.08	4.16	6.24	8.32

The furnace (retort) was made with Aluminum pipe, the dimensions are shown in Figure 2.1. The retort was 4-inch in diameter and 52-inch in length. The retort was wrapped with flexible strip heaters. A number of thermal experiments were performed where the retort was heated to set temperatures (see experimental matrix). The power to the strip heater was controlled by a rheostat. The rheostat was experimentally calibrated to attain the desired retort temperature. This was done by adjusting the percentage power on the rheostat and allowing the retort to reach steady state temperature. After steady state was obtained this temperature and the rheostat reading were recorded. A set of data was collected, and served as a calibration curve, see Figure 2.16. It should be noted that the calibration served only as a reference, it provided an approximate starting point to attain any desired temperature. During the actual experiment the rheostat was adjusted to obtain the desired temperature. Also, for the thermal experiments, where the objective was to observe the effect of elevated temperature (above room temperature) of the retort, the retort was insulated with glass-wool. This insulation was sealed to prevent off gassing. For all of the isothermal (room-temperature) experiments, the insulation was not present. For the thermal experiments where the objective was to study the effect of elevated furnace module gas temperature, the insulation was not present.

Figures 2.2 and 2.3 show the top of the furnace module without an argon reservoir. A sliding gate with a gasket was used to prevent gas flow through the port. In Figure 2.2, the gate is open and in 2.3 it is closed. As shown in the Figures 2.2 and 2.3, two tightening screws are used to loosen and slide the gate, after the gate has been positioned in the open or closed position the screws are tightened to achieve a leak tight seal. The scale-furnace module with the argon reservoir is represented in figures 2.4 and 2.5.

Figure 2.6 shows the location and dimension of the sampling ports used for collecting the gases from the furnace module. As can be seen from the figure there are six ports; three for taking the gas sample from the furnace module to the O2X1 Oxygen Analyzer (supplied by Panametric Corp.) and the other three are for returning the gases. No gas from the furnace module is discharged into the atmosphere, instead all of it is returned to the module. Therefore, the actual concentration is not affected by the measurement process. Miniature air pumps Model-SP 300 from Smart Products were used for sample collection and recirculation.

Figure 2.7 shows the bottom region of the furnace. The hole in the bottom of the retort provides an entry for the argon when filling the furnace module, and the other inlet is in the bottom of the module (note that these are not the make-up ports). A 30-cfm electric blower was installed in the bottom of the furnace module to mix the gas before and after each experiment.

Figures 2.8 and 2.9 show the detailed dimension of the experimental furnace module with the argon reservoir. Figure 2.10 shows the details of the spool-spacer, which connects the module and the reservoir. Figures 2.11 and 2.12 show the details of the sliding gate along with its sealing screws. Figure 2.13 is the furnace module without the argon reservoir.

The model-extraction basket was made from aluminum tube with the ends seal welded. Its outside diameter is 2.5-inches and it has a length of 40-inches. The basket withdrawal and insertion system consists of a cable-pulley mechanism driven by a variable speed DC-motor. Figure 2.14 shows the system schematically. The cable is attached to the top of the basket, and passes through two overhead pulley blocks before reaching the DC-motor driven pulley. Withdrawal and insertion is accomplished by

wrapping the cable on the pulley. This was calibrated for the speed range of interest, Figure 2.17 shows the basket speed as a function of DC motor dial-setting.

A 30-cfm blower was used for simulating HVAC air-flow rate. The blower was placed on top of the furnace module. Figure 2.1 shows the location of the HVAC blower. The air velocity was measured with a Model-8100, anemometer, manufactured by Alnor Instrument Co. Figure 2.19 shows the some photos of model experimental setup.

2.2 Leak Testing the Furnace Module

Several leak detection tests were performed to eliminate any leaks from the furnace module. Two different tests were performed to detect the leakage in the furnace module. After closing the sliding gate and all the feed throughs (i.e., ports for sample collection and temperature measurements), the furnace module was pressurized by argon to a pressure of 5-inches of water. In order for the furnace module to be leak-proof, the pressure had to remain constant for 1-2 hours. During the pressure test a soap-water solution was applied to all the locations, joints, and penetrations which are prone to leak. All detected leaks were fixed by tightening the screws (sliding gate), applying epoxy, or by changing the gasket. During the pressure test, a cable was wound around the furnace module to monitor the deformation of the furnace module caused by the internal pressure. There was no detectable restoration of the deformation during the period of the test, confirming a sealed furnace module. The second test consisted of filling the module with argon, mixing it thoroughly with a mixing blower and measuring the concentration in the furnace module. The module was then allowed to sit for a period of over 24-hours. The concentration measurement of the argon was repeated. The furnace module showed no detectable change in concentration during this 24-hours.

2.3 Instrumentation and Data Acquisition

Eight different thermocouples were used for measuring the temperature. Three of these are located on the retort to measure the retort temperature. The other five are used to measure the gas temperature in the furnace module. The locations of the thermocouples are shown schematically in Figure 2.14. The thermocouples were connected to a National Instrument Data Acquisition system connected to a personal computer. Lab-View Software was used for collecting and storing the data. Figure 2.15 shows the detailed schematic of the argon flow lines and the control valves.

Oxygen concentration was measured with O2X1 Oxygen Analyzer, which had three different ranges (range#1 1: 0-1000 parts per million; range #2: 0 - 1%; range #3: 0-10%). Calibration of the analyzer was performed using calibrated gas mixtures. These mixtures were obtained from Matheson Tri-Gas Company. The mixtures (argon and oxygen) were .001%, 0.08%, 0.8%, 5% and 8% oxygen.

2.4 Experimental Test Matrix

An experimental matrix representing the experimentally studied operating conditions is shown in Table 2.3 below.

The table below indicates that a total of 42 tests were performed. Seven of the experiments were repeated to check the accuracy of the experimental test results. There were six thermal tests, of these six, four were with elevated retort temperature and two were cases where the furnace module had elevated temperature (delta T). There are three tests which study the effect of closing and opening the sliding gates with a delay. These tests were done to simulate the situation where there is an operator delay

during the withdrawal or insertion of the basket. Also, there were 6-tests performed with the AR. The results of these findings are presented and discussed in the results section.

Table 2.3: Experimental Test Matrix.

Basket	Model HVAC (ft/m)	Basket speed (ft/m)		Makeup Rate		Test at Room Temp. (Isothermal)	Delay (5 mins)	Thermal (Retort Temp 167 to 176 F)	With Reservoir	Temp Diff (Module gas 50 F above Room Temp)	Repeat of Isothermal
		Model	Production	Model (cfh)	Production (cfm)						
Withdrawal	10	0.50	2.50	0.00	0.00	Yes					
				0.75	1.56	Yes					
				1.00	2.08	Yes	Yes	Yes	Yes	Yes	Yes
				2.00	4.16	Yes					
		1.00	5.00	0.00	0.00	Yes					
				1.00	2.08	Yes					
				2.00	4.16	Yes	Yes	Yes	Yes		Yes
				4.00	8.32	Yes					
		2.80	14.00	0.00	0.00	Yes					
				5.60	11.65	Yes	Yes	Yes	Yes		Yes
				9.00	18.72	Yes					
	No	0.50	2.50	**1.00**	2.08	Yes					
		1.00	5.00	**2.00**	4.16	Yes		Yes			Yes
		2.80	14.00	**5.60**	11.65	Yes					
Insertion	10	0.50	2.50	0.00	0.00	Yes					
				1.00	2.08	Yes			Yes	Yes	Yes
		1.00	5.00	0.00	0.00	Yes					
				2.00	4.16	Yes			Yes		Yes
		2.80	14.00	0.00	0.00	Yes					
				5.60	12.48	Yes			Yes		Yes

Note: In 'Makeup Rate' columns the ratio of 'Production(cfm) column and 'Model(cfh)' column is 2.08. (Production(cfm)/ Model(cfh)=(125*model scale/1*model scale)*(1cfm/60*cfm)=2.08).
Colored data indicates nominal cases (argon make-up rate is equal to volume withdrawal rate)

2.5 Experimental Procedure

A. Filling the Furnace Module with Argon

Note: The source of the Argon, shown in Figure 2.15, is a conventional 5 ft. high and 9 in. diameter Argon cylinder containing 99.99% Argon.

A.1. Ensure valve ***BG3*** and pressure regulator ***TR2*** are closed.

A.2. Open valves ***AG1, AG2, AG3, GG,*** and ***TG***.

A.3 Open the Furnace Module ***Gate*** and connect the gate opening with the safety exit – ***SE.***

A.4 Open pressure regulator ***TR1*** and observe the Argon cylinder pressure on pressure gage ***TPr1.***

A.5. To begin filling the Module, slowly and carefully open pressure regulator ***TR2*** until air flow meter ***AF*** indicates a flow at 10.0 cfh.

A.6. After approximately 5.0 hours, close the Furnace Module ***Gate*** and stop supplying Argon by closing pressure regulator ***TR2.***

A.7. Take oxygen % readings from sample lines ***C, D,*** and ***E*** using Oxygen Analyzers ***CO, DO,*** and ***EO*** respectively.

A.7.1. Ensure the range (scale) of each oxygen analyzer is set at 0-10%. (If necessary, set to proper range per pages 6 and 7 of the attached manual, Figure 2.18.)

A.7.2. Open valves ***CG1, CG2, CG3, CG4, DG1, DG2, DG3, DG4, EG1, EG2, EG3,*** and ***EG4.***

A.7.3. To establish a closed loop for each sample point, start pumps ***CP, DP,*** and ***EP*** using switches ***CS1, DS1***, and ***ES1***; **AND**, as indicated on flow meters

CF, DF, and ***EF,*** set the flow rate for each loop at 2.0 cfh using valves ***CG3, DG3,*** and ***EG3*** for their respective sample loops.

A.7.4. Approximately 10 seconds after pumps are started, analyze sample line C contents as follows:

A.7.4.1. Ensure switches ***DS2*** and ***ES2*** are OFF.

A.7.4.2. Ensure switch ***CS2*** is in the ON position.

A.7.4.3 Record the ***AM*** reading in mA.

A.7.5. Analyze sample line D contents as follows:

A.7.5.1. Ensure switches ***CS2*** and ***ES2*** are OFF.

A.7.5.2. Ensure switch ***DS2*** is in the ON position.

A.7.5.3. Record the ***AM*** reading in mA.

A.7.6. Analyze sample line E contents as follows:

A.7.6.1. Ensure switches ***CS2*** and ***DS2*** are OFF.

A.7.6.2. Ensure switch ***ES2*** is in the ON position.

A.7.6.3 Record the ***AM*** reading in mA.

A.7.7. Ensure switches ***CS1, DS1, ES1, CS2, DS2,*** and ***ES2*** are in the OFF position.

A.7.8. Convert the mA readings taken to Oxygen % using formula: $\%O_2 = (R-4.0)*S/16.0$; where S is the maximum range of the Analyzer (here 10), R is the mA reading of the ammeter ***AM***.

A.7.9 Record the calculated Oxygen % for each sample line.

A.8 To mix the gas in the Module, turn on blower ***B1*** by placing switch ***S3*** (figure 2.15) in the on position.

A.8.1 Mix the module gas for five minutes then turn off blower ***B1*** by placing switch ***S3*** in the OFF position.

A.8.2 Wait 2 minutes for the Module gas to stabilize, then perform steps A.7.1. through A.7.9.

A.9. If Oxygen concentration is less than 0.5%, then record concentration and proceed to step A.10. If Oxygen concentration is greater than or equal to 0.5%, then repeat filling and sampling steps until Oxygen concentration is less than 0.5%.

A.10. Close the Module ***Gate*** and valves ***TR1, TR2, TG, AG3, AG1, AG2,*** and ***AG3.***

A.11. Turn on the computer ***Comp*** and the Analog Digital Converter Device ***A/D*** by placing switches ***S5*** and ***S4*** in the ON position. When ***Comp*** is on, open the programmed Labview file, Thermocouples.vi from directory C:\Rafat\Src\. Start running it and record all temperature readings.

B. Insertion of the Basket (With HVAC)

B.1. Turn on the motor controller ***MC*** by setting switch ***MCS1*** to the On position.

B.2. Using switch ***MCS2***, position the Basket such that the bottom of the basket is approximately 1 inch above the top of the Module.

Note: Instructions for performing the next step are on page 8.

B.3. Set the motor controller regulator ***MCR*** at 18 (0.5 ft/m).

B.4. If Argon makeup is not going to be provided, then skip this step and proceed to the next step. If Argon makeup is to be provided, ensure valve ***AG3*** is closed, then open valves ***TG, BG1, BG2, BG3,*** and ***TR1.***

B.5. Determine the Module initial Oxygen % as follows:

B.5.1 If mixing and sampling of the Module gas has been performed as per steps A.8. through A.8.2. within the last 5 minutes and no changes have been made to the Module gas makeup, then record the last documented Oxygen concentration and proceed to Step B.6.

Note: Long delay causes settling down of Argon. Uniform mixture in the module is recommended before starting any test. Also by any chance there may have some infiltration of air inside, so don't rely on the sampling done before 5 minutes and possibly do it immediately before Step B.6.

B.5.2 If mixing and sampling of the Module gas has not been performed within the last 5 minutes, or if changes have been made to the Module gas makeup, then perform steps A.8. through A.8.2. and A.9 and record results.

B.6. Turn on blower ***B2*** by setting switch ***S1*** in the On position. This will simulate the flow of HVAC across the Module top at 10 f/m.

B.7. Open the Module ***Gate***, start Motor ***M*** by placing switch MCS2 in the forward setting, and immediately go to the next step.

B.8. If Argon makeup is not to be provided, then skip this step and proceed to the next step. If Argon makeup is to be provided, slowly and carefully open ***TR2*** and establish a flow rate of 1.0 cfh, as indicated on flow meter ***BF***.

B.9. When the Basket reaches the bottom of the furnace (this will take approximately 10 minutes), stop the motor by setting ***MCS2*** at Brake position.

B.10. If Argon makeup was not being provided, then skip this step and proceed to the next step. If Argon makeup was being provided, then close ***TR2, TG***, and ***BG3*** and turn off B2.

B.11. Uncouple ***H2*** from ***H1*** and remove ***H2*** from the Module.

B.12. Close the Module ***Gate***.

B.13. Perform two sets of Module gas analysis (before and after mixing gas) per steps A.7. through A.7.9 and A.8. through A.8.2, and record results.

B.14. Subtract respective oxygen concentrations (after mixing) in step B.5. from oxygen concentrations in step B.13. to determine the increase in Oxygen concentration during the basket insertion.

B.15. Turn on the computer ***Comp*** and the Analog Digital Converter Device ***A/D*** by placing switches ***S5*** and ***S4*** in the ON position. When ***Comp*** is on, open the programmed Labview file, Thermocouples.vi from directory C:\Rafat\Src\. Start running it and record all temperature readings.

C. Withdrawal of the Basket (With HVAC)

C.1. Ensure switch MCS1 is in the On position.

C.2. Set the motor controller regulator ***MCR*** at 18 (0.5 ft/m)), see figure 2.17.

C.3 Ensure valve ***AG3*** is closed, then open valves ***TG, BG1, BG2, BG3,*** and ***TR1.***

C.4. Determine the Module initial Oxygen % as follows:

C.4.1 If mixing and sampling of the Module gas has been performed per steps A.8.theough A.8.2.within the last 5 minutes and no changes have been made to the Module gas makeup, then record the last documented Oxygen concentration and proceed to Step B.6.

C.4.2 If mixing and sampling of the Module gas has not been performed within the last 5 minutes, or if changes have been made to the Module gas makeup, then perform steps A.8. through A.8.2. and A.9 and record results.

C.5. Open the Module ***Gate*** and couple H1 and H2.

C.6. Turn on blower ***B2*** by placing switch ***S1*** in the On position. This will simulate the flow of HVAC across the Module top at 10 f/m.

C.7. Turn on motor ***M*** by setting ***MSC2*** at the backward position and proceed immediately to the next step.

C.8. Slowly and carefully open ***TR2*** and establish a flow rate of 1.0 cfh, as indicated on flow meter ***BF***.

C.9. When the Basket reaches the bottom of the furnace (this will take approximately 10 minutes), stop the motor by setting ***MCS2*** at Brake position.

C.10. Close valves ***TG, BG1, BG2, BG3,*** and ***TR1.***

C.11. Close the Module ***Gate***.

C.12. Perform two sets of Module gas analysis (before and after mixing gas) per steps A.7. through A.7.9 and A.8. through A.8.2, and record results.

C.13. Subtract respective oxygen concentrations (after mixing) in step C.4. from oxygen concentrations in step C.12. to determine the increase in Oxygen concentration during the basket Withdrawal.

C.14. Turn on the computer ***Comp*** and the Analog Digital Converter Device ***A/D*** by placing switches ***S5*** and ***S4*** in the ON position. When ***Comp*** is on, open the programmed Labview file, Thermocouples.vi from directory C:\Rafat\Src\. Start running it and record all temperature readings.

D. Rest of the tests matrix.

D.1. To do tests without HVAC, always keep switch S1 in the Off position.

D.2 To perform different insertion and withdrawal rates, set the motor controller regulator ***MCR*** per the attached figure 2.17.

D.3. To get different Argon makeup flow rates, turn ***TR2*** clockwise or counter clockwise as necessary to obtain the desired rate. For no flow rate, keep ***TR2*** and ***TG*** closed.

Note: Due to the low flow rates required, some fluctuation in the flow rate will occur. Therefore, flow meter ***BF*** must be monitored closely and ***TR2*** adjusted as necessary to maintain the desired flow rate.

D.4. Tests so far done is mentioned as ***At Room Temp.*** Cases in the test matrix means do the tests at room temperature everywhere.

D.5. A test instruction specifying a ***Delay(5 mins)*** means that after opening and before closing the Module ***Gate*** wait 5.0 minutes before proceeding to the next step which is actually operator delay. These tests are performed at room temperature everywhere.

D.6. A test instruction specifying a ***Repeat*** means that test results must be verified by repeating the test. These tests are performed at room temperature everywhere.

D.7. A test instruction specifying a ***With Reservoir*** means that do the mentioned tests with the Argon Reservoir. To do this, replace the top ***Gate*** attachments with the Reservoir and its attachments. These tests are performed at room temperature everywhere.

D.8. A test instruction specifying ***Temp Diff (Module gas 50 F above Room Temp)*** means that the tests will be conducted with a module temperature at 50^{o} F higher than the room temperature. To do the tests remove the heater from the furnace and uniformly spread it on the bottom of the module. Make sure to put some heat insulation between the heater and the floor of the module, otherwise the floor will melt as it is made out of Plexi Glass. Now after everything is OK, keep the ***Gate*** close, start the mixer ***B1*** and the heater at the Variac, ***V*** setting of 120 for 5 minutes and then ***V*** setting of 30 for another 10 to 15 minutes to get the desired temperature. This time setting is for Room temperature of 78^{o} F to 80^{o} F. If it is different, time for heating the module may vary. After getting the desired temperature do the tests as was done previously.

D.9. A test instruction specifying a ***Thermal (Retort Temp 167 to 176 F)*** means to do the mentioned tests with the Furnace average temperature of 150^{o} F. To do the test, uniformly wrap the heater around the furnace and then wrap the insulation

(1” thick) around it. When everything is OK, turn on the heater at the Variac, ***V*** setting of 120 for 5 minutes and then at 25 for about 10 to 15 minutes to get the desired temperature of the furnace. Now do the tests as were done for isothermal cases.

E. Consecutive Tests.

Everyday perform two or three tests. Initial Oxygen % must be less than 0.5 % and after any test the reading of Oxygen % will be the initial reading for the next test. If this % is more than 0.75, go through necessary steps in ***A***. fill the module to less than 0.5% and do the next test.

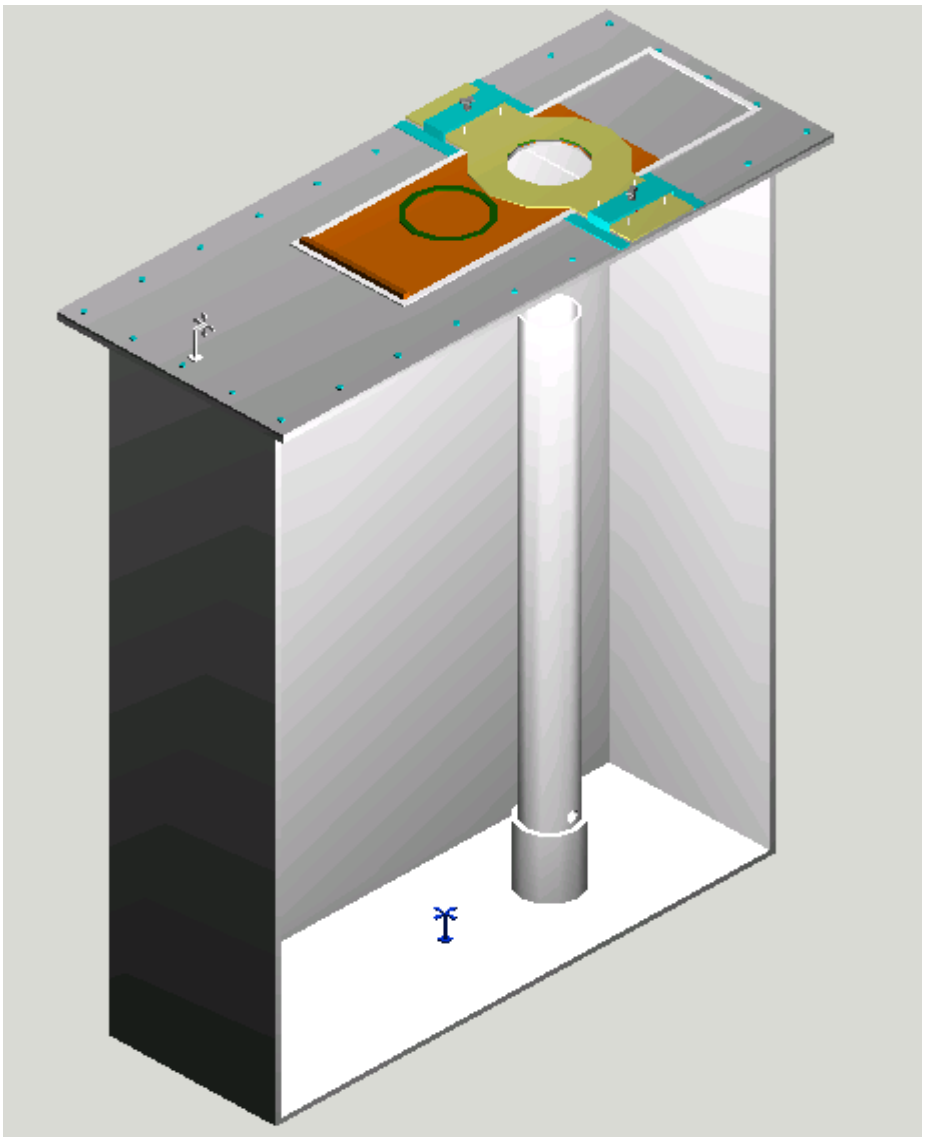

	Furnace Module				Retort	
	Length	**Width**	**Height**	**Vol (ft^3)**	**Dia (ID)**	**Height**
Production	19’-9"	6’-6"	26’-7"	3600	20"	260"
Model	54"	17"	64"	30	4"	52"

Figure 2.1: Schematic of the experimental facility without argon reservoir.

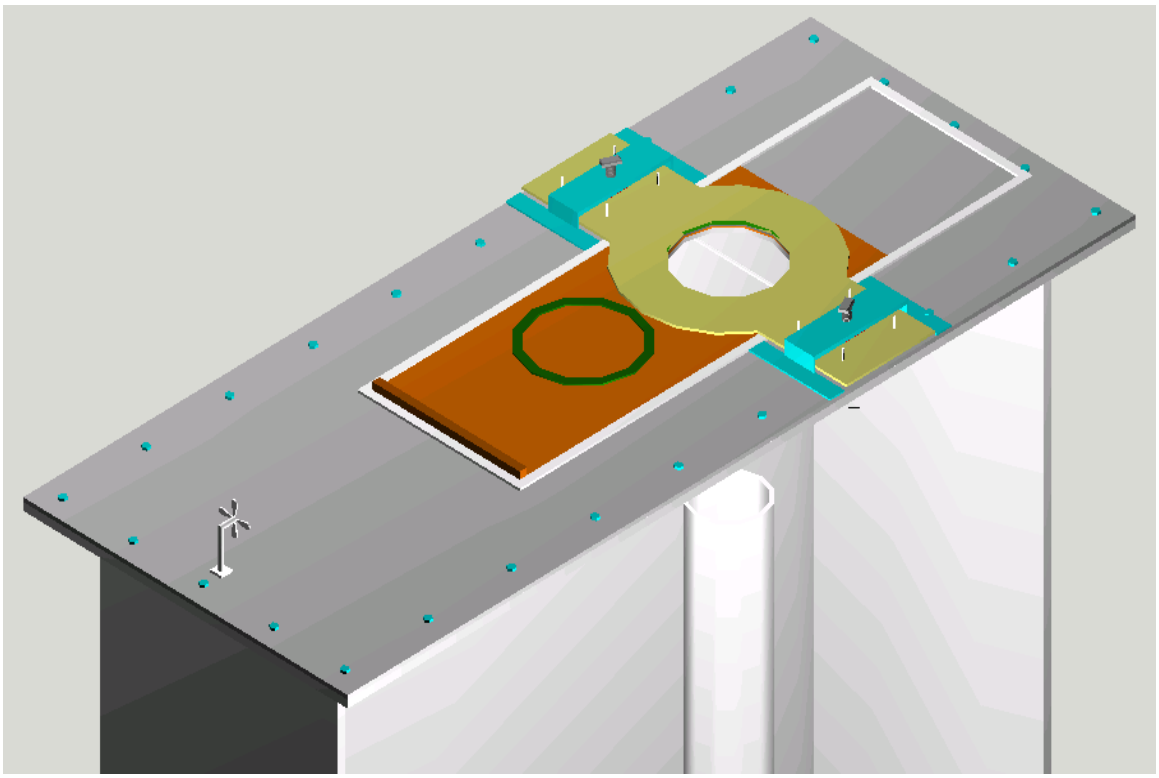

Figure 2.2: Figure showing top of the furnace module without the reservoir (open gate).

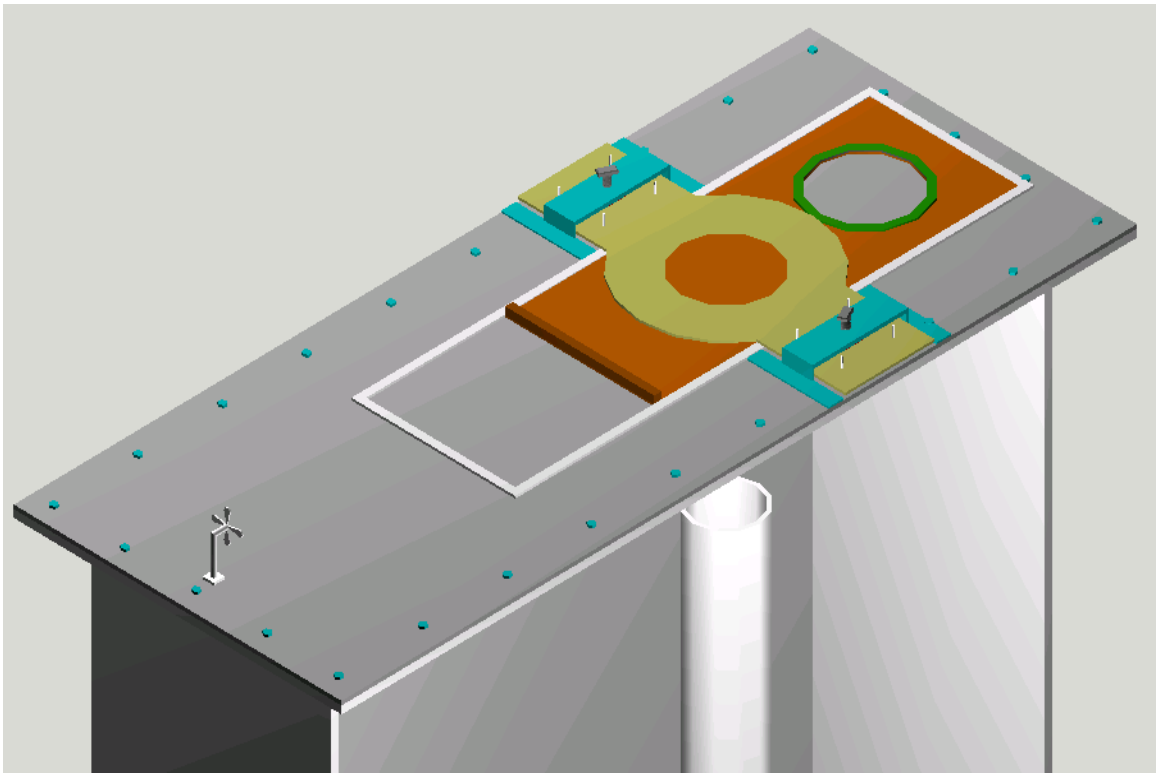

Figure 2.3: Figure showing the furnace module without the reservoir (closed gate).

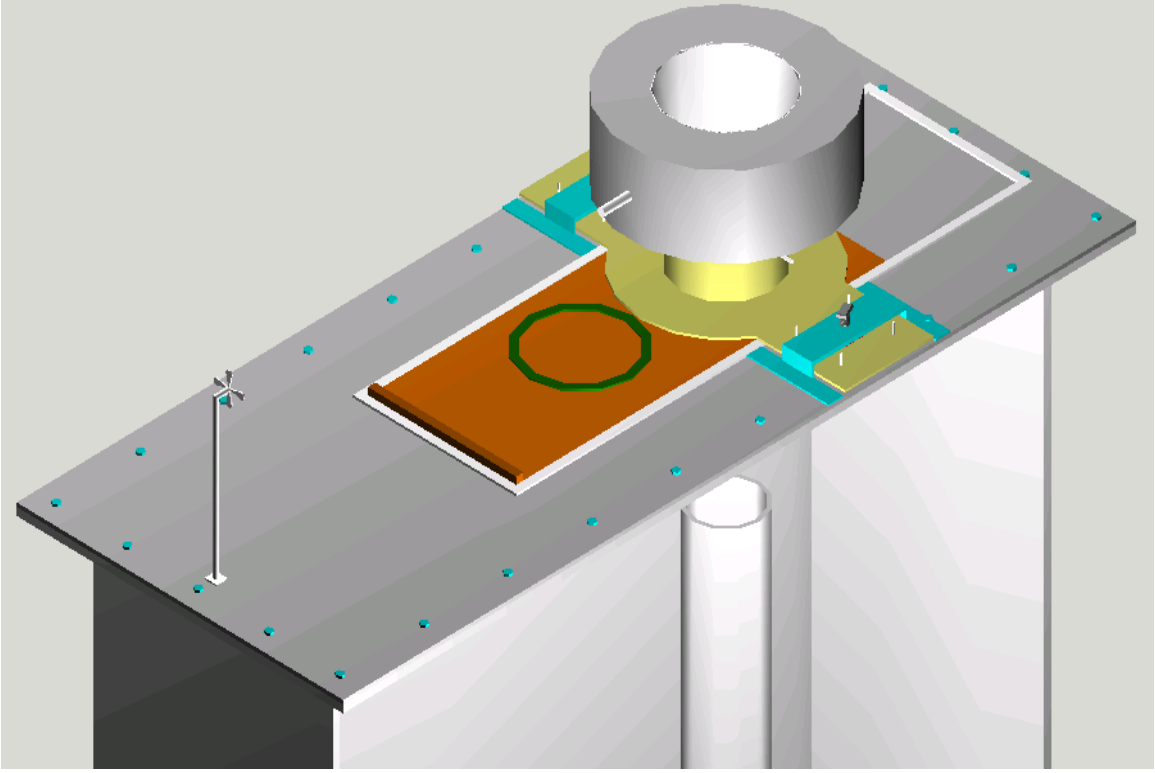

Figure 2.4: Figure showing top of the furnace module with the reservoir.

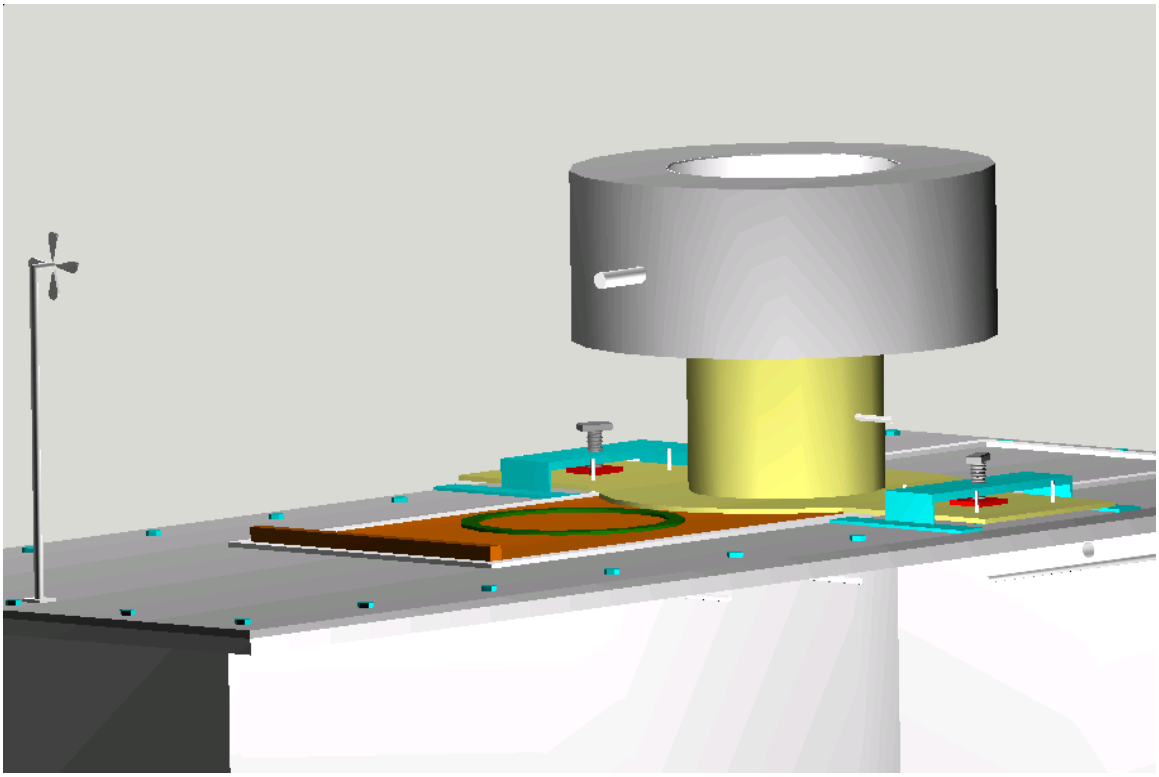

Figure 2.5: Figure showing top of the furnace module with the reservoir.

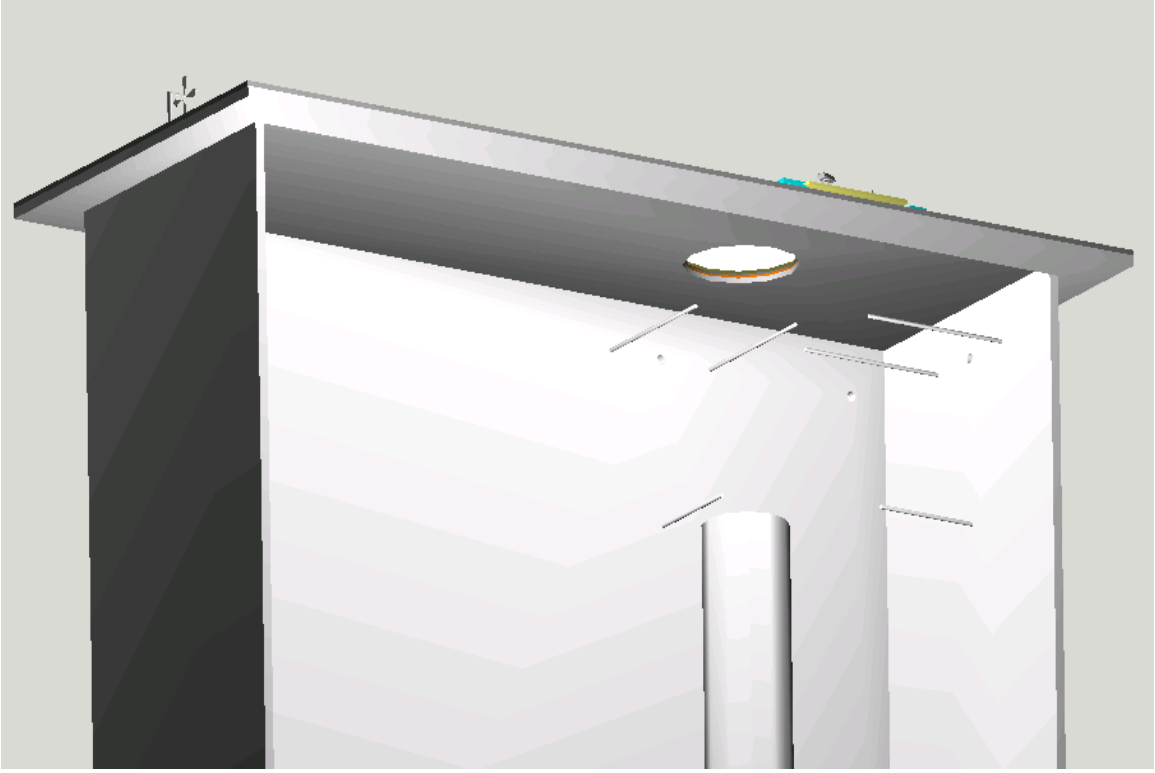

Figure 2.6: Figure showing the location of argon sampling ports.

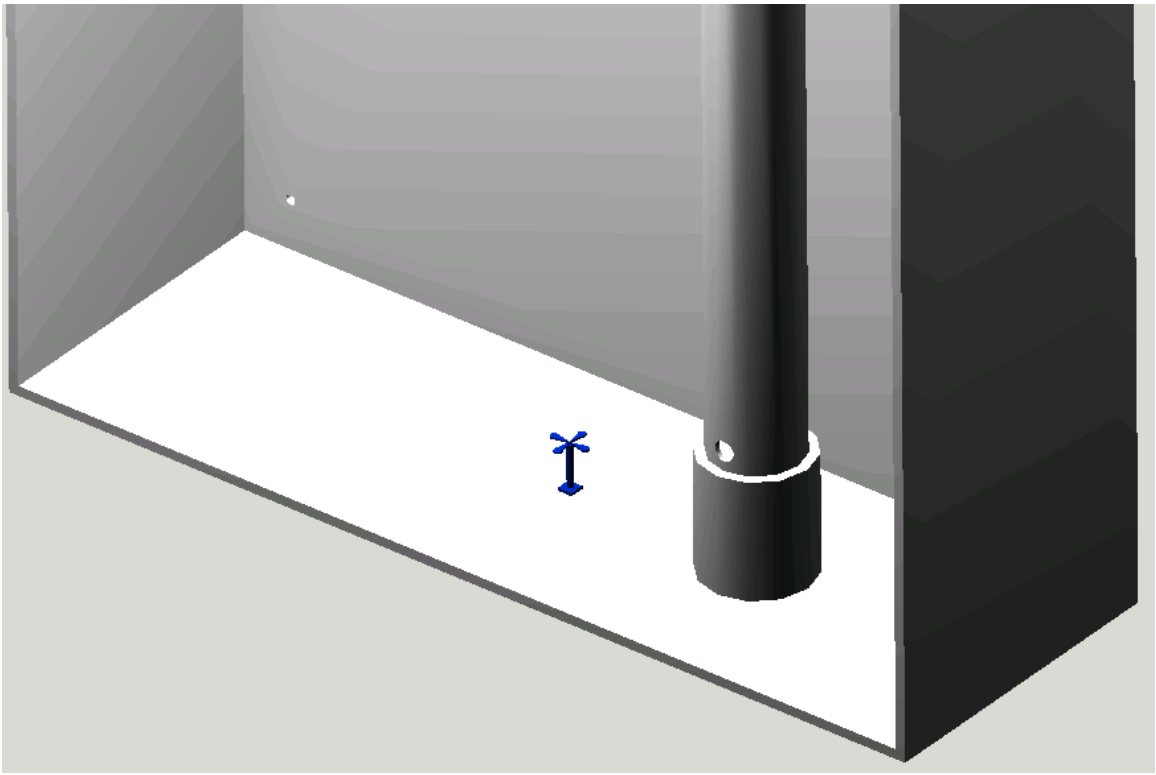

Figure 2.7: The detail of the furnace retort.

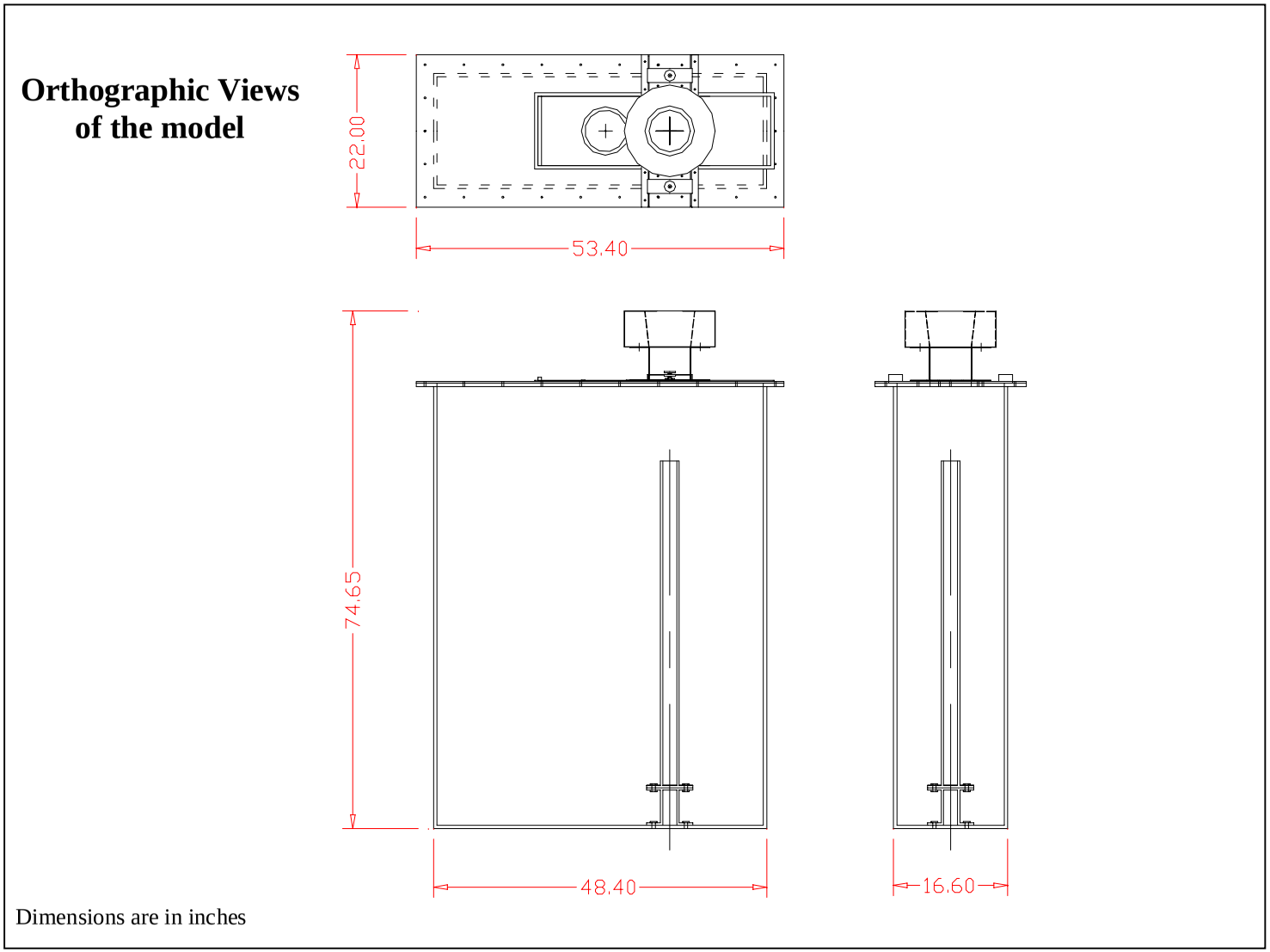

Figure 2.8: Dimensions of the furnace module with argon reservoir.

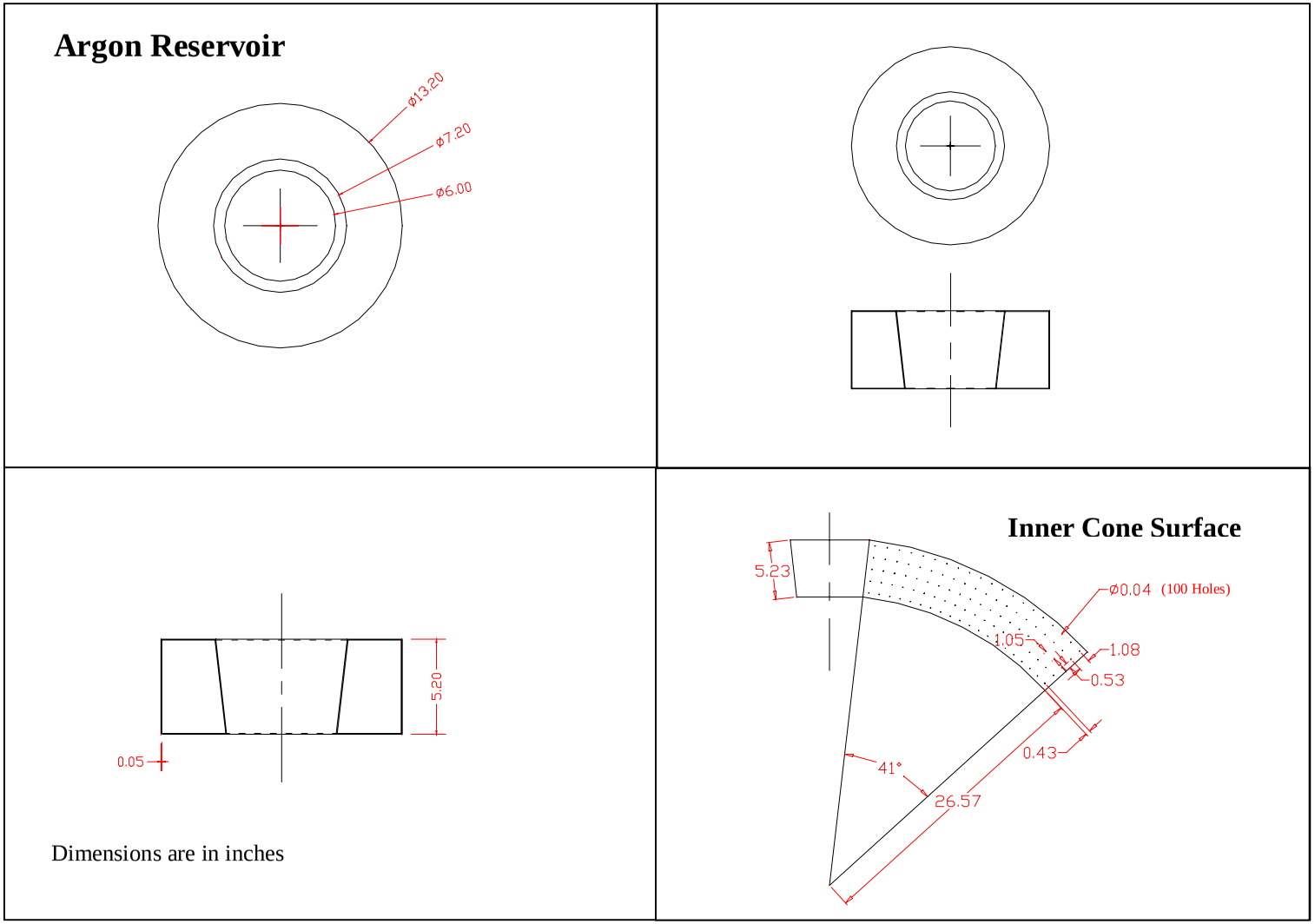

Figure 2.9: Dimensions of the argon reservoir and its holes.

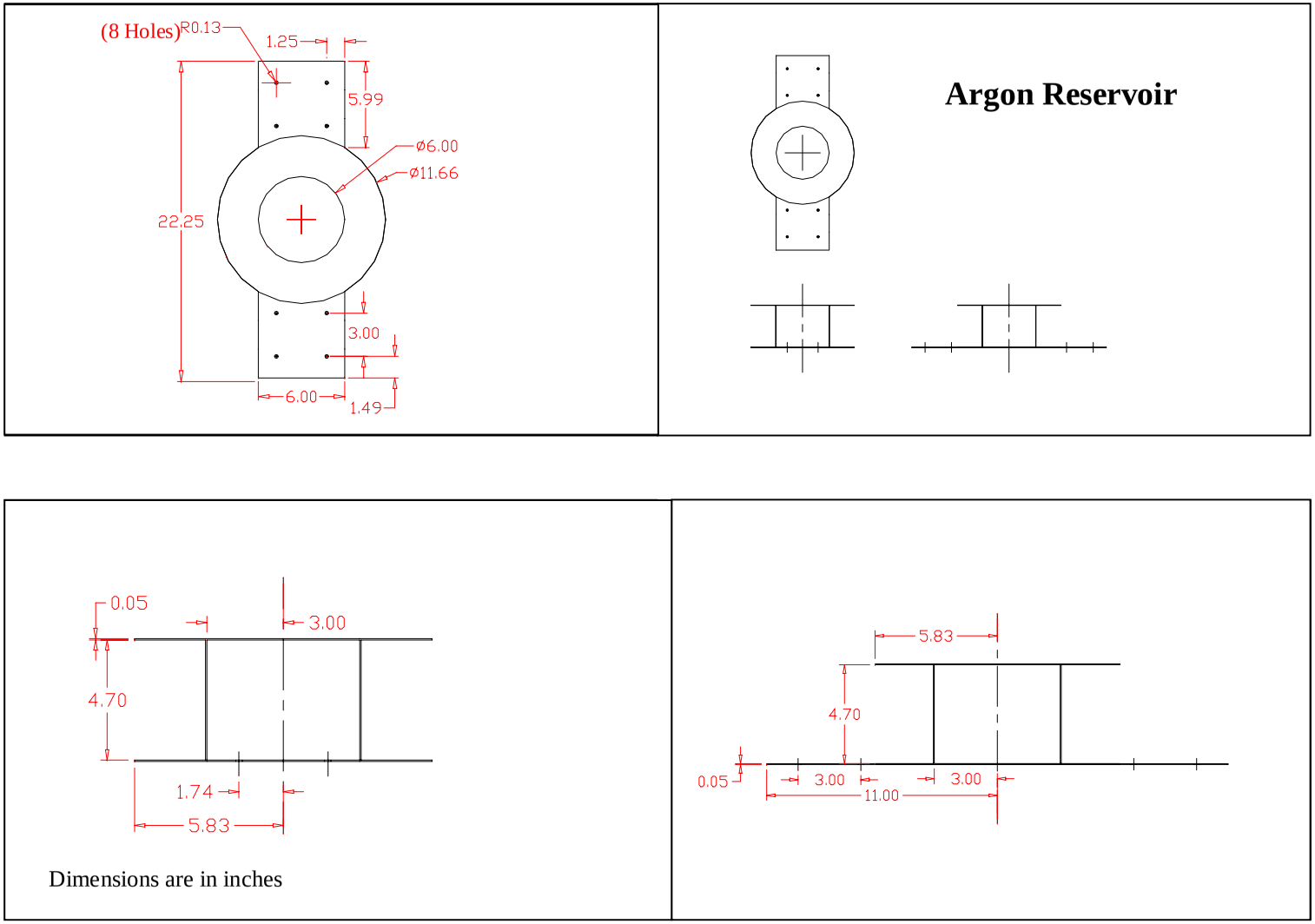

Figure 2.10: Dimensions of the sliding gate component.

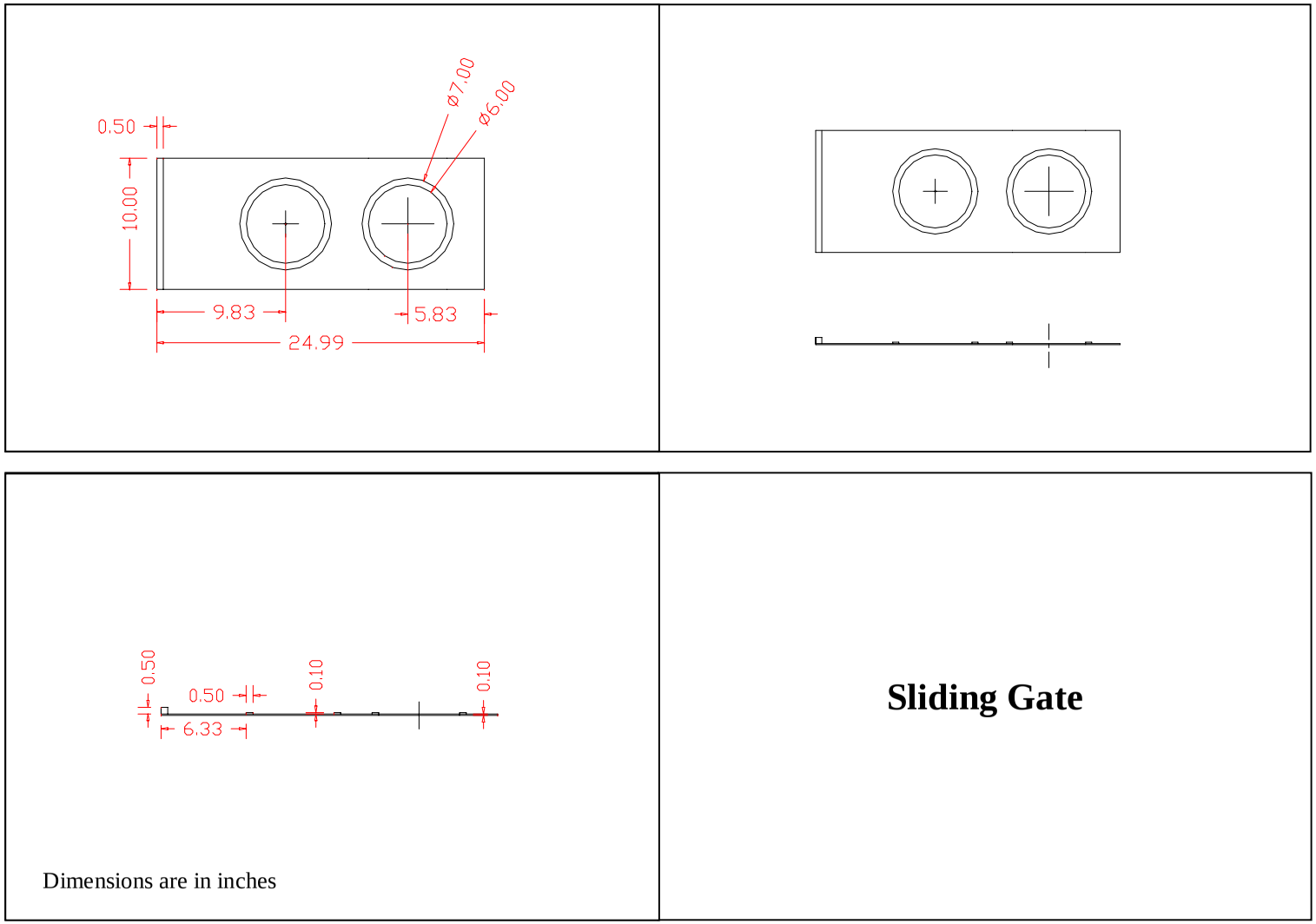

Figure 2.11: Dimensions of the sliding gate.

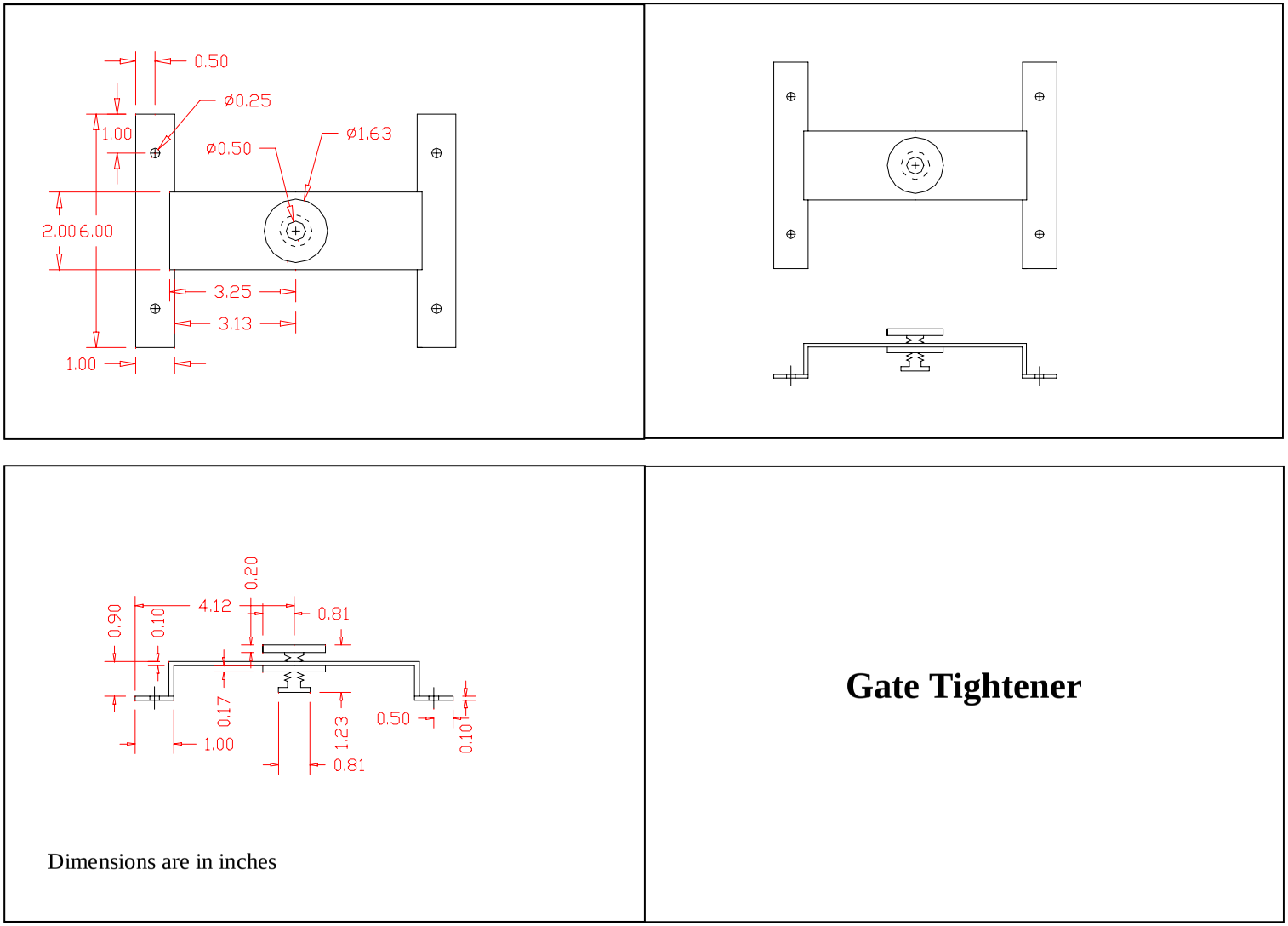

Figure 2.12: Dimensions of the tightening mechanism.

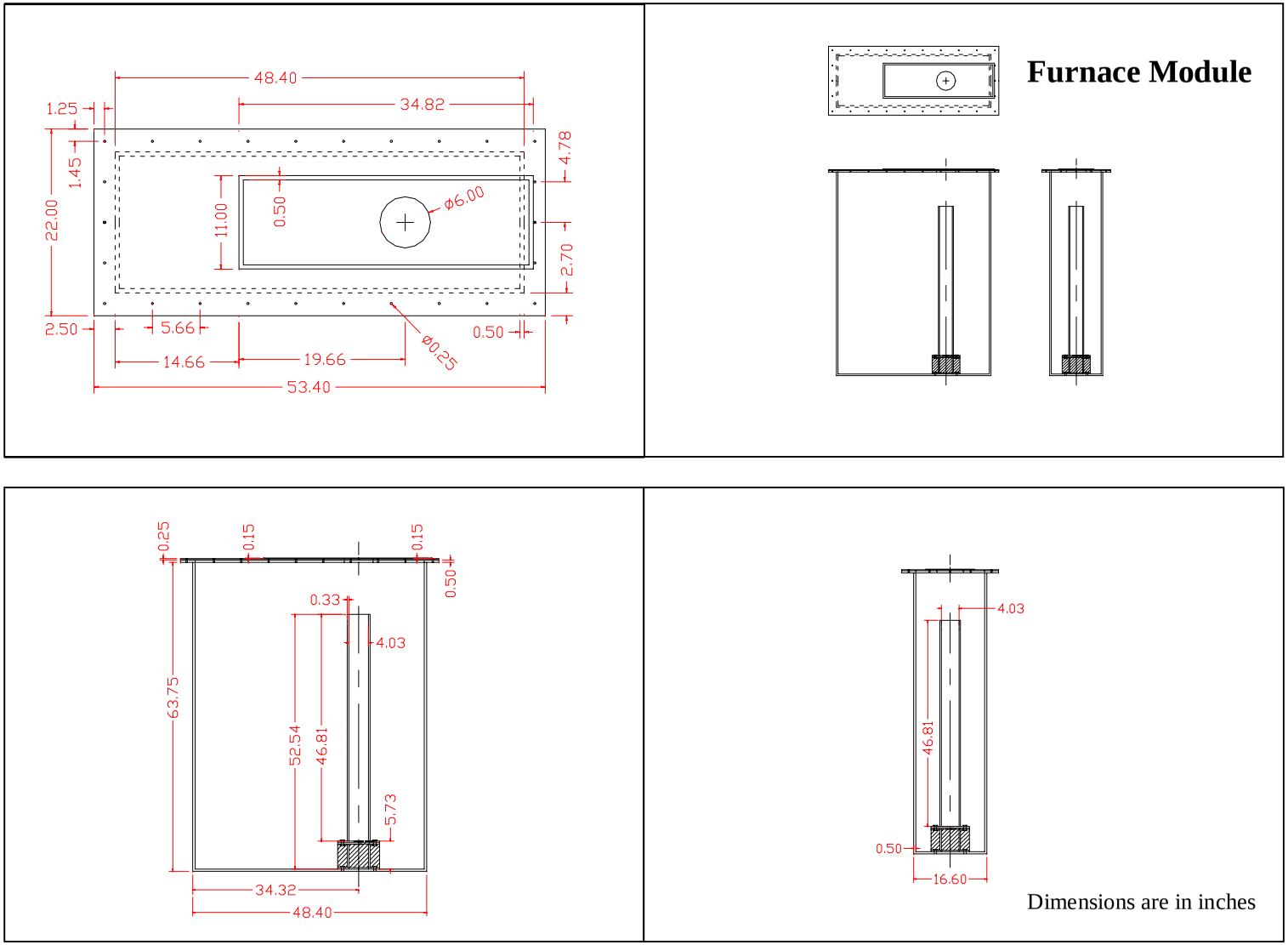

Figure 2.13: Dimensions of the furnace module without argon reservoir

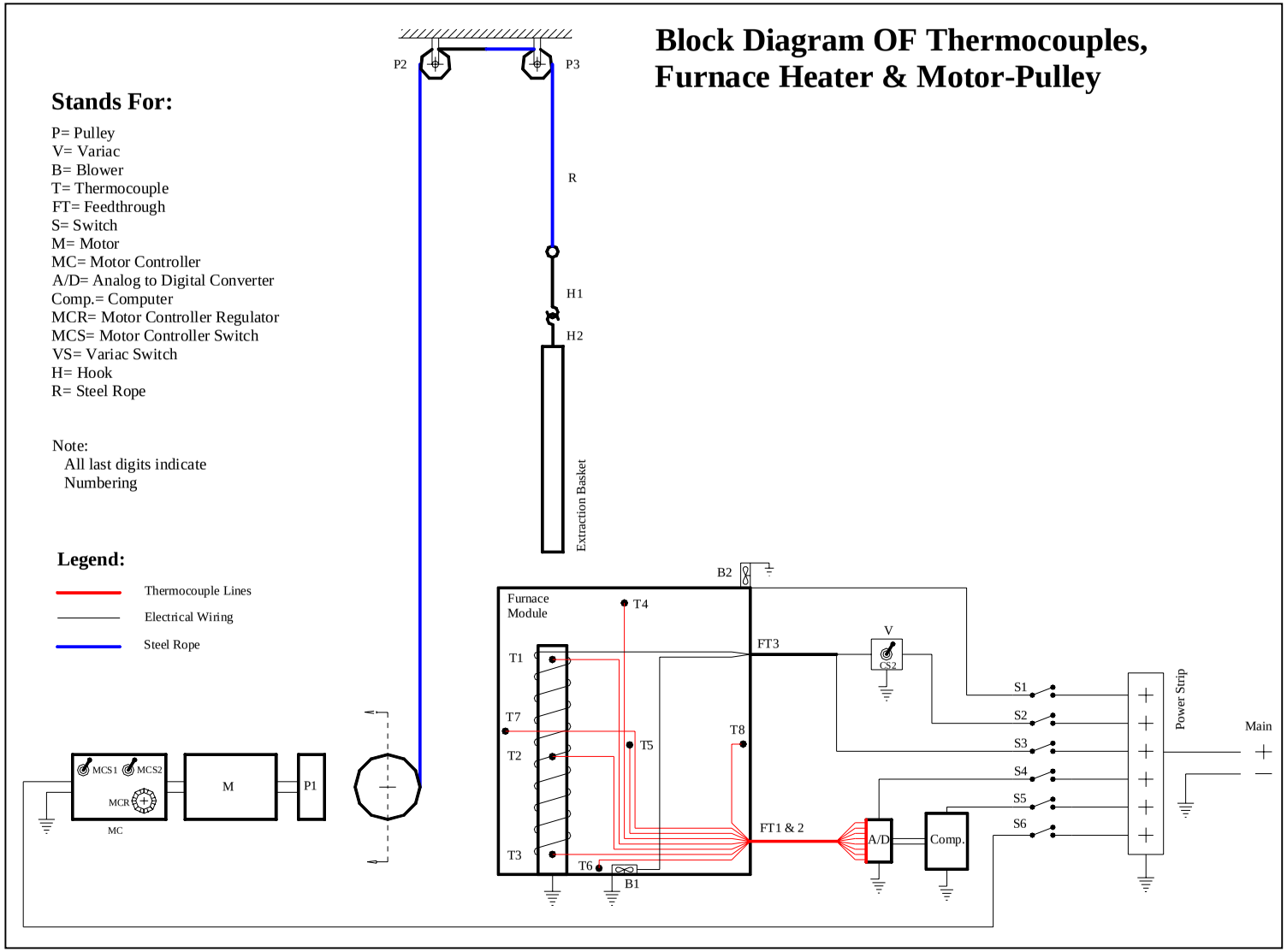

Figure 2.14: Schematic of experimental system showing the locations of the thermocouples

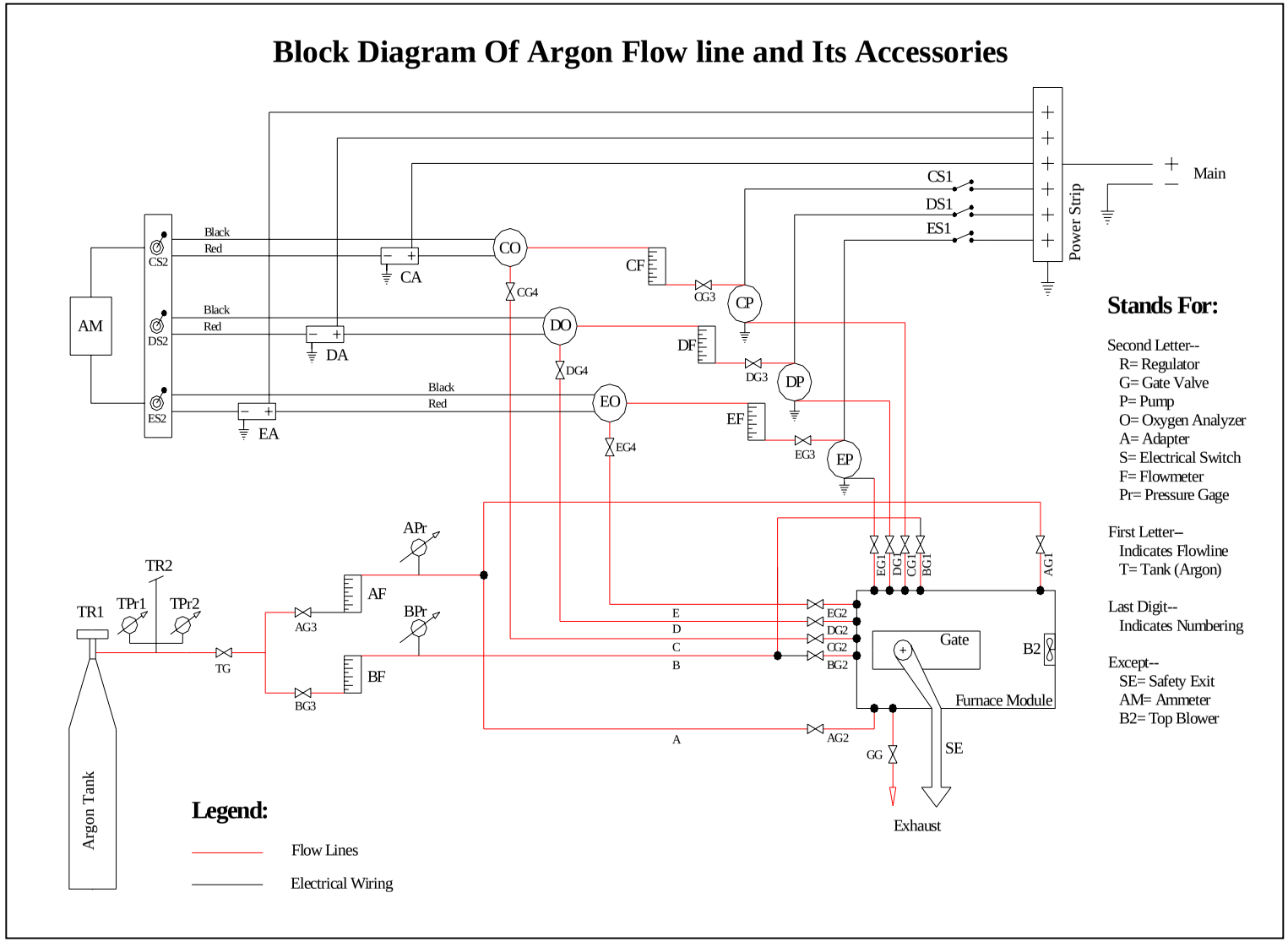

Figure 2.15: Location of the Thermocouples and the Pulley System

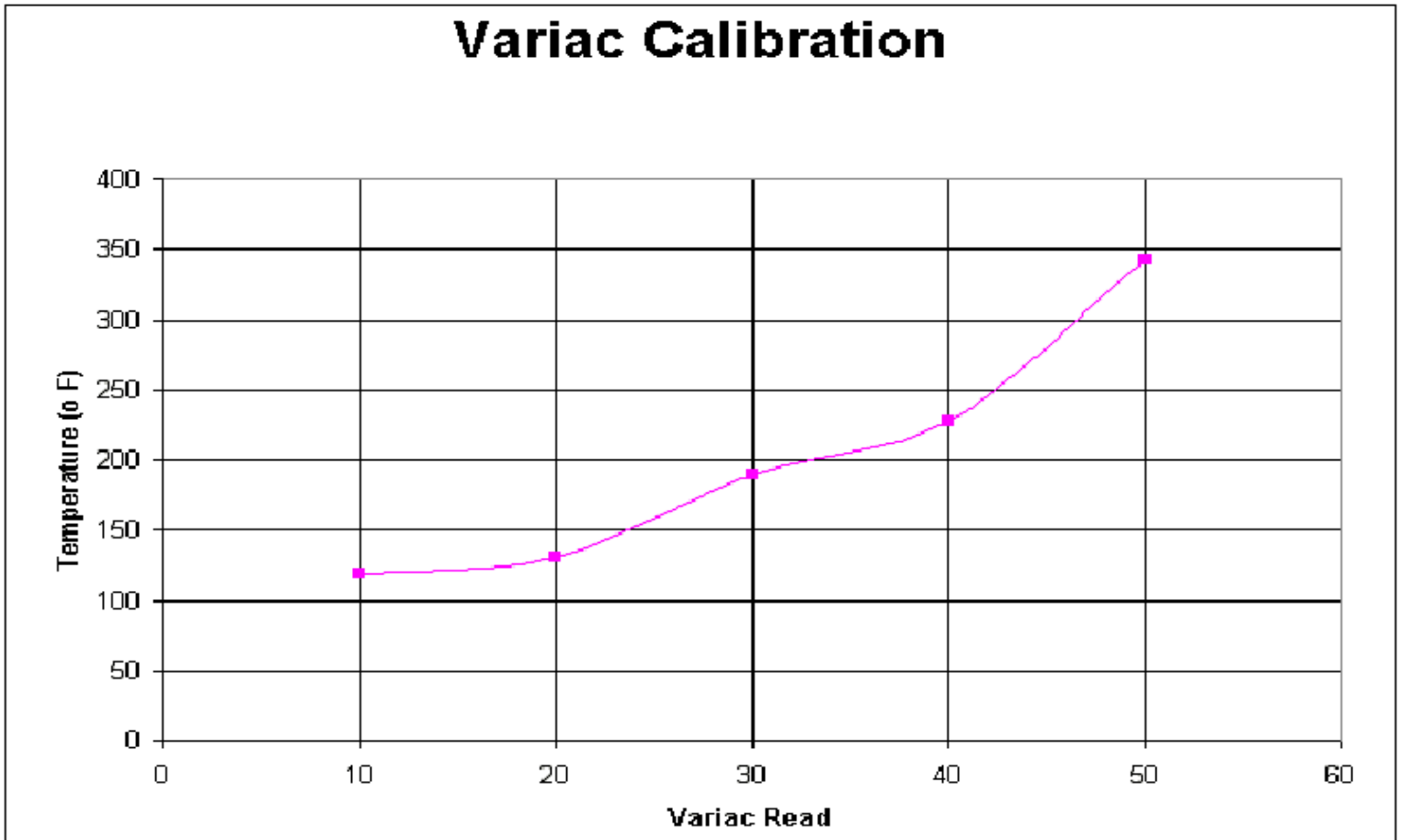

Read	10	20	30	40	50
o F	119.00	131.00	189.10	227.20	342.00

Figure 2.16: Calibration curve for the retort temperature.

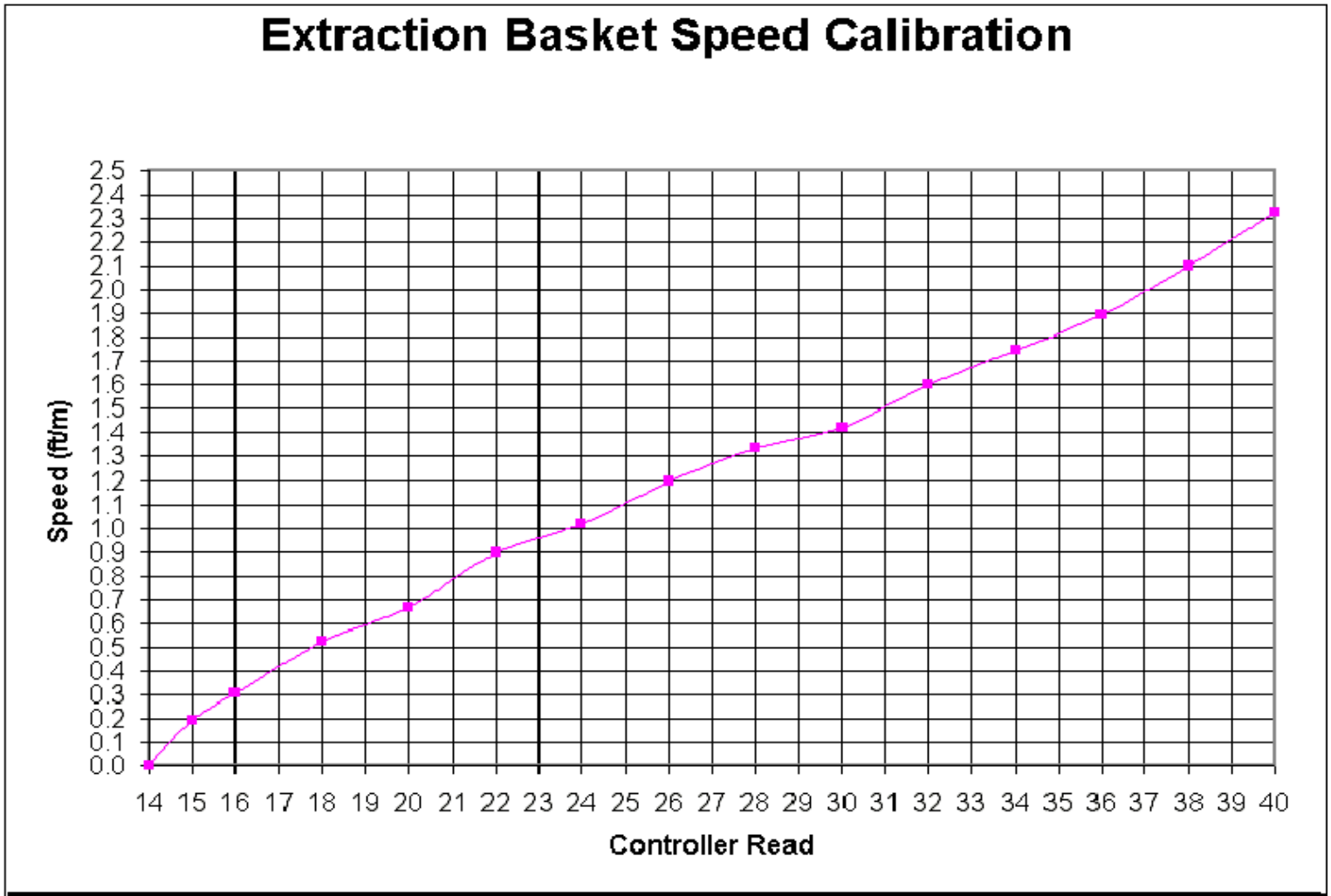

Read	14	15	16	18	20	22	24	26	28	30	32	34	36	38	40
ft/m	0.00	0.19	0.31	0.53	0.66	0.90	1.02	1.19	1.33	1.42	1.60	1.75	1.90	2.10	2.33

Figure 2.17: Calibration curve for the basket insertion and withdrawal.

Entering the Main Menu (cont.)

1. Press and hold down the ▽ key until ☼ 3 comes ON.
2. Press the MODE/SET key and ☼ 2 comes ON.
3. Press the ▽ key and ☼ 1 starts blinking. This indicates that you have entered the *Main Menu*.

Note: *The O2X1 operates on a 4-20 mA loop current, which varies as the LEDs turn ON and OFF. Therefore, do not take any measurements while in the* User Program.

Exiting the Menus

To exit and save changes:

From the *Main Menu*, press and hold down both the MODE/SET and ▽ keys until all three LEDs flash simultaneously. This indicates that any changes are being saved. All LEDs then turn OFF.

Note: *If any LEDs are blinking, this means you are in the* Main Menu.

To exit without saving changes:

Disconnect the power to the O2X1 for at least five seconds, or stop pressing keys. The O2X1 resumes normal operation if no keys are pressed within 60 seconds.

Programming and Calibrating the O2X1

Upon startup, a five-step adjustment and calibration procedure must be performed on the O2X1:

1. Select the desired measurement range.
2. Trim the low (4 mA) and high (20 mA) outputs.
3. For the initial installation, calibrate the unit with air for either a ppm or % sensor.
4. For ppm sensors only, purge the sensor with a low ppm oxygen gas.
5. For all subsequent calibrations, use an appropriate span gas for the sensor and range selected.

The above tasks must be performed from the *Main Menu*. See Figure 7, *O2X1 Menu Map*, by folding out the inside back cover of this guide.

Selecting the Range

1. At the *Main Menu*, with ☼ 1 blinking, press the △ key to display the current range. See Table 1 below to determine the current range from the status of the LEDs.

Table 1: LED Range Codes

☼ 1	☼ 2	☼ 3	Range
OFF	ON	ON	0-10 ppm
ON	OFF	OFF	0-100 ppm
OFF	ON	OFF	0-1,000 ppm
OFF	OFF	ON	0-10,000 ppm
ON	ON	OFF	0-10%
ON	ON	ON	0-25%

2. To select the desired range, press the △ or ▽ key to scroll through the available options until the desired range is displayed.
3. When done, press the MODE/SET key. The blinking of ☼ 1 indicates that you have returned to the *Main Menu*.

Trimming the Output

To trim the analog output, calibrate the low (4 mA) end of the output then the high (20 mA) end.

Note: *The low and high adjustments interact with each other. Therefore, recheck the calibration after the procedure has been completed.*

Preparing to Trim the Output

In preparation for trimming the analog output, complete the following steps:

1. Connect an ammeter in series with the power supply, to monitor the analog output.
2. Enter the *Main Menu* as described in *Entering the Main Menu* on page 5. (Refer to the menu map in Figure 7 inside the back cover foldout.)
3. Press the MODE/SET key repeatedly until ☼ 2 blinks. This is the beginning of the *Output Trim* submenu.

Proceed to the next section on page 8.

Figure 2.18: Oxygen Analyzer manual pages 6 and 7.


a


c


b

Figure 2.19: (a) Experimental set up without Argon Reservoir, (b) Accessories- Motor-Pulley, Motor Controller, Air Sampling Pump, Oxygen Analyzer, Flow Meters, Digital Multi-Meter and (c) Shows basket Withdrawal, gate, anemometer.

Chapter 3 : Computational Investigation

As mentioned in Introduction section, the computational study was performed for cases with and without the AR. The computational model was broken-up into calculations performed using FLUENT and using FIDAP, both of which are commercially available software.

Withdrawal and insertion was modeled using the moving body constraint capability of FIDAP. This capability is used to model a moving solid through a continuum of a fluid. The methodology used by FIDAP consists of applying and removing constraints to nodes as a function of time and position. The constraints may be applied to, velocity vector, temperature and species concentration. A user-supplied FORTRAN sub-routine is used to specify the location of the nodes in the region of the extraction-basket as a function of time and assign the values of the constraints. The position of the nodes at any time is determined from the withdrawal or insertion velocity of the basket. The velocity vector of the nodes located in the region of the basket is set to that of the withdrawal or insertion velocity. Temperatures and species concentrations are set to the required values. Because the basket is moving, the moving body constraints are applied

to different nodes at different times. For all the computational studies, 2-D studies, 3-D studies and study of the reservoir filling process, the following steps were followed:

- Mesh Generation
- Input Proper Boundary Conditions
- Parametric Numerical Simulations
- Verification of Grid Independence of the Numerical Calculations
- Compilations of results:
    - Plot species concentration (Oxygen, and Argon) in the Computational Domain
    - Plot of Velocity Vectors in the Computational Domain
    - Plot temperature contours in the Computational Domain (only for thermal cases)

Figure 3.1 shows the mesh used for 2-D computational simulations for the case without the reservoir. The HVAC air-flow is simulated with a 2-D plenum created over the furnace module. Air at a uniform velocity is allowed to flow from one side as shown in the figure, and the top boundary of the plenum is not a solid wall. Make-up argon is allowed to enter through two openings as shown in this figure. After performing grid independence studies a total of 5,500 cells were used for this study. The 2-D computations were performed using FIDAP.

Figure 3.2 shows the mesh used for 2-D computational simulations for the case with the reservoir. The HVAC air-flow in this case is simulated with a 2-D plenum created over the neck of the furnace module. The actual argon reservoir is not modeled in this case, instead a uniform make-up argon velocity is assigned to the inner wall of the reservoir. Make-up argon is allowed to enter through two openings as shown in this figure. Based on grid independence studies a total of 5,234 cells

were used for this study. It can also be mentioned that the 2-D computations were performed using FIDAP. For simulating numerical calculations for the model, similar meshes were used except the number of grid points used were 15,024 for both cases.

Figures 3.3 and 3.4 show the computational 3-D mesh used for numerical studies, the first figure shows the mesh without the reservoir and the second one shows mesh for cases with the argon reservoir. The number of grids used without the reservoir was 55,482 and with the reservoir it was 34,185. FIDAP was used for 3-D simulations.

Figure 3.5 shows the computational domain and grids used to simulate the argon filling process. FLUENT was used to simulate these results.

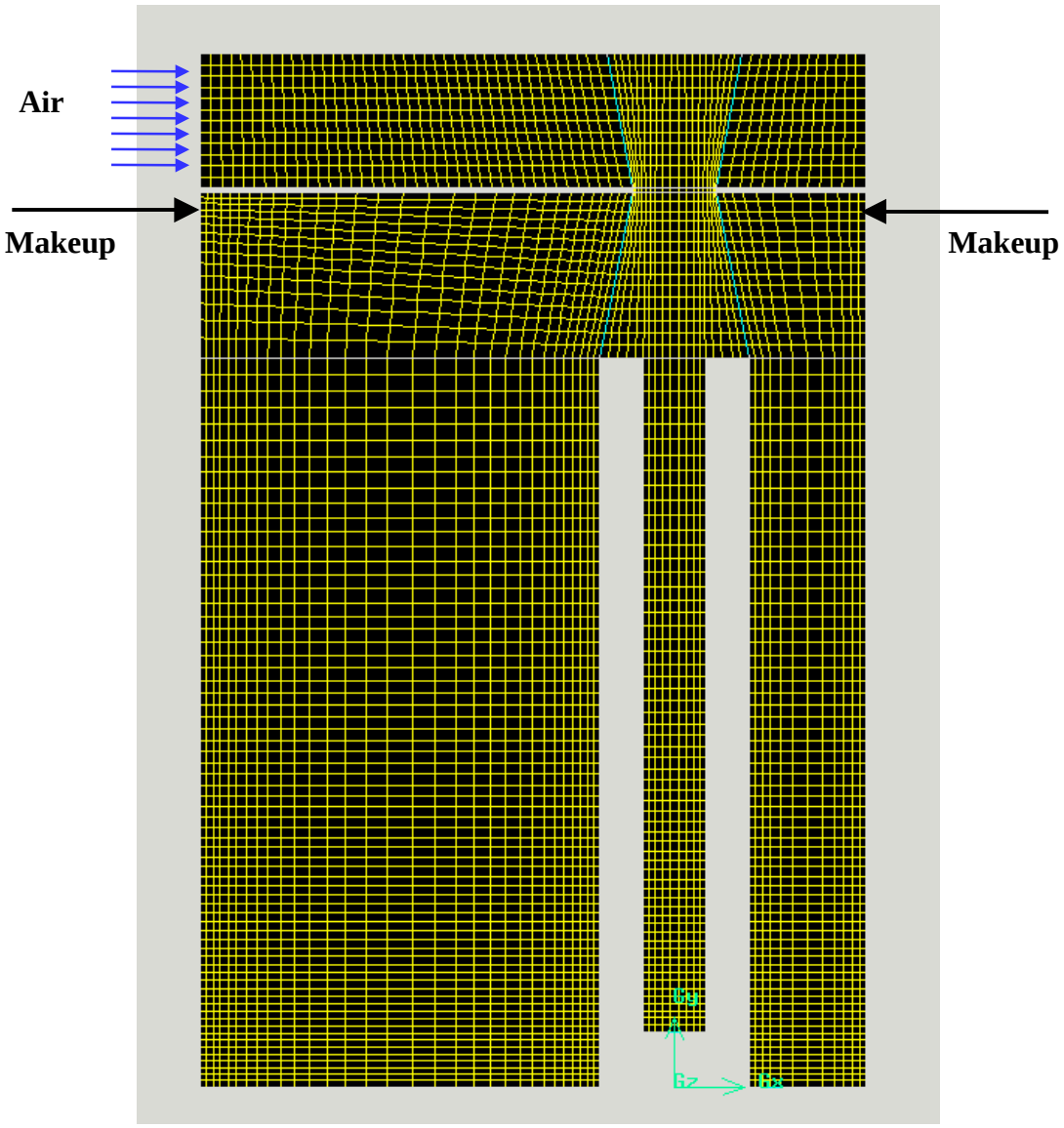

Figure 3.1: Mesh for 2-D computations (without reservoir).

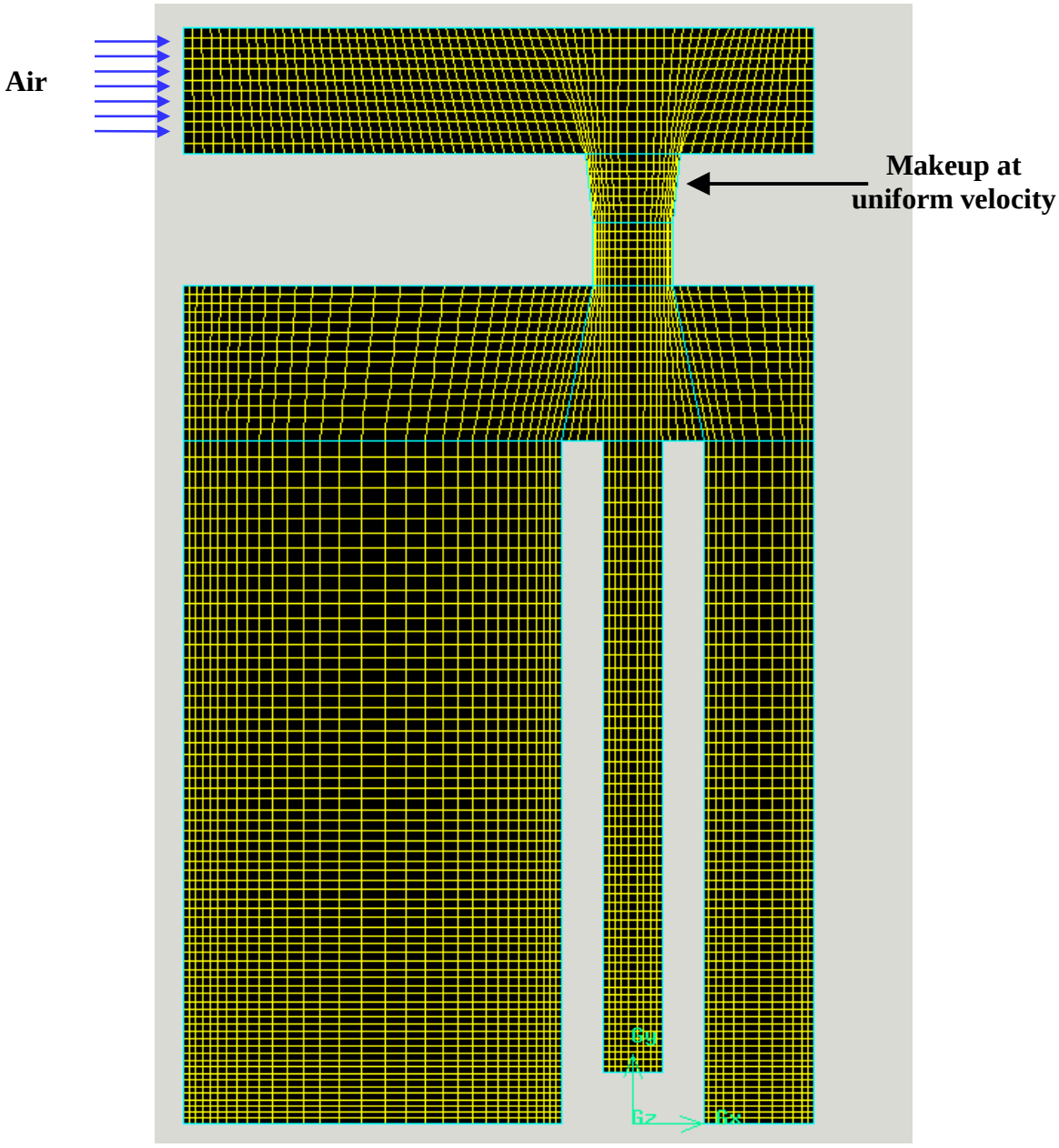

Figure 3.2: Mesh for 2-D computations (with reservoir).

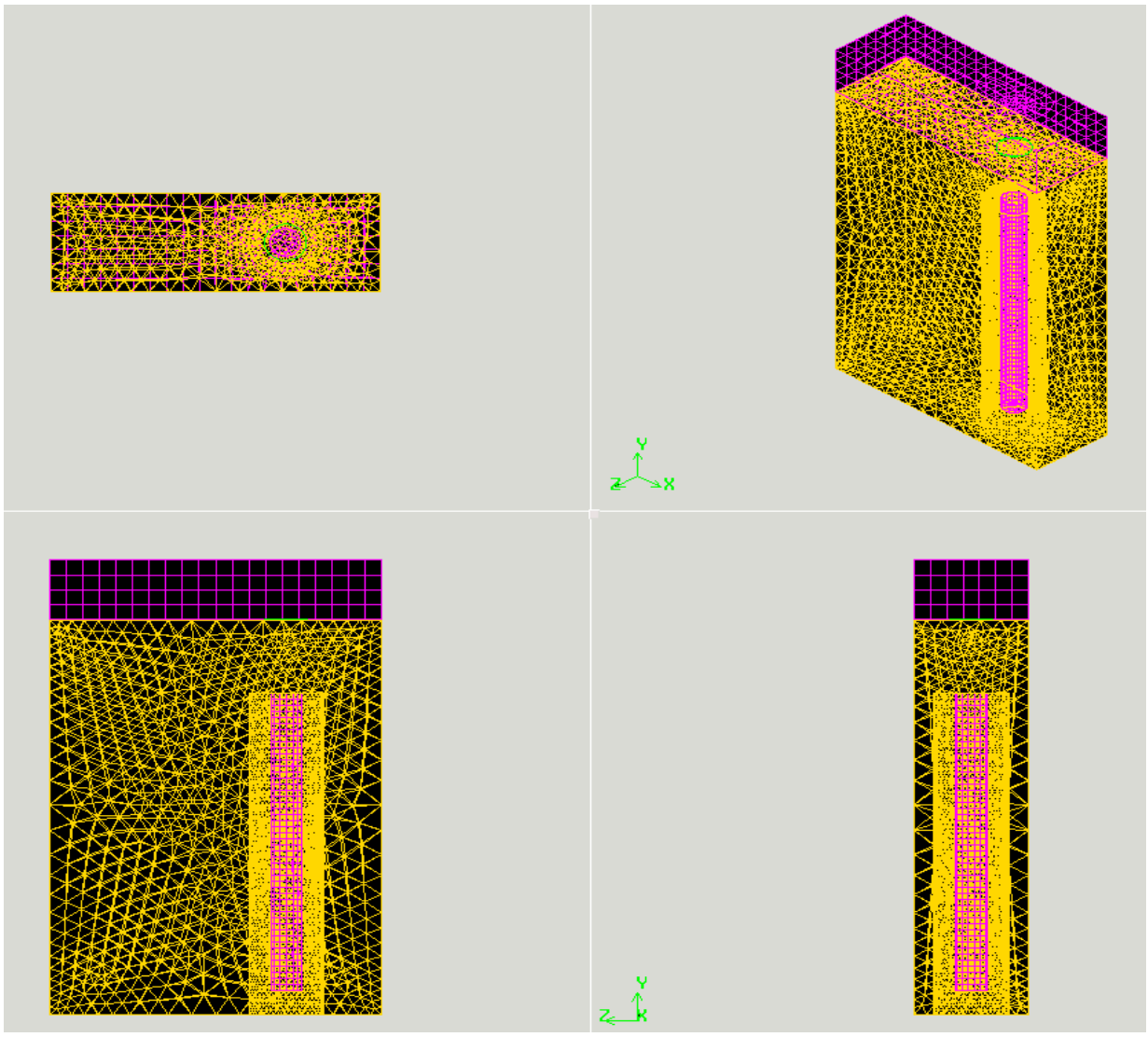

Figure 3.3: Mesh for 3-D computations without the argon reservoir.

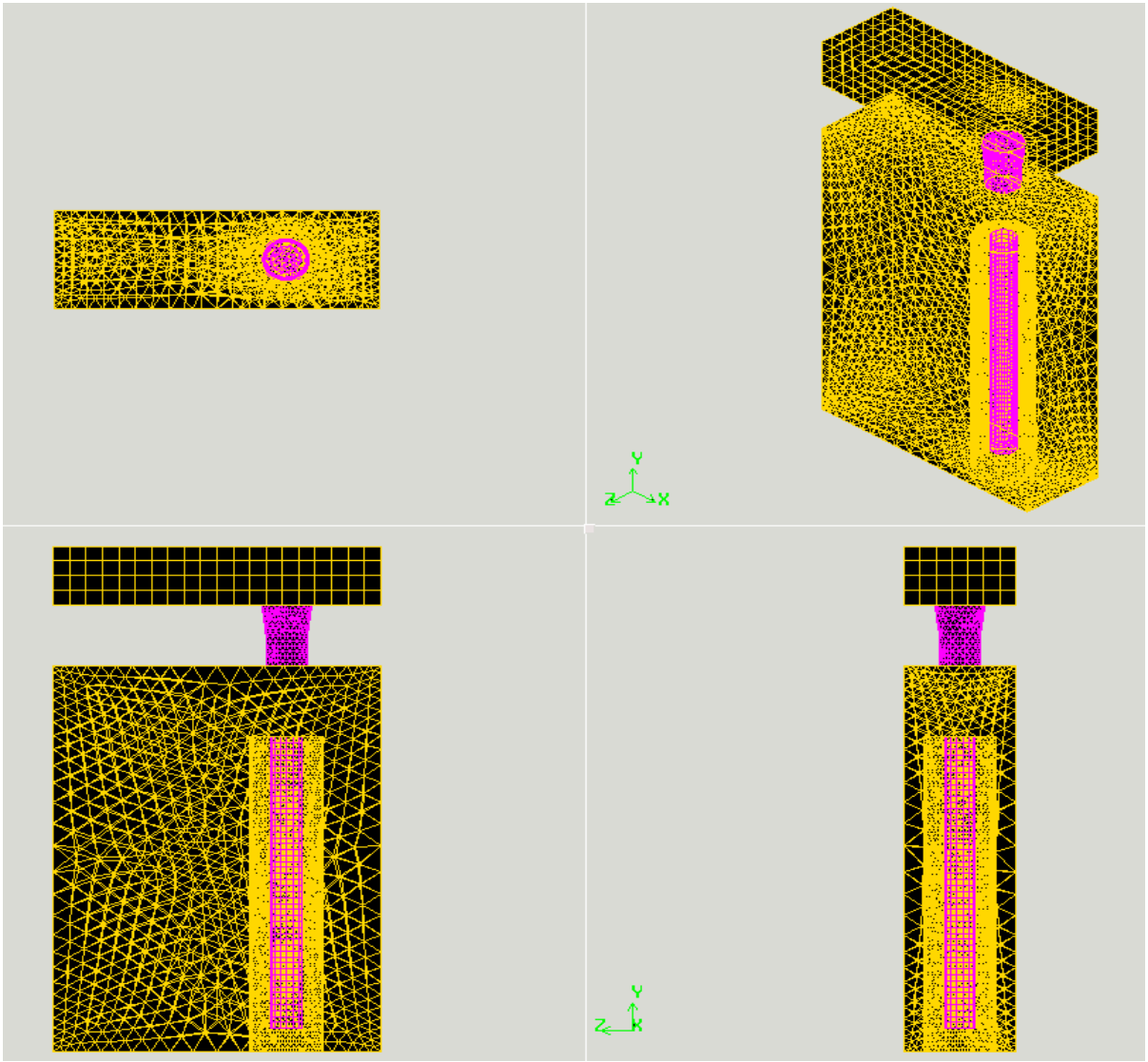

Figure 3.4: Mesh for 3-D computation with the argon reservoir.

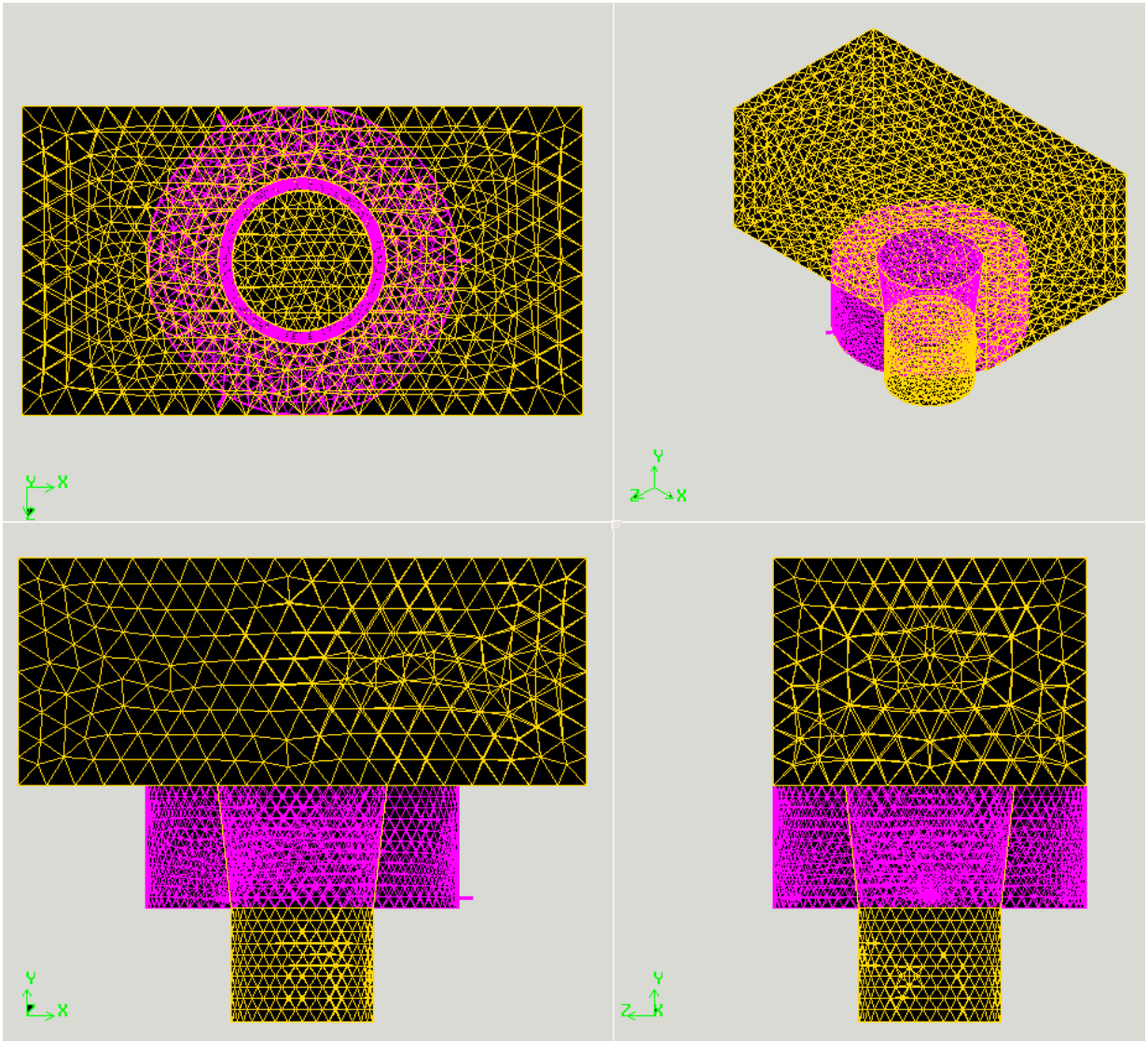

Figure 3.5: 3-D Computational mesh used for filling of the reservoir.

Chapter 4 : Results & Discussions

The results of the study are presented in two sections, first the results of the experimental investigation and then the results of the numerical calculations.

4.1 Experimental Results

The test matrix, i.e., the operating parameters at which the tests are performed is presented in Table 2.3. In the experimental matrix table, the HVAC column represents the velocity of the HVAC air, the column “model” represents the values of the parameter actually used in the model experiment, and “production” represents the corresponding value of the same variable for the production furnace/module. Isothermal experiments represent experiments performed at room temperature. The values “yes” represent the experiments that were performed. For each of the experiments, initial and final concentrations of argon, temperatures and flow conditions were measured. The range of withdrawal and insertion speed (crane speed) varied from 0.5 ft/min to 2.8 ft/min which correspond to production crane speeds of 2.5 ft/min to 15 ft/min. The maximum production-crane speed is approximately 15 ft/min.

Table 4.1 provides a summary of the experimental results, this table presents the average ingress of oxygen during each of the experiments performed. The data presented is the difference between final mixed and the initial concentrations of the

oxygen in the experimental furnace module. The rows shown in color are for the cases where the volume flow rate of make-up argon is equal to the volumetric withdrawal rate of the basket (these cases are referred to as nominal cases in this report). One can observe from the data that, compared to the nominal case, there is significantly more ingress of oxygen/air when there is no make-up argon. For example, 155% more oxygen/air infiltrates the chamber with no make-up argon compared to the nominal make-up case with 2.5 ft/min (production) withdrawal rate (0.2794 vs. 0.1800), the same is 304% more for 14 ft/min withdrawal rate (0.0362 vs. 0.01102). It is also observed from the table that when there is no HVAC air flow the ingress of oxygen/air is less than the case HVAC air flow. This difference is 133% when the withdrawal rate is 2.5 ft/min (0.1356 vs. 0.1800), and is 134% when the withdrawal rate is 14 ft/min (0.0271 vs. 0.0362).

Another observation from the results is that air ingress is less for faster withdrawal rates. This is intuitive, because the duration for which the sliding gate remains open is inversely proportional to the withdrawal rate. When the gate is open for a shorter time there is less ingress of air due to lower diffusive and convective transport.

For the isothermal case, with no make-up argon, the maximum ingress of oxygen was 0.28% which is equal to about 1.33% ingress of air (factor of 4.76). These values were well within the design requirements of 3% oxygen. For the cases that were repeated, it was observed that the ingress in both cases was within the limits of experimental uncertainty. Small differences between the two can be attributed to the experimental uncertainty in controlling the make-up argon flow rate. This flow rate was very low, and fluctuated by as much as 50%.

Results from the thermal cases showed a larger ingress; in some cases the ingress was larger than allowed in the design criteria. For the □T case where the furnace module gas temperature was 50^{o}F above the room temperature, the infiltration oxygen/air was the greatest. With a basket speed of 2.5 ft/min (production) with 2.5 cfm (production) make-up argon flow rate approximately 14.35% air (3.0137% O_2) was observed, for the same conditions for insertion of the basket, the air addition was about 11.1% (2.3137% O_2).

For the case when the retort is at 150^{o}F with the withdrawal rate of 2.5 ft/min (production) with HVAC air at 10ft/min and with 2.08 cfm make-up argon, the air added was about 4.78% (1.0042% O_2) Although for the same retort temperature if the withdrawal rate is 14 ft/min the infiltration of air is about 0.68% (0.1421% O_2).

Figure 4.1.1 shows comparative studies for various cases at three different withdrawal rates, 0.5 ft/min, 1 ft/min and 2.8 ft/min (corresponding production crane speeds of 2.5 ft/min, 5ft/min and 14 ft/min) with nominal make-up flow rates of argon. These are the same results as presented in Table 4.1. It is clear, that the experiments that are repeated yielded similar results, showing confidence in repeatability of the experiments. Also, it is seen that with argon reservoir the ingress of air is lower. Higher crane speed always resulted in lower ingress of oxygen/air. Also, apparent from this figure is the fact that for cases with longer period of opened gate (delay-cases), the ingress of oxygen is larger. The argon reservoir allowed lower ingress.

Figure 4.1.3 is a compilation of results for ingress of air/oxygen without the HVAC air flow rate. Compared with the data in Figure 4.1.1 it can be seen that with no-HVAC air the ingress is lower. Again as expected, as the crane speed increases the total ingress volume decreases. This figure also shows the results the results of three cases for

which the experiments were repeated. These show very good repeatability of the experimental results.

Figure 4.1.3 presents the results for insertion of the basket with nominal make-up argon. For these cases the insertion of the extraction basket always allows lower air-ingress. Figure 4.1.2 and 4.1.3 have similar trends in that the thermal case predicts high ingress of air and the argon reservoir allows the least amount of ingress. For all isothermal cases the ingress is within design limits with no-reservoir. Insertion with (△T cases) the furnace module gas temperature 50^{o}F above the room temperature is shown in Figure 4.1.4.

The thermal cases (hot retort or hot furnace module gas) produced undesirable results during the withdrawal of the basket. These results are shown in Figures 4.1.1 and 4.1.4. Figure 4.1.4 shows the □T cases where the furnace module gas temperature was 50^{o}F above room temperature. The withdrawal of the basket allowed the maximum ingress, whereas, the insertion allowed lower ingress, but this was still above the allowed design criteria.

Figure 4.1.5 shows the ingress of oxygen during withdrawal and insertion for isothermal cases with no argon reservoir as a function of make-up argon flow rate. All the cases are for basket speed of 0.5 ft/min (2.5 ft/min production), for which the nominal make-up rate is 1.00 cfh (2.1 cfm production). The blue bars in the figure represent withdrawal with HVAC air, the yellow bars are insertion with HVAC and the maroon bar withdrawal with no HVAC air. From the results the following points can be observed: that with increasing make-up rate the ingress is lower, during insertion of the basket the ingress of air/oxygen is lower than withdrawal for the same conditions, and that with no HVAC air flow the ingress is lower.

Figures 4.1.6 and 4.1.7 show ingress of oxygen during withdrawal and insertion of the basket for isothermal cases with no argon reservoir, as functions of make-up argon flow rates. The basket speeds are of 1.0 ft/min (5 ft/min production) and 2.8 ft/min (14 ft/min production), for which the nominal make-up rates are 2.00 cfh (4.2 cfm production) and 5.6 cfh (11.65 cfm production) respectively. The blue bars in the figures represent withdrawal with HVAC air, the yellow bars are insertion with HVAC and the maroon bar withdrawal with no HVAC air. Again the same conclusions as in figure 4.1.4 can be drawn.

Figure 4.1.8 shows the effect of basket speed during withdrawal at different make-up rates. This figure includes the cases with HVAC air flow. Two clear observations can be made, they are that with increasing basket speeds the duration for which the furnace module is open results in lower ingress; and with increased make-up argon flow rate lowers the ingress. Figure 4.1.9 is similar to figure 4.1.8 except it is for withdrawal with no HVAC air flow. Figure 4.1.10 shows the ingress during insertion of the basket with HVAC air flow. Again, the conclusions are similar to that discussed for Figure 4.1.8.

Table 4.1: Summary of experimental results showing the ingress of % of Oxygen.

Basket Movement	HVAC (ft/m)	Basket speed (ft/m)		Makeup Rate		Test at Room Temp. (Isothermal)	Delay (5 mins)	Thermal (Retort Temp 167 to 176 F)	With Reservoir	Temp Diff (Module gas 50 F above Room Temp)	Repeat of Isothermal
		Model	Production	Model (cfh)	Production (cfm)						
Withdrawal	10	0.50	2.50	0.00	0.00	0.2794					
				0.75	1.56	0.2379					
				1.00	2.08	0.1800	0.3677	1.0042 (167)	0.0298	3.0137 (46)	0.1396
				2.00	4.16	0.1646					
		1.00	5.00	0.00	0.00	0.1777					
				1.00	2.08	0.1600					
				2.00	4.16	0.1198	0.2900	0.7394 (176)	0.0138		0.1146
				4.00	8.32	0.0867					
		2.80	14.00	0.00	0.00	0.1102					
				5.60	11.65	0.0362	0.2096	0.1421 (171)	0.0037		0.0258
				9.00	18.72	0.0210					
With-drawal	No	0.50	2.50	1.00	2.08	0.1356					
		1.00	5.00	2.00	4.16	0.0785		0.2711 (175)			0.0735
		2.80	14.00	5.60	11.65	0.0271					
Insertion	10	0.50	2.50	0.00	0.00	0.1115					
				1.00	2.08	0.0892			0.0027	2.3173 (50)	0.0758
		1.00	5.00	0.00	0.00	0.0506					
				2.00	4.16	0.0198			0.0004		0.0252
		2.80	14.00	0.00	0.00	0.0148					
				5.60	11.65	0.0054			0.0000		0.0037

Note:
1. In the following three pages Figure 4.1.1 to Figure 4.1.3 color of the Titles of the plots correspond the color of the Data of this table-4.1.
2. Black data is not the nominal cases (volume displacement rate of the basket is equal to make up flow rate)
3. All the tests except those at column 10 “with Reservoir” were done without reservoir.
4. Tests ‘Delay’ is explained at Page-25 in D.5.

Nominal Cases Percent Increase of Oxygen for Different Test Variables (Withdrawal and HVAC on)

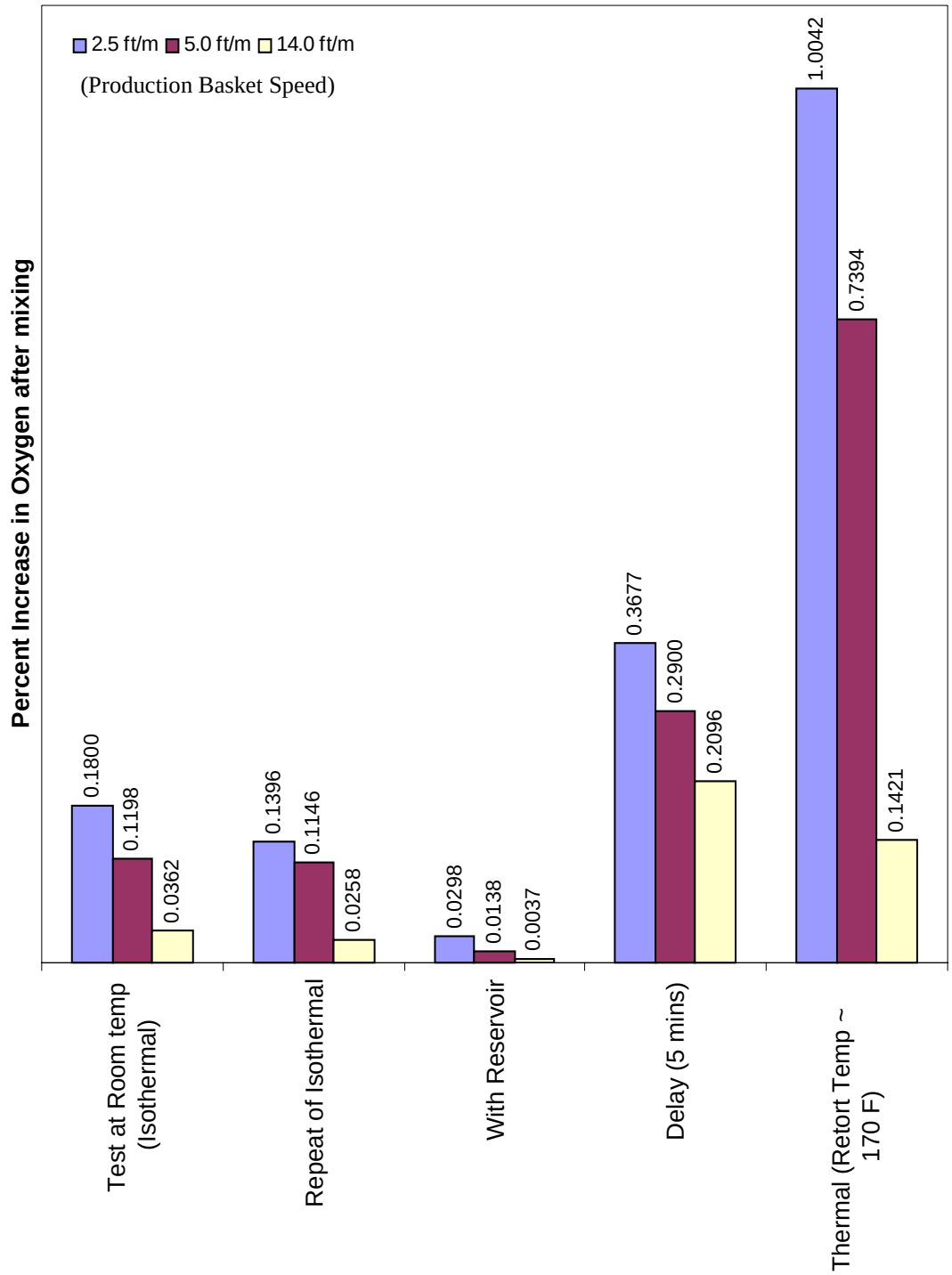

Figure 4.1.1: Oxygen ingress at three different withdrawal speeds with nominal argon make-up.

Nominal Cases Percent Increase of Oxygen for Different Test Variables (Withdrawal and HVAC Off)

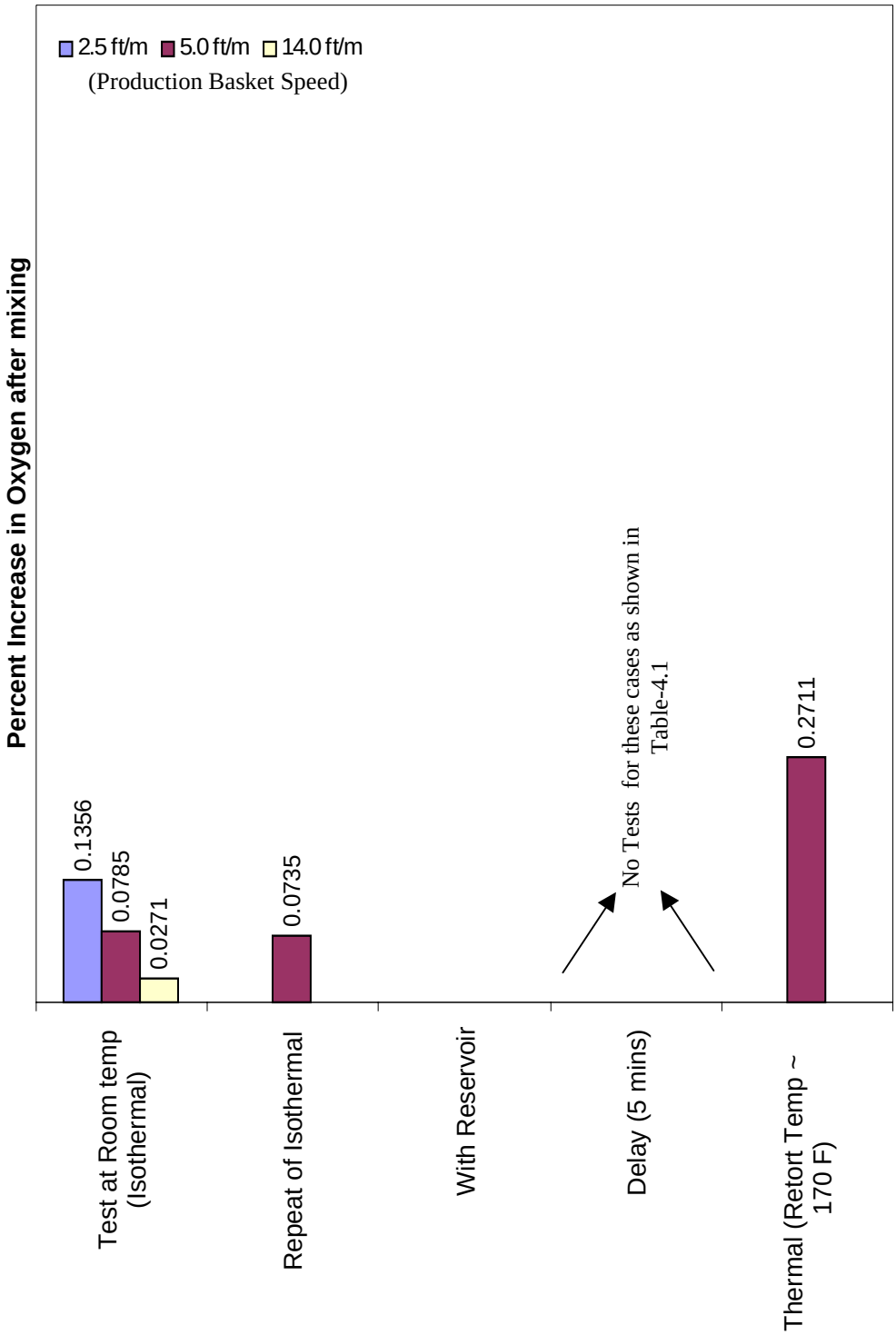

Figure 4.1.2: Compilation of results without the HVAC air flow.

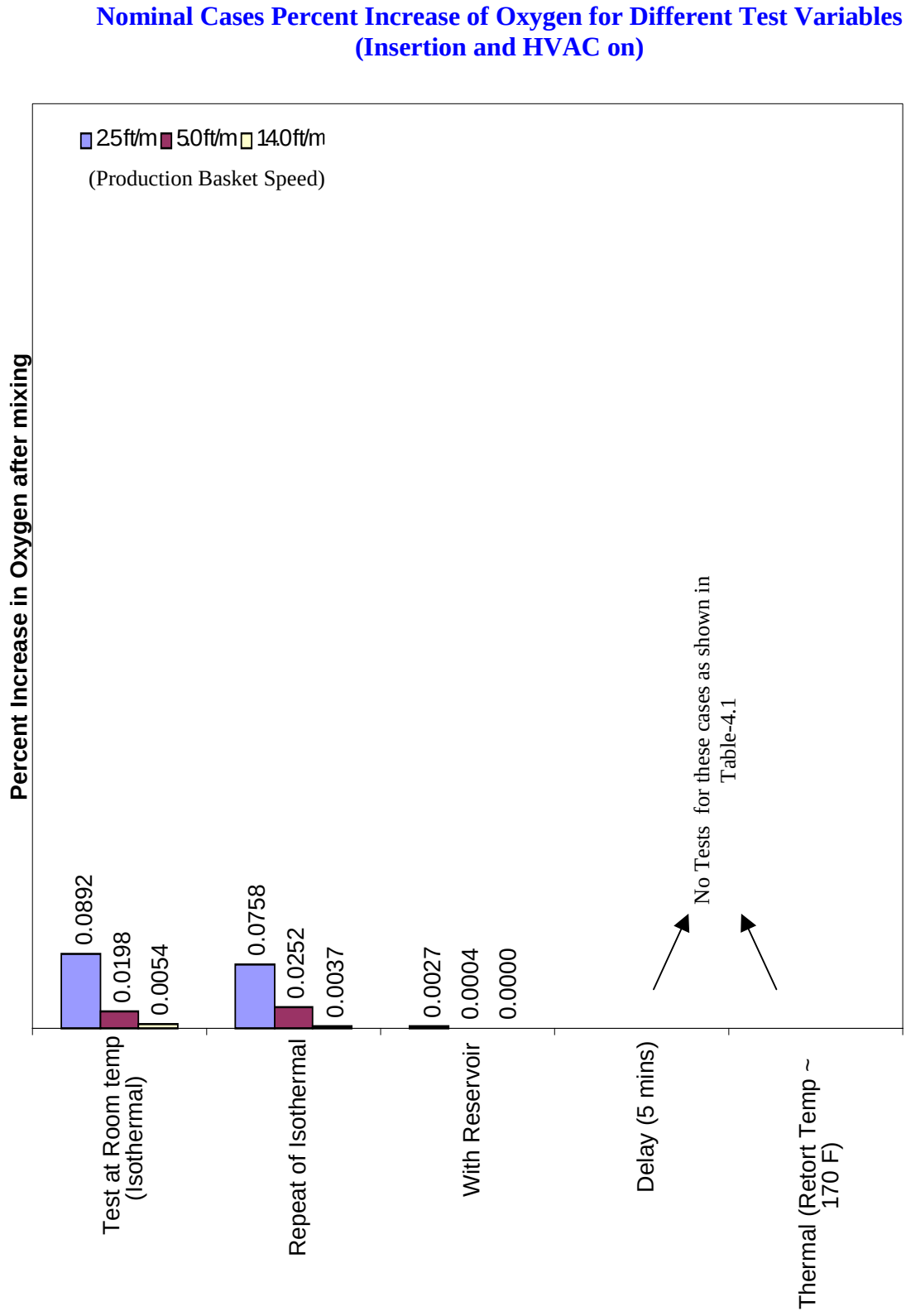

Figure 4.1.3: Figure shows the ingress of air with nominal make-up argon during insertion of the basket.

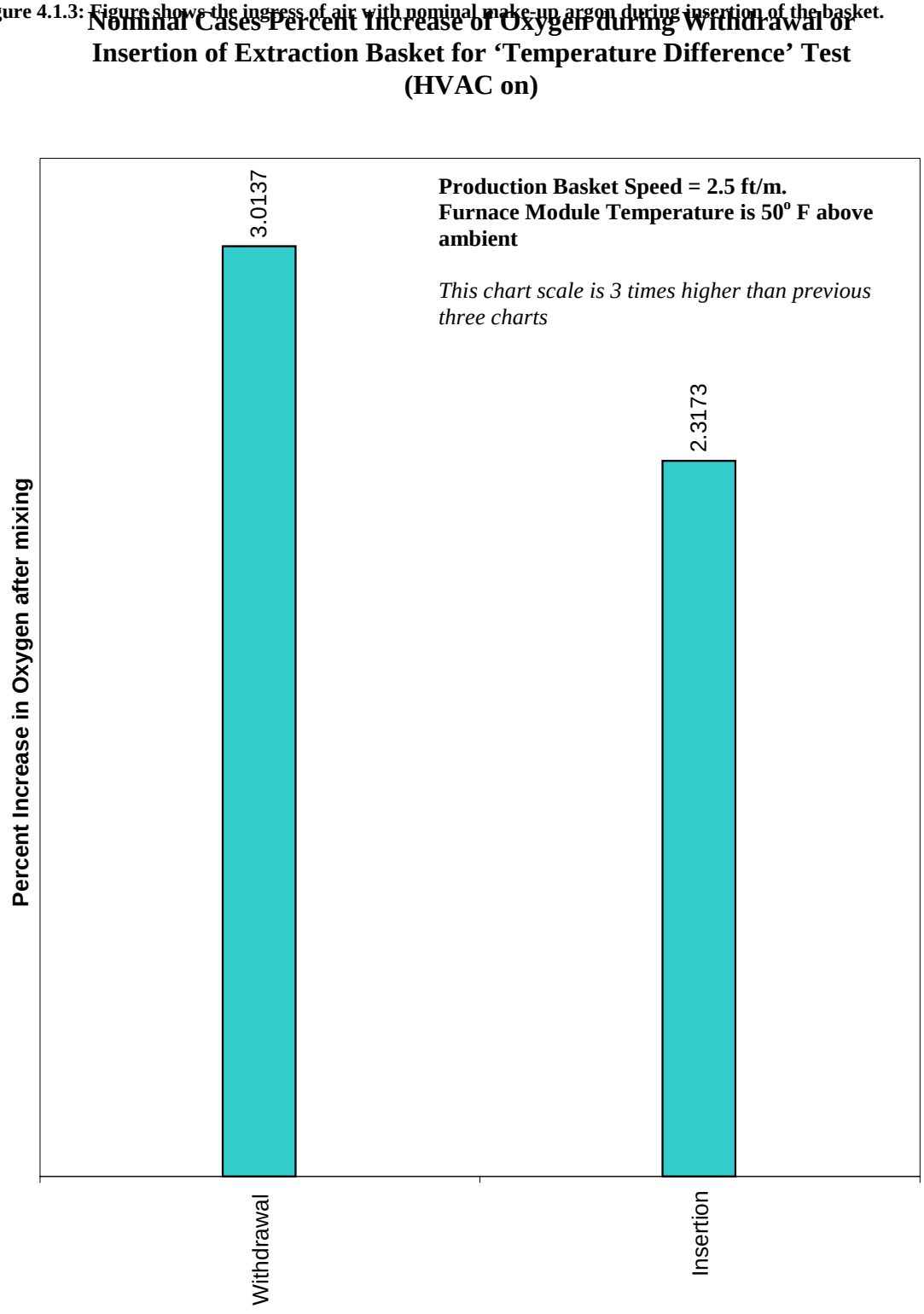

Figure 4.1.4: Figure shows the ingress of air with nominal make-up argon for Temperature Diff. Case.

Nominal Cases Percent Increase of Oxygen at 2.5 ft/min Production Basket Speed for different Argon makeup rate

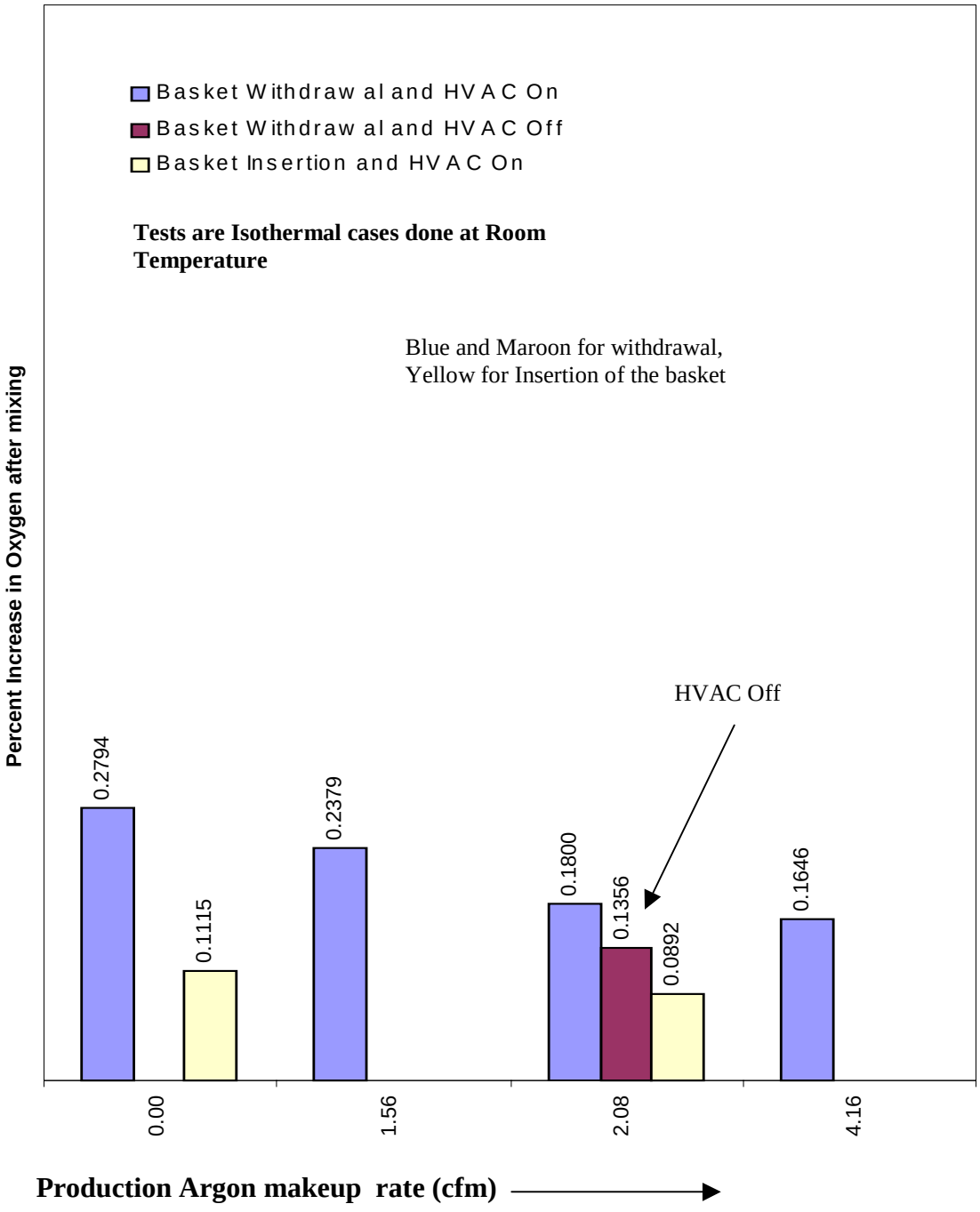

Figure 4.1.5: Ingress of oxygen as a function of Argon make-up rate for insertion and withdrawal of the basket at 0.5 ft/min (Production 2.5 ft/min & no-argon reservoir).

Nominal Cases Percent Increase of Oxygen at 5.0 ft/min Production Basket Speed for different Argon makeup rate

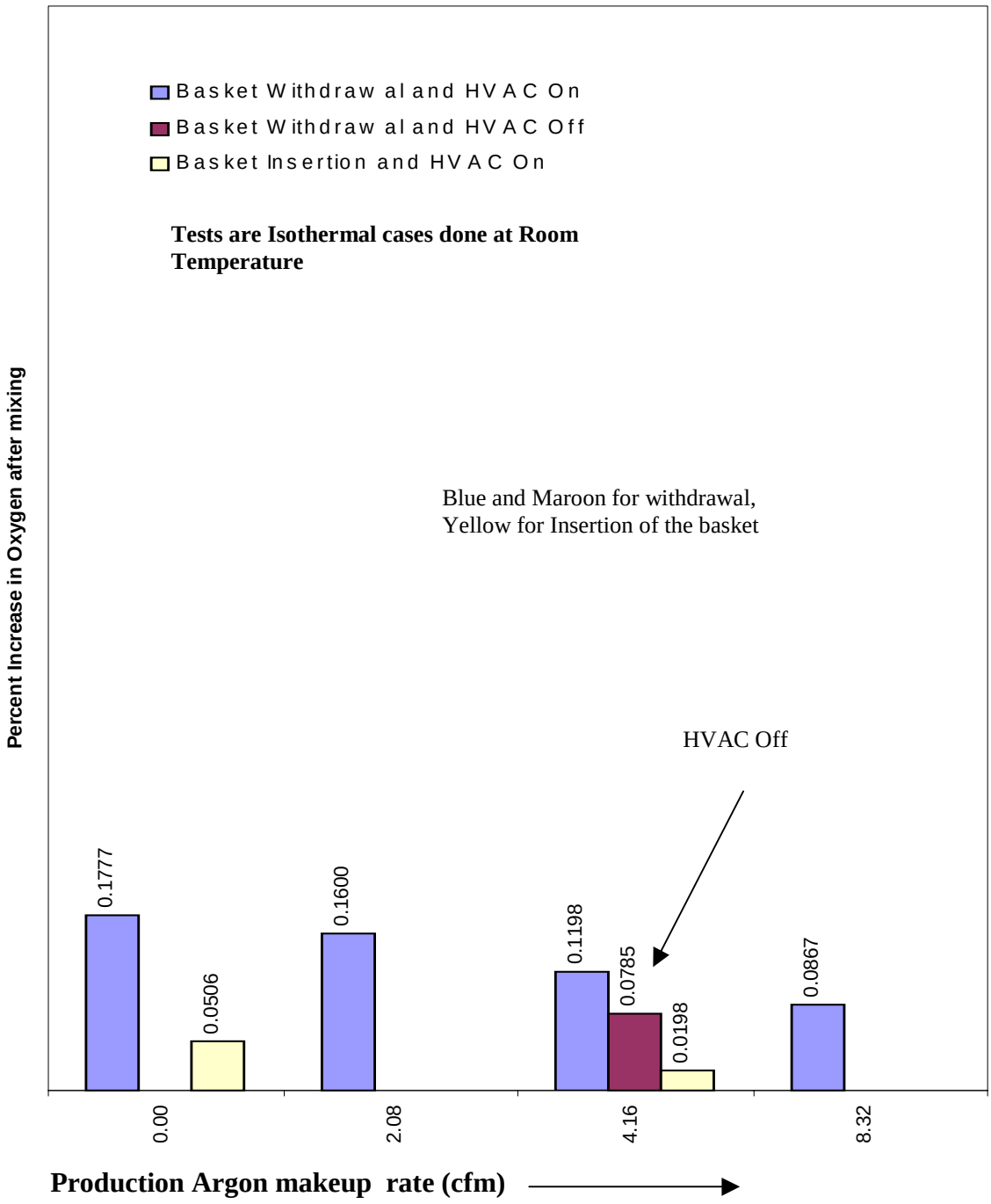

Figure 4.1.6: Ingress of oxygen as a function of Argon make-up rate for insertion and withdrawal of the basket at 1 ft/min (Production 5 ft/min & no-argon reservoir).

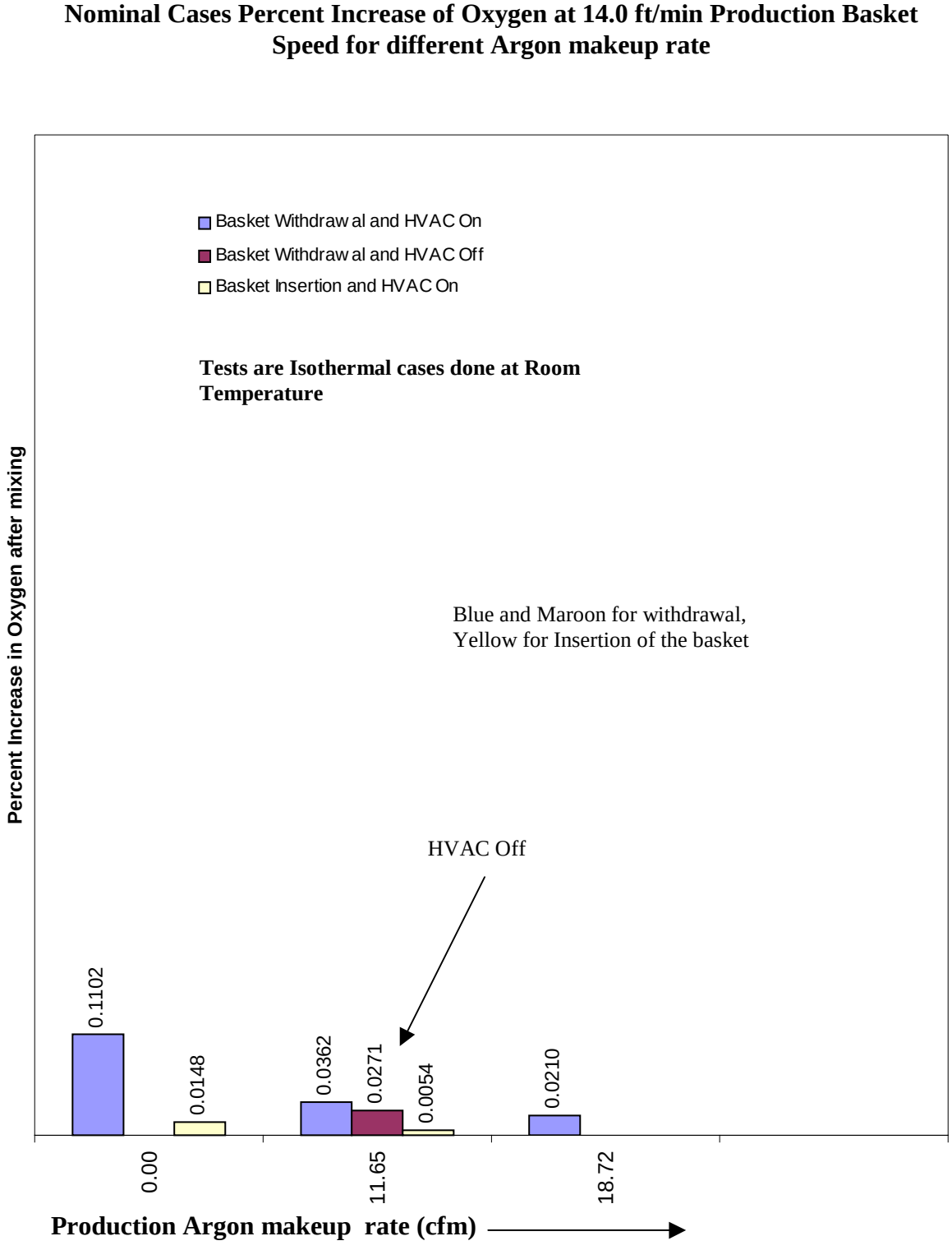

Figure 4.1.7: Ingress of oxygen as a function of Argon make-up rate for insertion and withdrawal of the basket at 2.8 ft/min (Production 14ft/min & no-argon reservoir).

Nominal Cases Percent Increase of Oxygen for different extraction basket speed (Withdrawal of the basket and HVAC On)

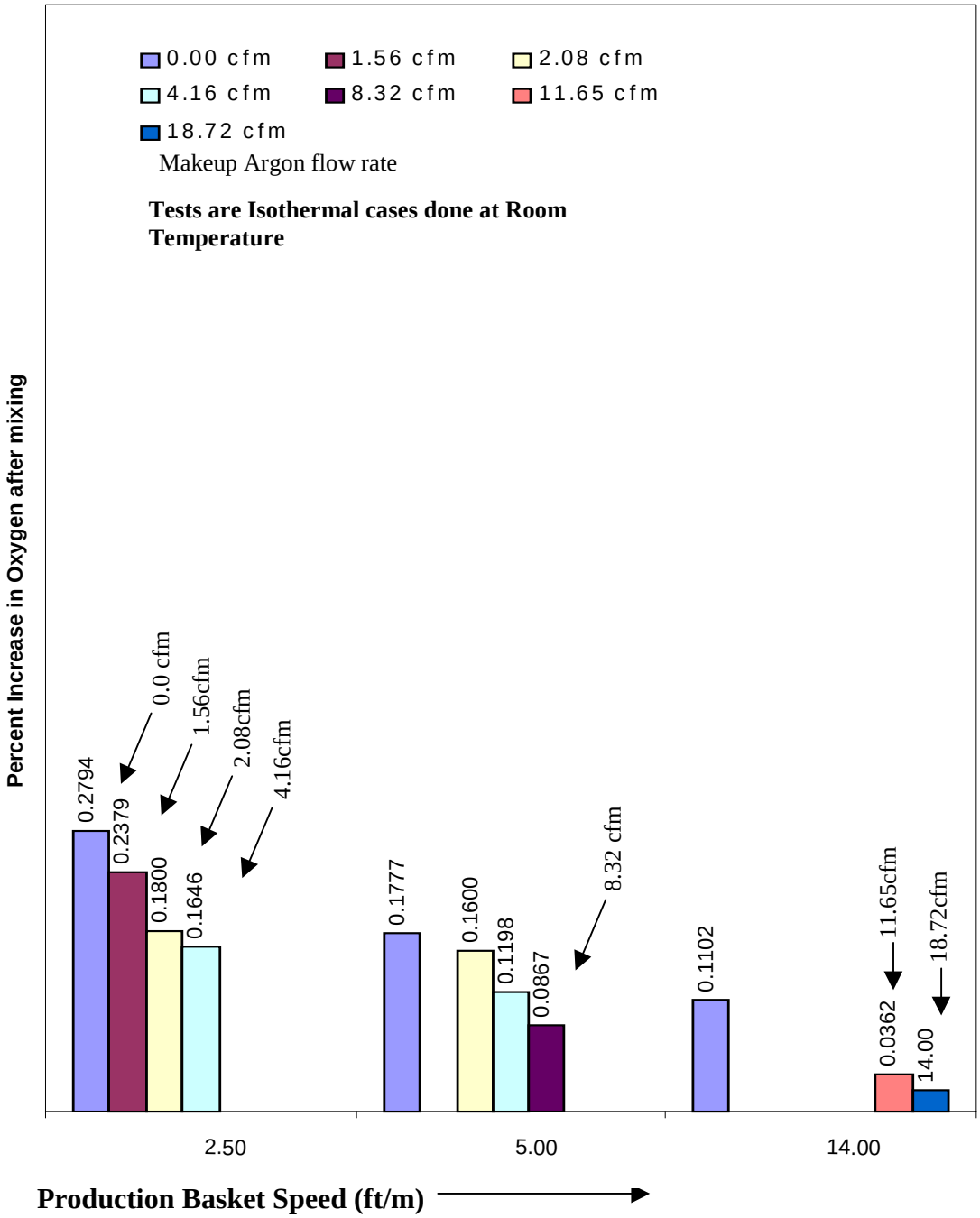

Figure 4.1.8: Effect of three different basket speeds (withdrawal) with different make-up rates with HVAC air flow.

Nominal Cases Percent Increase of Oxygen for different extraction basket speed (Withdrawal of the basket and HVAC Off)

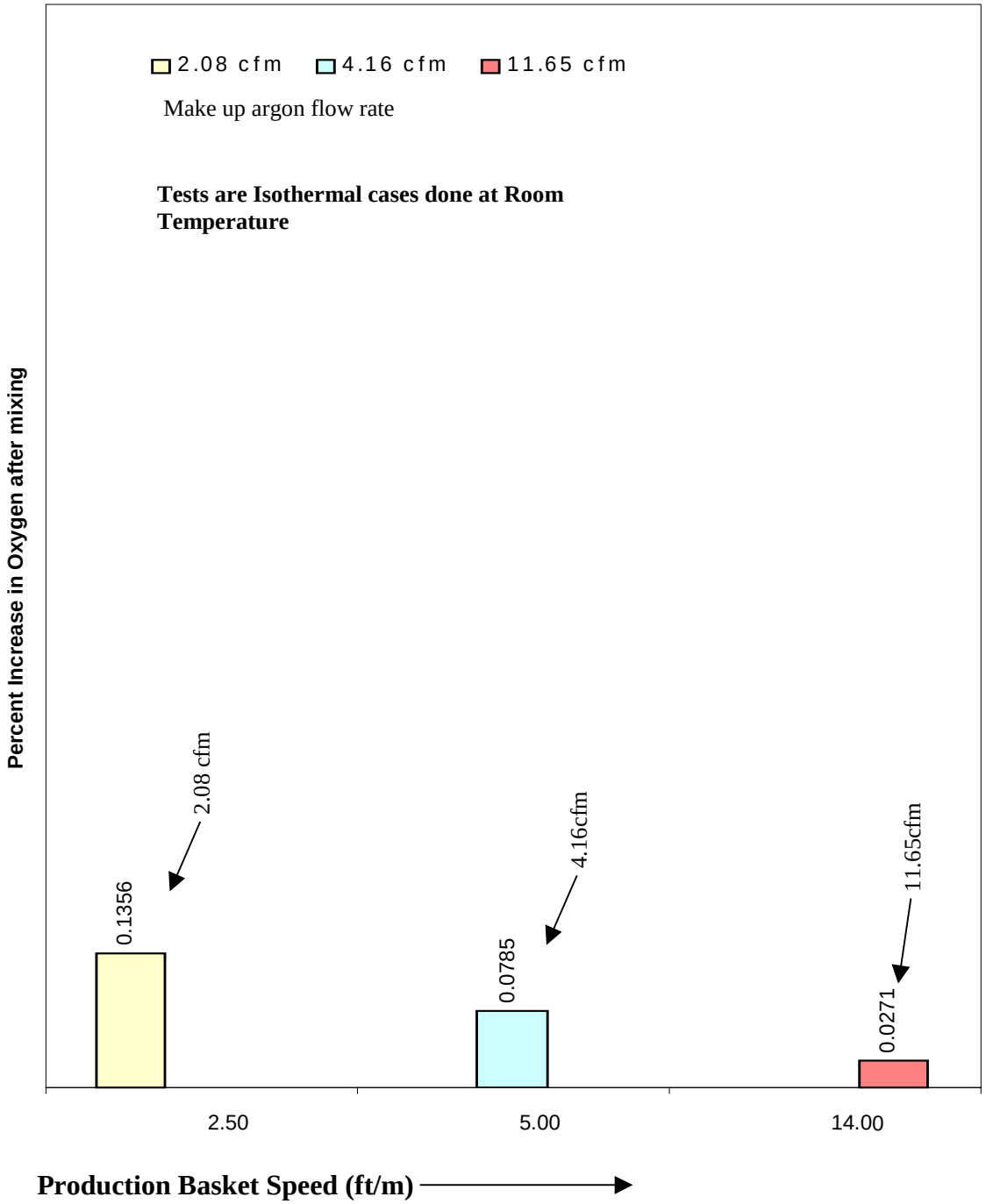

Figure 4.1.9: Effect of three different basket speeds (withdrawal) with different make-up rates without HVAC air flow.

Nominal Cases Percent Increase of Oxygen for different extraction basket speed (Insertion of the basket and HVAC On)

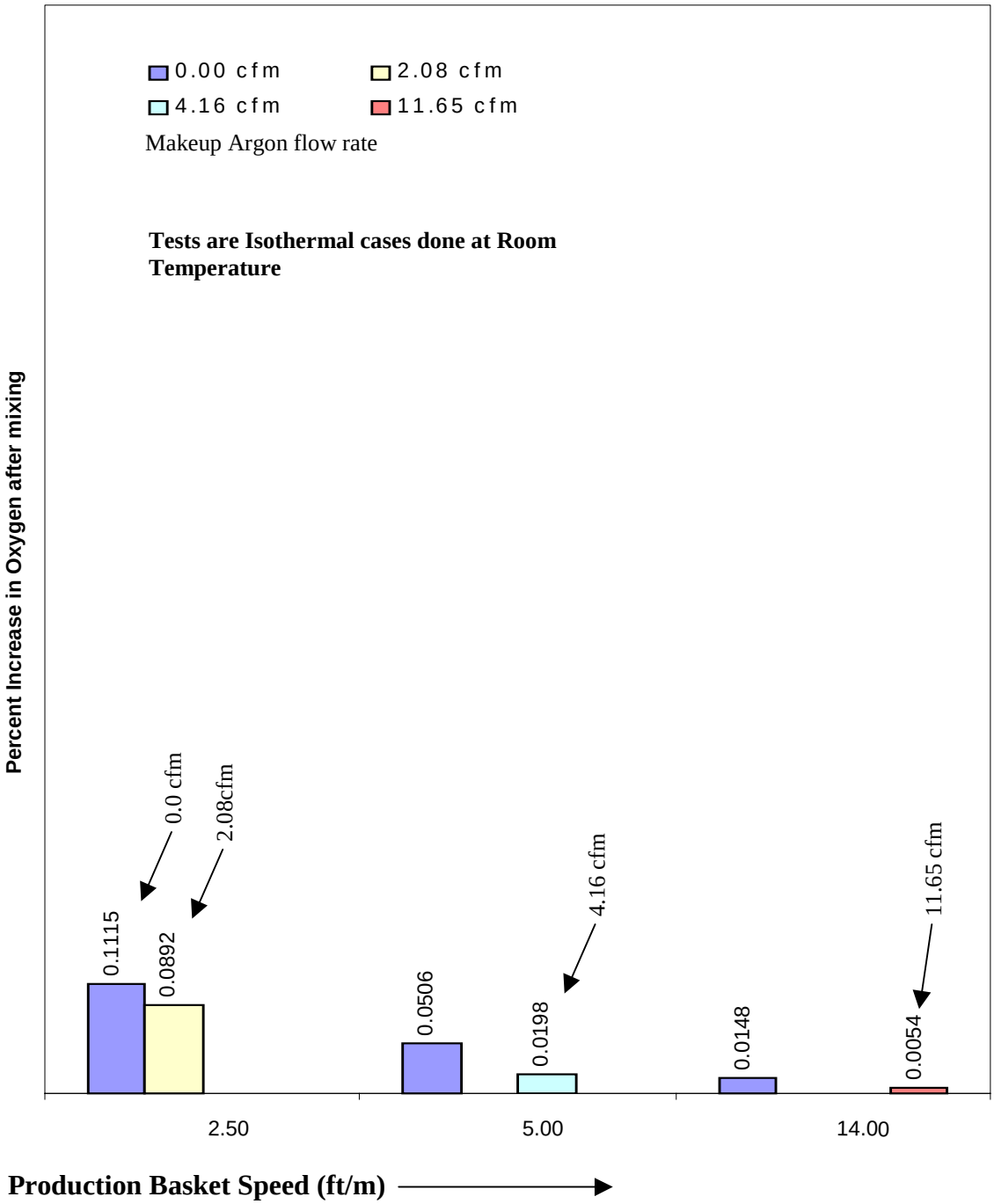

Figure 4.1.10: Effect of three different basket speeds (insertion) with different make-up rates with HVAC air flow.

4.2 Computational Results

This section presents computational results obtained from the computational fluid dynamics codes FLUENT and FIDAP. The insertion and withdrawal of the extraction basket constitute time dependant phenomena. Therefore unsteady state governing equations for conservation of mass, momentum, energy and species are solved. The generated results are a function of time. For isothermal cases, i.e., for experiments performed at room temperature, the parameters of interest are the velocity filed in the module and the concentration of argon and air in the module (species). For thermal cases the temperature is the third important variable. Presented results include cases with and without argon reservoirs; and cases with and without HVAC air flow. The room temperature cases will be discussed first, followed by thermal cases, 3-D case, reservoir filling, results showing effect of the plug, and finally validation of the computational results.

4.2.1 Room Temperature Studies (isothermal cases)

Figures 4.2.1 and 4.2.2 show the withdrawal of the extraction basket at 2 ft/min. The figures represent the case with no make-up argon and without the argon reservoir. Figure 4.2.1 represents the velocity vector (velocity of the air or argon) after 602 seconds from the beginning of the withdrawal process and Figure 4.2.2 shows the concentration of argon (0 to 100%) and air at the same instant in time. Figure 4.2.1 shows velocity vector representing the ingress of air into the furnace module to fill-up the vacuum created due to the withdrawal of the basket. Therefore, these figures demonstrate the need for make-up argon to avoid ingress of room air.

Figures 4.2.3 to 4.2.6 show the velocity profiles and the species concentration (argon and air) during the basket insertion process. The case shown in the figures is with an argon reservoir and no make-up argon flow rate. During the basket insertion, the introduction of the basket on the furnace module displaces a volume of the argon equal to the volume of the inserted basket. The insertion rate is 2 ft/min, at 402 seconds about 12 feet of the basket has moved into the furnace module. Figure 4.2.3 shows the velocity vector, at the throat the velocity of argon leaving the module is in the range of 0.3-0.4 ft/min. From Figure 4.2.4 it is apparent that due to this forced expulsion of argon from the furnace module, there is no ingress of air even without any make-up argon flow during the insertion process. Figure 4.2.6 shows the species concentration later at 802 seconds, when the basket is almost completely in. There is virtually no air infiltrated into the module.

From the two cases just discussed, it is concluded that with an argon reservoir, during the basket-withdrawal make-up argon is required, whereas, for the basket-insertion process make-up argon is not necessary. Similar cases were investigated at other flow rates, and the same conclusions were reached.

Figures 4.2.7 to 4.2.12 show withdrawal of the basket in the presence of an argon reservoir with make-up argon flow. The make-up argon is supplied to the argon reservoir, which allows a flow of argon through the inner porous wall. The figures present velocity vectors and species concentrations at three different times (202 seconds, 424 seconds, and 602 seconds). At 202 seconds there is movement of the basket, but none of the volume of the basket has exited the furnace module. As a result the volume of gases convecting out of the furnace module equals the make-up argon volume. In Figure 4.2.8 one can see the plume of argon being pushed to the right by the HVAC air. At 402 seconds (Figures 4.2.9 and 4.2.10) a little less than half of the basket has exited the

furnace module and an ingress of argon from the reservoir is obvious. As argon is constantly being made-up, there is no ingress of atmospheric air in the furnace module. The same observations are more pronounced at 602 seconds. It was concluded from these and other numerical calculations that, with make-up argon flow an argon reservoir is effective in preventing ingress of atmospheric air into the module and furnace.

Figures 4.2.13 to 4.2.15 show that during the basket withdrawal process without an argon reservoir; if there is no argon make-up then there will be significant ingress of atmospheric air. At 602 seconds both the velocity vectors (Figure 4.2.13) and the species concentrations (Figures 4.2.14 and 4.2.15) validate this conclusion. Figure 4.2.14 is color contour, showing the concentrations of argon from 0 to 100%. Figure 4.2.15 shows the line contours of the same to show more detailed concentration of argon in the module, thus these lines show the amount of air infiltrated.

Figures 4.2.16 to 4.2.18 show that basket insertion process without an argon reservoir, make-up argon is not necessary to prevent ingress of atmospheric air. Figure 4.2.17 shows the plume of argon that is forced out due to the basket insertion and the plume is being pushed to the right due to the HVAC air. Figure 4.2.17 is a color contour, showing the concentrations of argon from 0 to 100%. Figure 4.2.18 shows the line contours of the same to show more detailed concentration of argon in the module, thus these lines show the amount of air infiltrated. The wake region created behind the basket allows a small plume of air getting in the module, but clearly this amount is negligible.

Figures 4.2.19 to 4.2.23 show the basket withdrawal process. In this case there was no argon reservoir, and argon was directly injected into the furnace module. The injection was from two ports as shown earlier (Figure 3.1). At 202 seconds the basket has not exited from the furnace module. The velocity vectors show argon leaving the furnace.

This volume is the make-up argon. Figure 4.2.20 shows the argon concentration and the plume of argon being pushed to the right by the HVAC air. At 402 seconds when the basket is exiting the module, the volume rate of make-up cancels the volume rate of basket exit, as a result velocity vector shows almost no ingress of room air at this time. This fact is confirmed by observing Figures 4.2.22 and 4.2.23 which show the concentration profile and the concentration contours. There is virtually no ingress of room air. It is concluded that for no argon reservoir with make-up argon the ingress of room air will be minimal (well within allowable limits).

4.2.2 Thermal Studies

Figures 4.2.24 to 4.2.29 show withdrawal of the basket in the presence of an argon reservoir. The make-up argon flow rate is nominal. The case depicted is a thermal case, where the retort was at a temperature of 150^{o}F. Figure 4.2.24 shows the temperature contour at 36.1 seconds of the withdrawal process. Localized effect of the heated retort can be seen from this figure, and this plot shows a hot plume rising due to buoyancy can be seen in this plot. The plume can be seen more distinctly in the next figure which shows the velocity vectors. Figure 4.2.26 shows the species concentration. At 280 seconds of the withdrawal (Figures 4.2.27-4.2.29) the effect of the buoyancy driven plume is stronger. At this time it is apparent the volume of argon lost due to buoyancy driven flow will allow ingress of room air.

Figures 4.2.30 to 4.2.38 show the withdrawal of the basket with no argon reservoir. The case depicted is similar to the previous case (with argon reservoir), where the retort was at a temperature of 150^{o}F. Figure 4.2.30 shows the temperature contour at 36.1 seconds of the withdrawal process. A hot plume rising due to buoyancy can be seen in this plot. The plume can be seen more distinctly in the next figure which shows the

velocity vectors with a maximum velocity as high as 1.95 ft/min. Figure 4.2.32 shows the species concentration at this time. At 200 seconds of the withdrawal (Figures 4.2.33-4.2.35) the effect of the buoyancy driven plume is stronger. At this time it is apparent the volume of argon lost due to buoyancy driven flow will force ingress of room air to fill up the empty volume. This phenomenon is evident from Figure 4.2.35 showing the species contour plot. Ingress of room air causes a region in the furnace module where the argon concentration is as low as 55%. Figures 4.2.36 to 4.2.38 show similar trends at 400 seconds. It is concluded from the above discussion that opening the gate-valve for basket withdrawal, when the retort is at an elevated temperature will result in ingress of room air due to the buoyant plume.

4.2.3 3-D Studies

Figures 4.2.39 to 4.2.44 show the computational results with 3-D computational domain. The case investigated was for withdrawal of the basket without an argon reservoir. The withdrawal rate was 2 ft/min with argon make-up rate of 2 cfm (nominal). Figure 4.2.39 shows the velocity vectors at 202 seconds. This is compared with Figure 4.2.19, which represents the same case in 2-D. Comparison of the velocity vector and their magnitude reveal similar trends. Figure 4.2.40 shows the species concentration, comparing it to Figure 4.2.20, one can see the similarity in the argon concentration, as well as the plume of argon emanating from the production furnace. Figures 4.2.41 and 4.2.42 are sectional views of the species concentration and the velocity vector respectively. Due to the ingress along the edge of the gate, a ring of lower concentration argon is visible. Figures 4.2.43 and 4.2.44 show velocity vectors and species concentrations at a later time (240 seconds). The ring is still visible, and on the velocity vector one can see that due to the blocking of the gate by the basket, the exit velocity is larger at the periphery of

the gate. From the 3-D computational results, it is concluded that the 2-D computations provide reliable results.

4.2.4 Filling of the Argon Reservoir

Figure 4.2.45 shows a typical concentration profile during the filling of the argon reservoir. This particular case shows the filling at 2 cfm argon with HVAC air blowing at 10 ft/min, the profile after about 2.1 hours shows that the top of the reservoir is not completely filled. The filling process is shown in more detail in Figure 4.2.46, the argon concentration is shown at 4-different depths of the reservoir as a function of time. It can be seen from the figure that about 90% argon filling is achieved in about 3500 seconds. From there filling is asymmetric that is it takes about another 3000 seconds to increase the argon concentration by another 5%. This figure also shows the effect of stopping the filling process and leaving the reservoir to the hot cell atmosphere. In 1-hour about 50% of the argon diffused into the ambient atmosphere. From this it is concluded that in order to fill and maintain a high concentration in the reservoir it must be continuously supplied with argon. This may result in large argon consumption. Figure 4.2.46 shows the filling at 4.0 cfm. The filling time is reduced to 2,300 seconds but again, the concentration attained is only 94%. Figure 4.2.47 shows the comparative filling time for the two filling rates.

Figure 4.2.48 shows the filling without HVAC air flowing across the reservoir. It is interesting to see that the filling time without HVAC is reduced by half for the same filling rate of 2 cfm. This indicates that the HVAC enhances convective transport from the top of the argon reservoir. This loss, in addition to the diffusive loss (with HVAC air in the room) results in longer filling time. This phenomenon is also responsible for lower argon depletion after the filling process was stopped at 2400 seconds. Figure 4.2.49 shows the

filling process without HVAC air at 4.0 cfm. Figure 4.2.50 Compares the filling and depletion for the two flow rates with no HVAC flow rate.

These studies demonstrate that the filling process of the reservoir is faster for cases when there is no HVAC air flow in the room.

4.2.5 Room Temperature at Faster Withdrawal Rates

Figures 4.2.51 to 4.2.56 present a case with faster withdrawal rate of the basket. The basket withdrawal speed was 15 ft/min (maximum speed of the production crane), and the argon make-up rate was 15 cfm. At 20 seconds (Figures 4.2.51 & 4.2.52) the velocity vectors show that argon is exiting the furnace module due to make-up argon. The velocity vectors show a faster flow speed than was observed previously at 2 ft/min withdrawal rate. At 60 seconds (Figures 4.2.53 & 4.2.54), it is observed that even though the basket is exiting the furnace module, there is no ingress of room air due to the fact that make-up argon is being supplied directly into the module. At 80 seconds (Figures 4.2.55 & 4.2.56) this trend is confirmed. From this study it is concluded that faster withdrawal with nominal argon make-up will meet the design requirement. In fact, as the withdrawal rate increases, there is lower total diffusion of room air into the module.

4.2.6 Effect of Plug

Figures 4.2.57 to 4.2.65 show the effect of having a tapered plug for closing the opening to the furnace module. The objective of this study was to see the effect of this shape in the infiltration of room air due to HVAC air flow. Figures 4.2.57 and 4.2.58 show the velocity vectors and argon concentration after 1.0 second of the opening process. It is

assumed that the plug is moved at 15 ft/min and that there is no make-up argon flow. It can be seen that as the plug is moved up, room air flows to fill the void and that the process is aided by the HVAC air flow. Figures 4.2.59 and 4.2.60 show the region near the module opening for species concentration and the velocity vector. It can be seen that the ingress of air is very localized. Figures 4.2.61 to 4.2.65 show the results when the plug has moved further (10 seconds). Again one can see very localized ingress. In fact, the total ingress of room air was negligible and well within the allowable design limits.

4.2.7 Validating The Computational Results

Figures 4.2.66 to 4.2.72 show results for computations performed on the 1/5th-scale model experiment. The results shown are for 200, 400 and 600 seconds of the withdrawal process. The basket speed studied was 0.5 ft/min and the argon make-up flow rate was 1 cfh. The computations were performed on a 2-D computational domain and the grids used are discussed in Chapter 3.0. Figure 4.2.67 shows the contour lines for the concentration of argon at 200 seconds. Near the module opening the concentration varies between 82% to 100%. Figure 4.2.68 shows the velocity profile at 200 seconds. Figures 4.2.69 and 4.2.70 show the species concentration contours and velocities at 400 seconds. At this time the concentration of argon near the module opening is about 92% - 100%. At 600 seconds, as shown in Figures 4.2.71 and 4.2.72, when the basket has completely exited the module, the concentration of argon is still high. A volumetric average for the entire model-furnace provided average air ingress of about 0.34% compared with the experimental result of about 0.87%. It can be mentioned here that during the experiment there was some time lag between opening the gate and starting the experiment. The actual computational time was about 70% of

the actual experimental time. In addition, controlling 1 cubic feet per hour of make-up argon had a very large uncertainty, nevertheless the computational results demonstrate good agreement with the experiment.

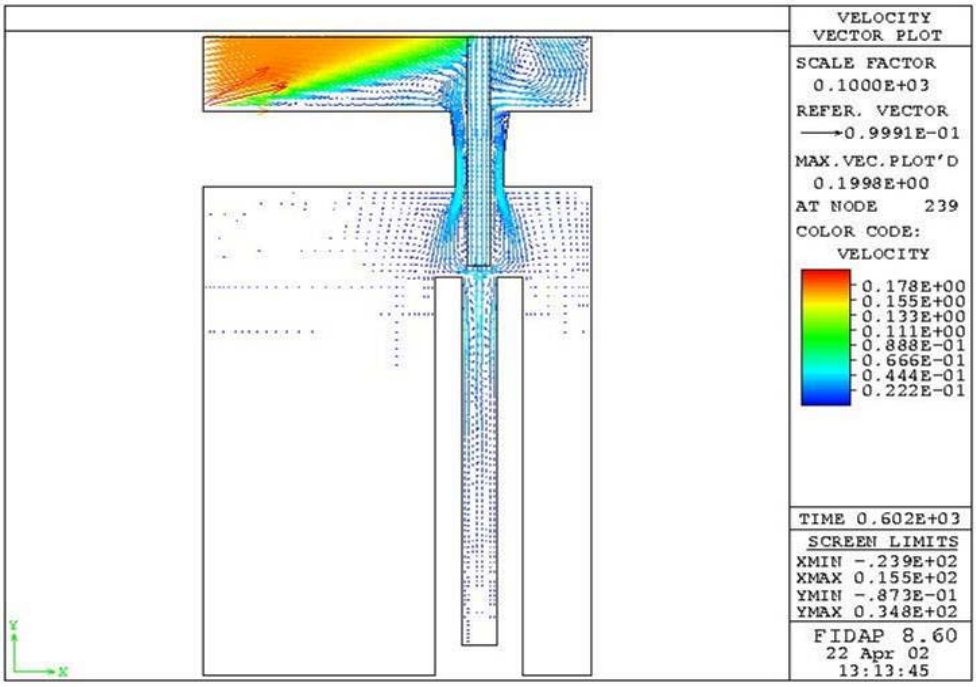

Figure 4.2.1: Withdrawal of the Extraction Basket with Argon Reservoir (No-make-up) 602 seconds (at 2 ft/min velocity)-Velocity Vector.

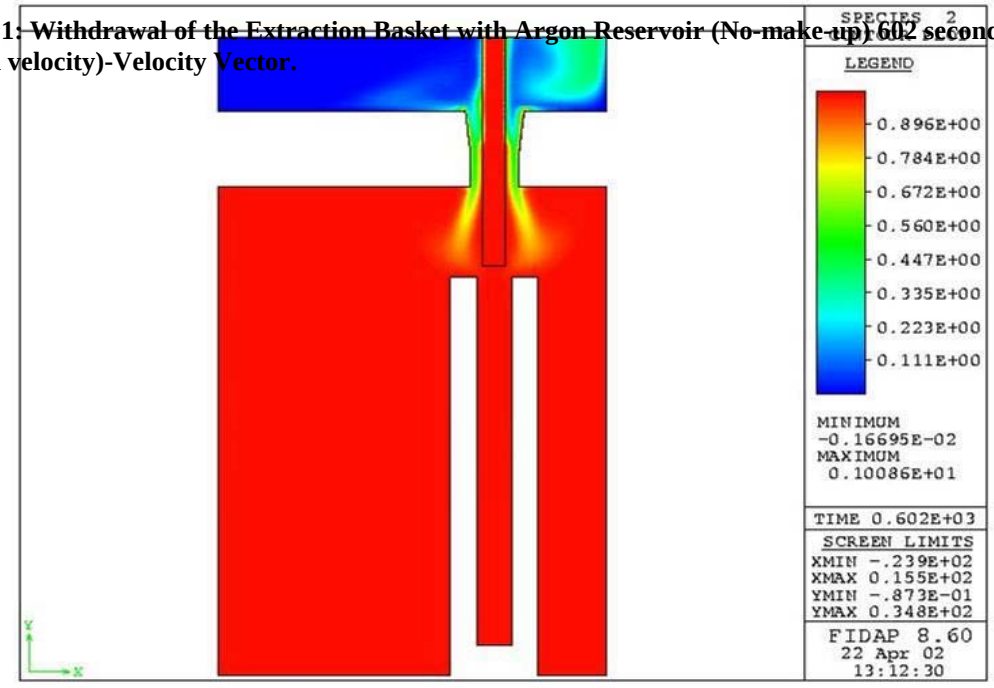

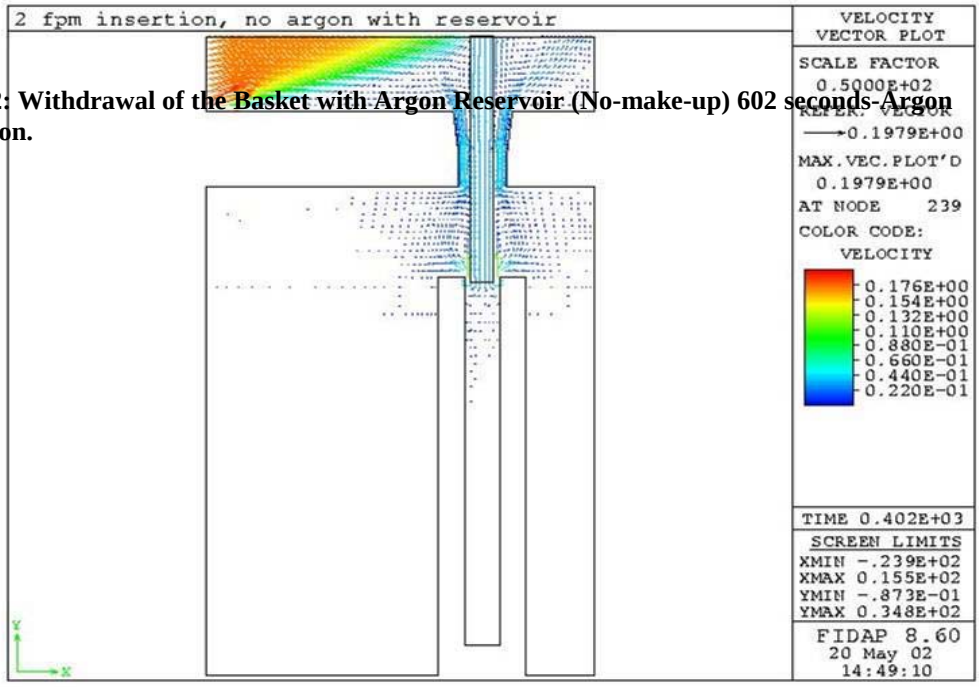

Figure 4.2.2: Withdrawal of the Basket with Argon Reservoir (No-make-up) 602 seconds-Argon Concentration.

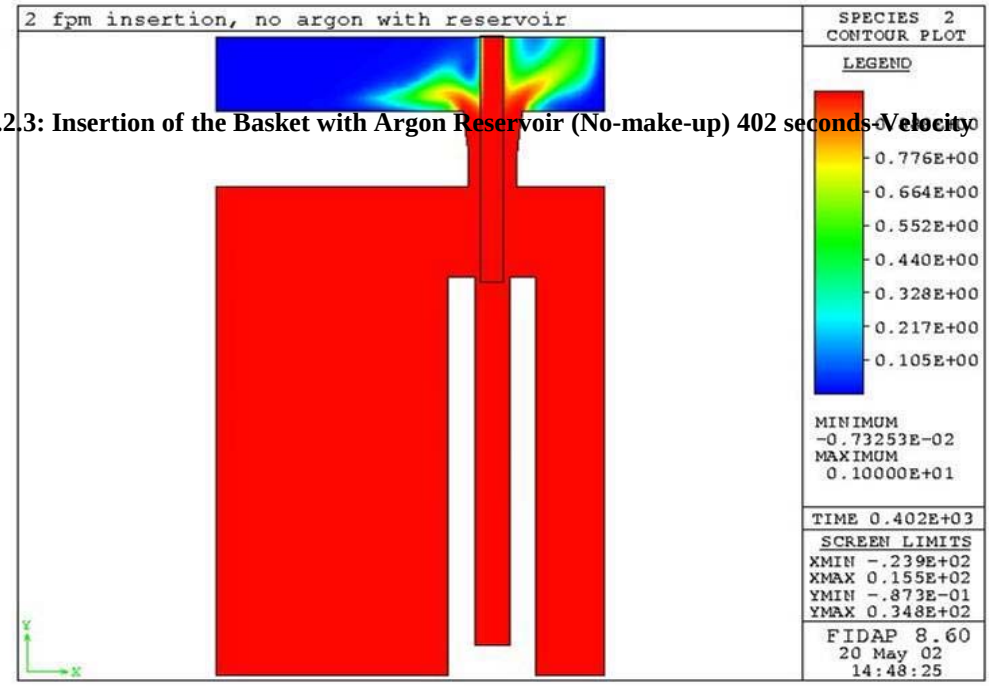

Figure 4.2.3: Insertion of the Basket with Argon Reservoir (No-make-up) 402 seconds-Velocity Vector.

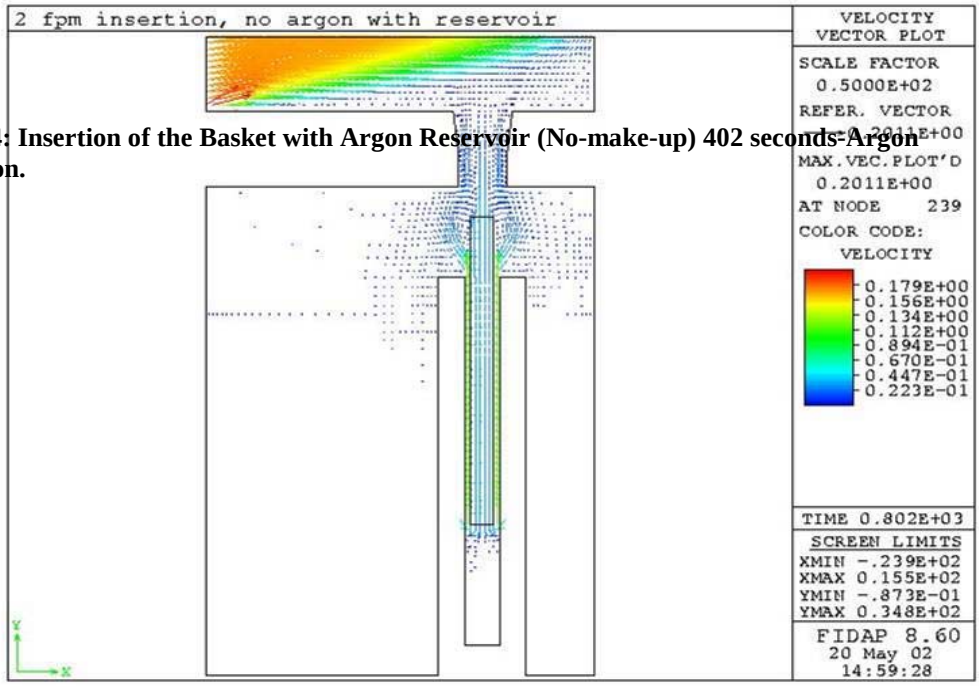

Figure 4.2.4: Insertion of the Basket with Argon Reservoir (No-make-up) 402 seconds-Argon concentration.

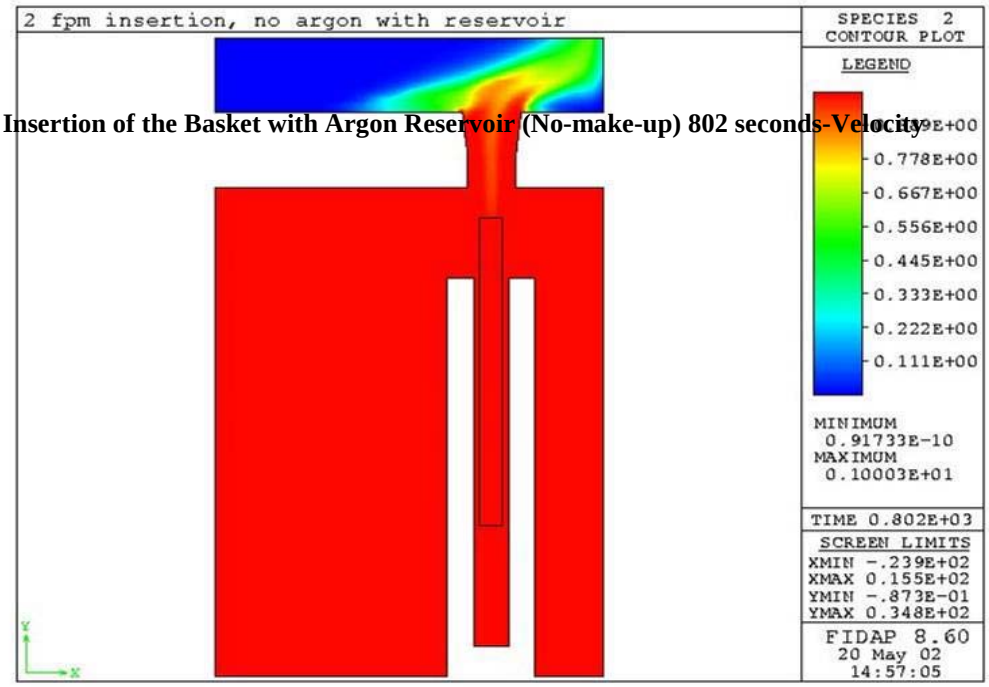

Figure 4.2.5: Insertion of the Basket with Argon Reservoir (No-make-up) 802 seconds-Velocity Vector.

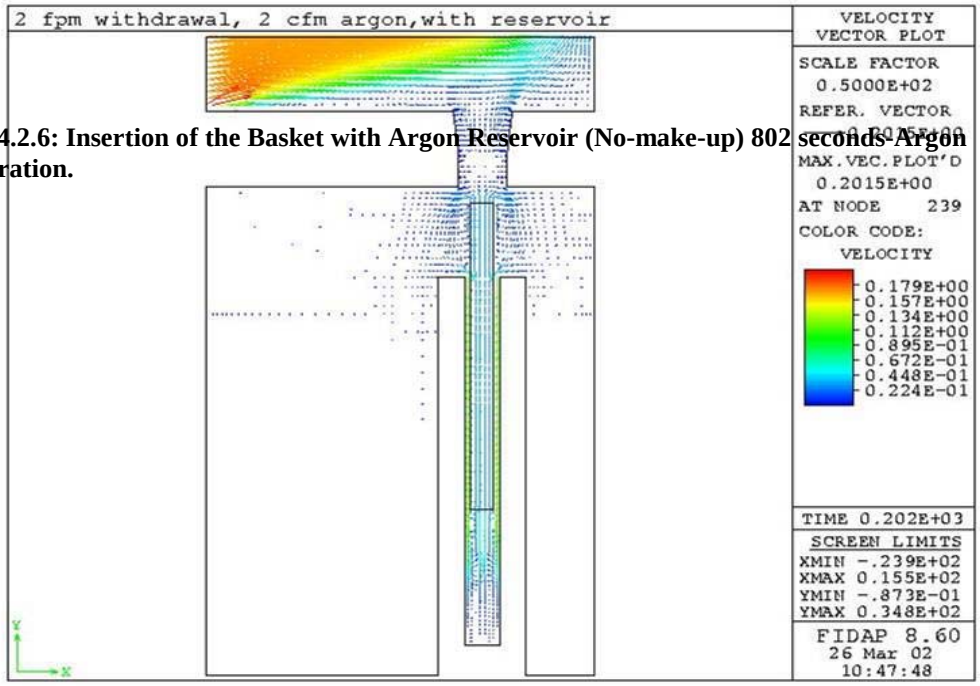

Figure 4.2.6: Insertion of the Basket with Argon Reservoir (No-make-up) 802 seconds-Argon concentration.

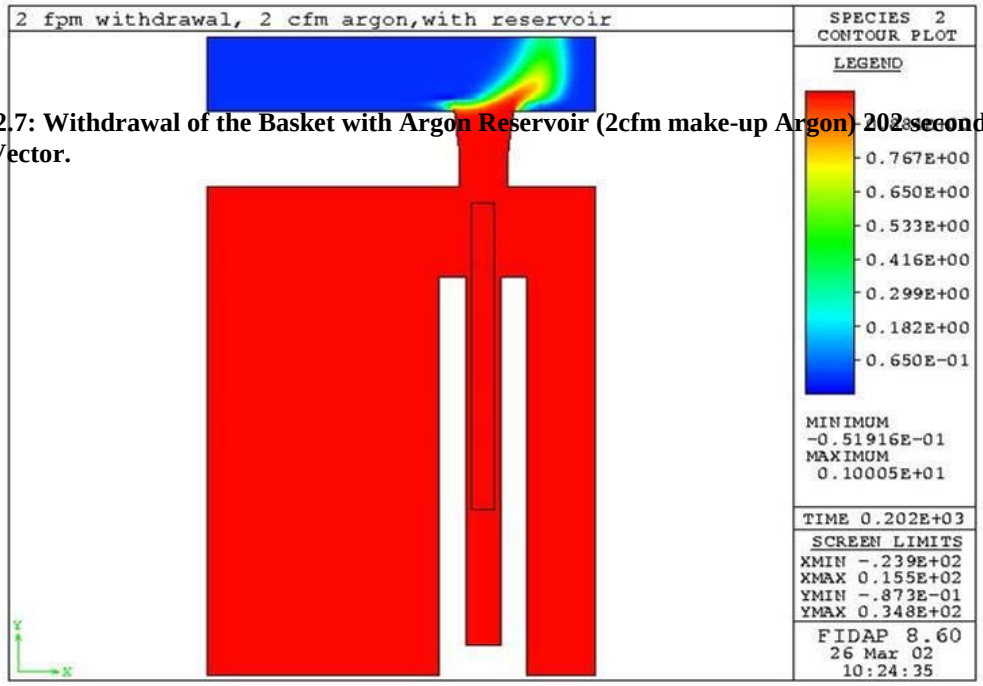

Figure 4.2.7: Withdrawal of the Basket with Argon Reservoir (2cfm make-up Argon) 202 seconds-Velocity Vector.

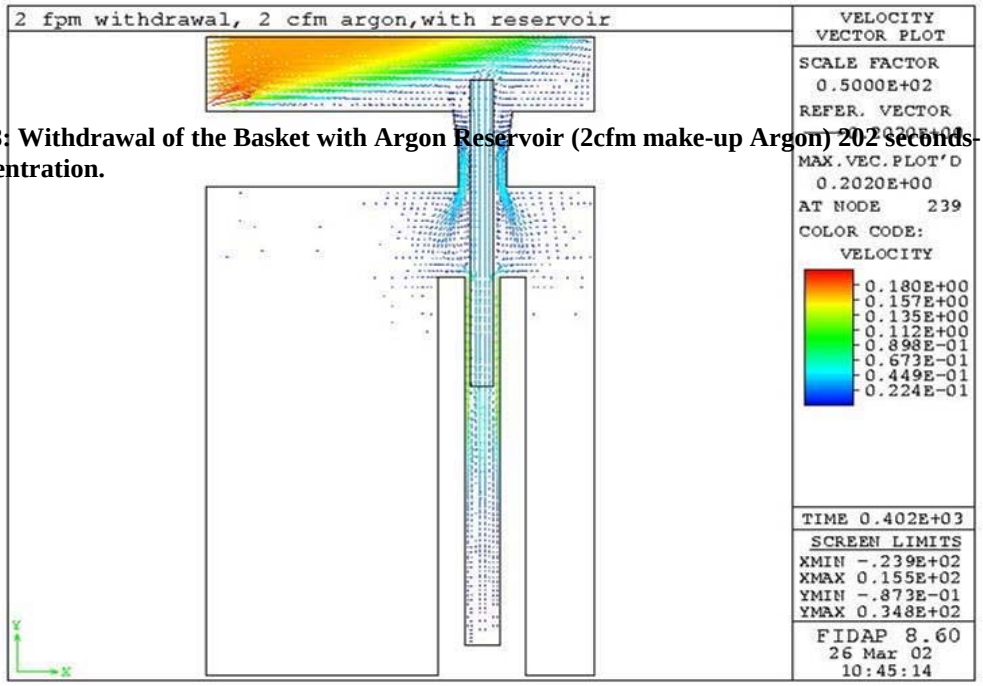

Figure 4.2.8: Withdrawal of the Basket with Argon Reservoir (2cfm make-up Argon) 202 seconds- Argon concentration.

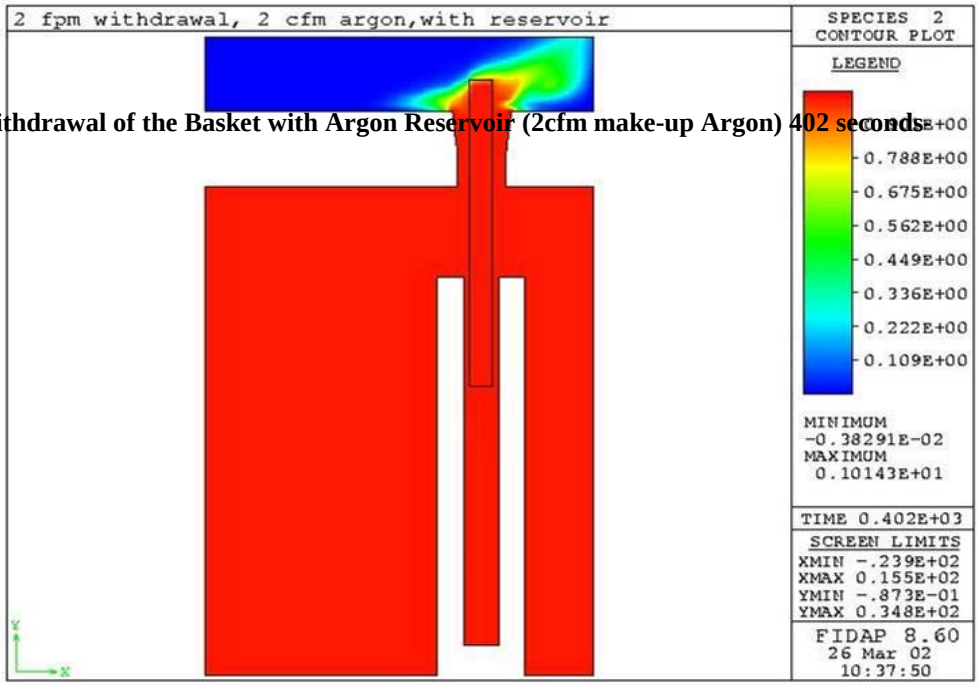

Figure 4.2.9: Withdrawal of the Basket with Argon Reservoir (2cfm make-up Argon) 402 seconds Velocity Vector.

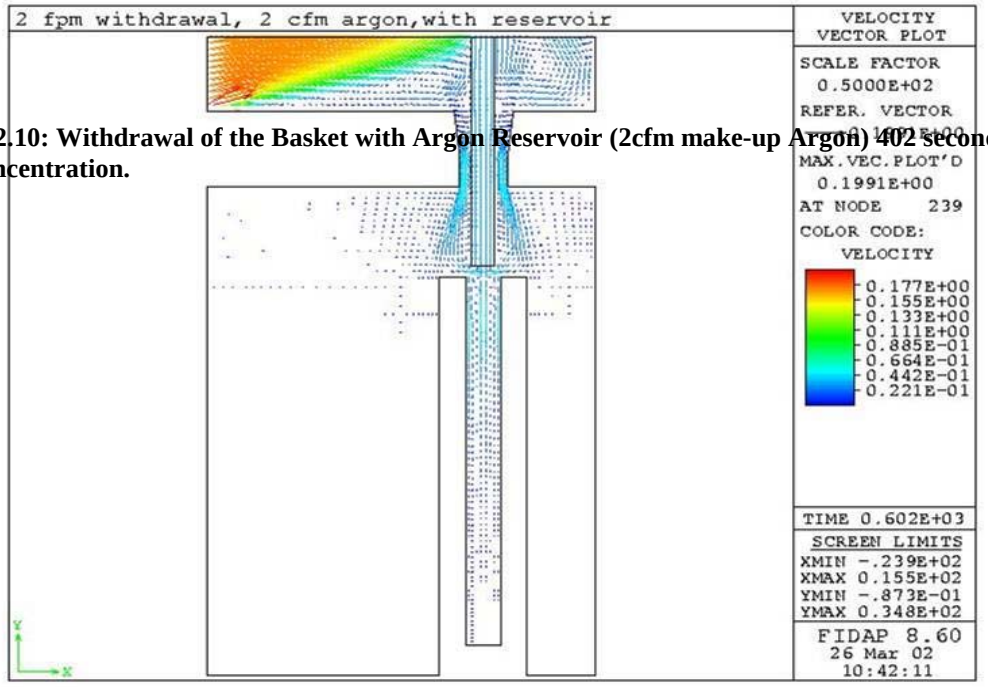

Figure 4.2.10: Withdrawal of the Basket with Argon Reservoir (2cfm make-up Argon) 402 seconds-Argon concentration.

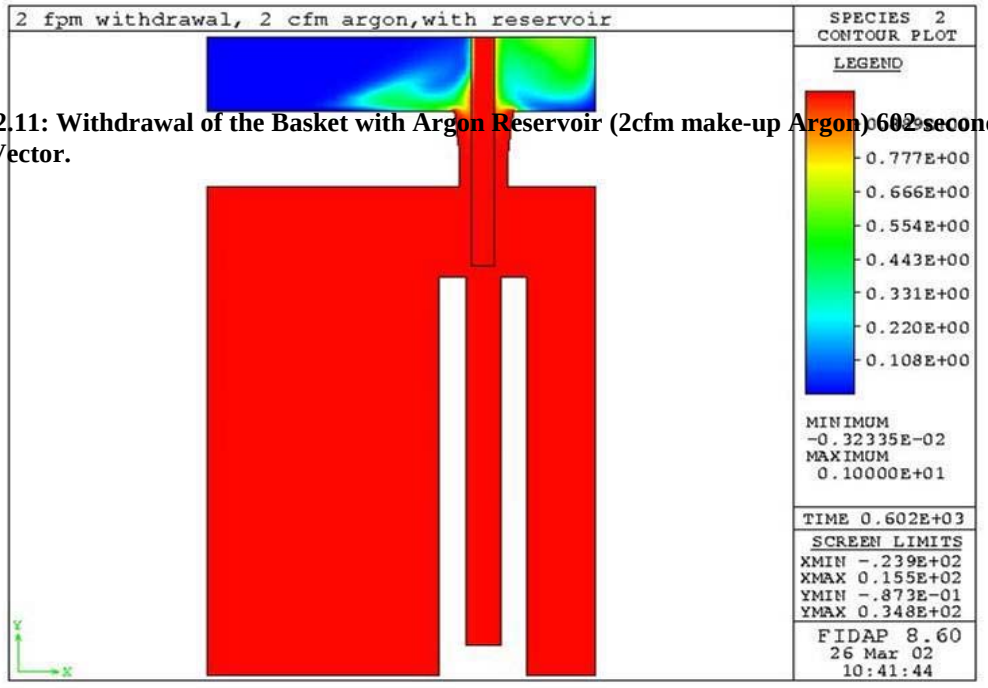

Figure 4.2.11: Withdrawal of the Basket with Argon Reservoir (2cfm make-up Argon) 602 seconds-Velocity Vector.

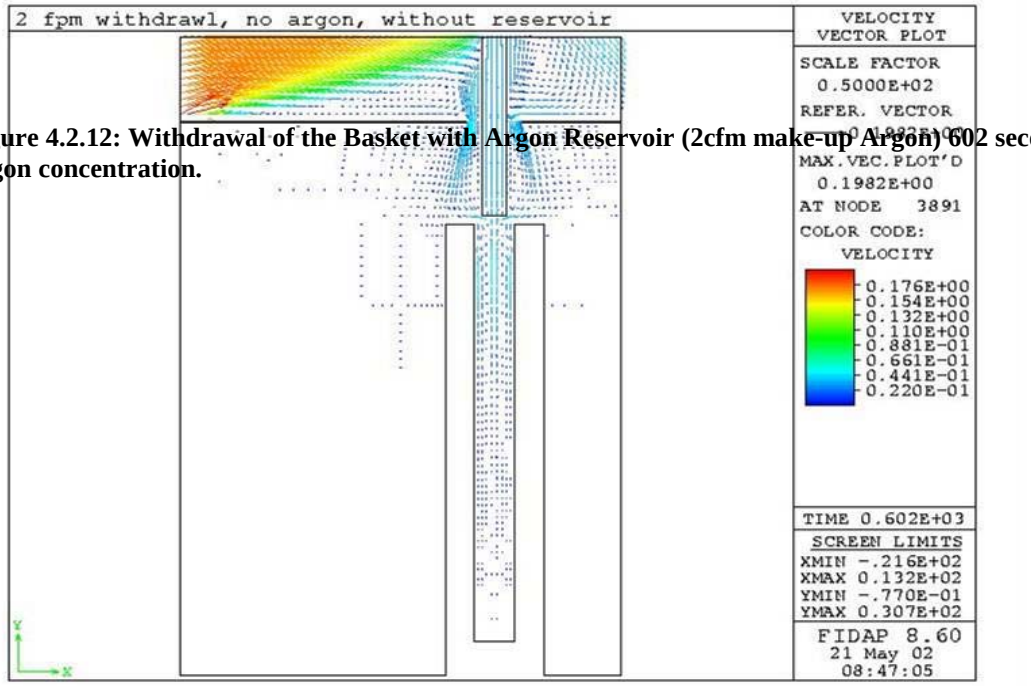

Figure 4.2.12: Withdrawal of the Basket with Argon Reservoir (2cfm make-up Argon) 602 seconds-Argon concentration.

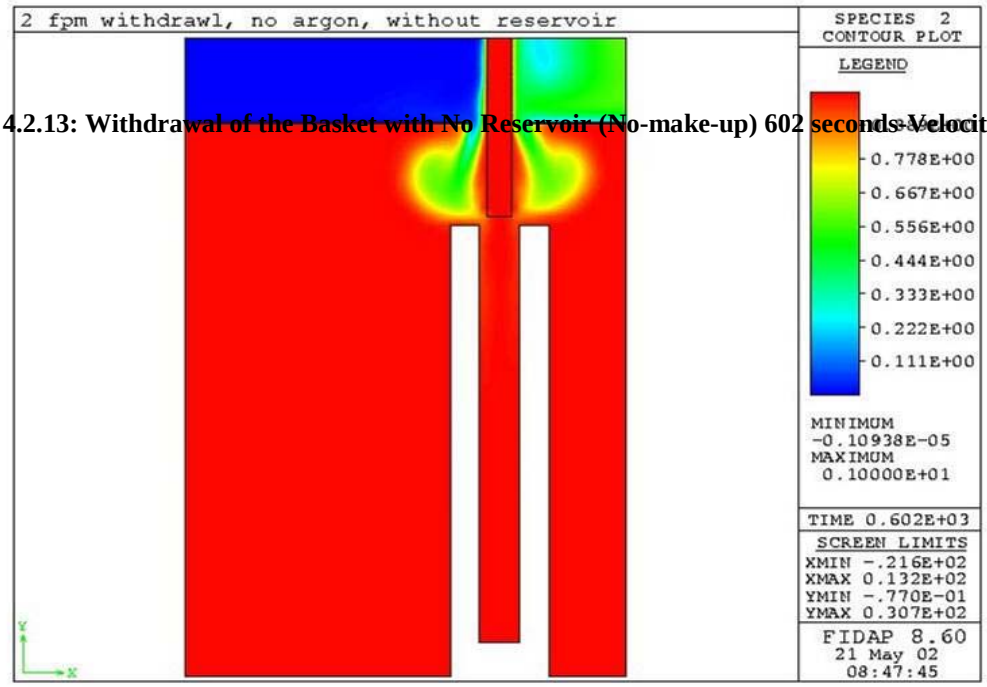

Figure 4.2.13: Withdrawal of the Basket with No Reservoir (No-make-up) 602 seconds-Velocity Vector.

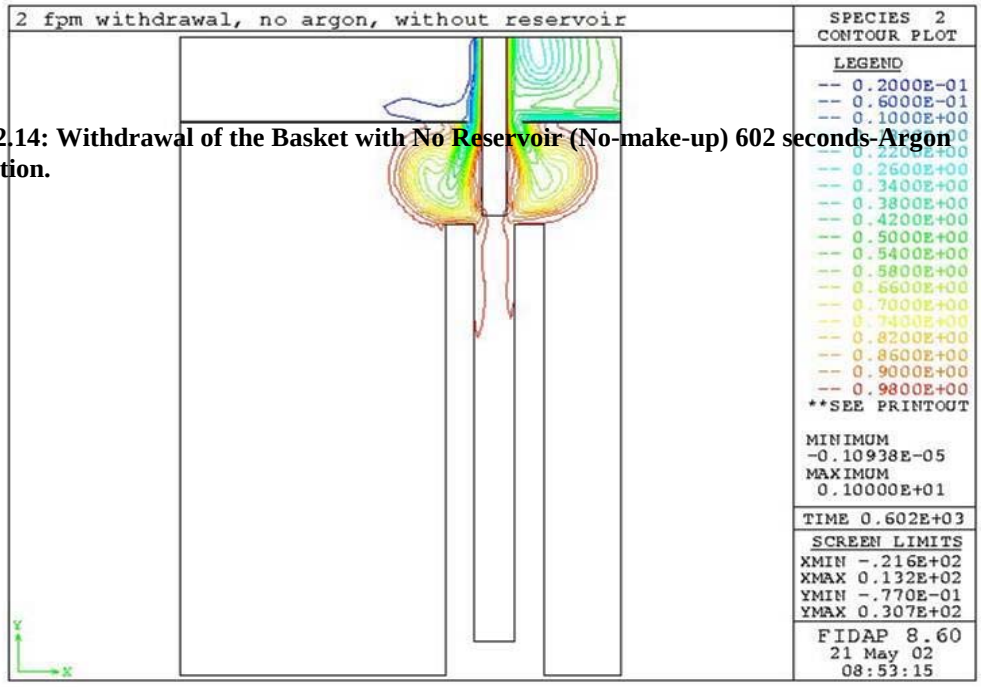

Figure 4.2.14: Withdrawal of the Basket with No Reservoir (No-make-up) 602 seconds-Argon concentration.

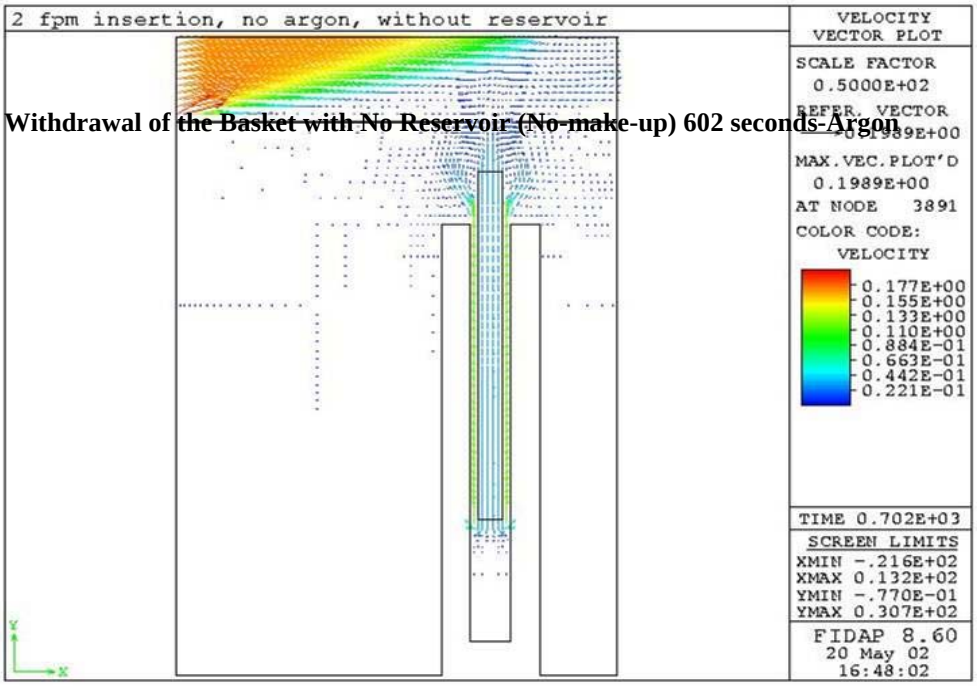

Figure 4.2.15: Withdrawal of the Basket with No Reservoir (No-make-up) 602 seconds-Argon contour.

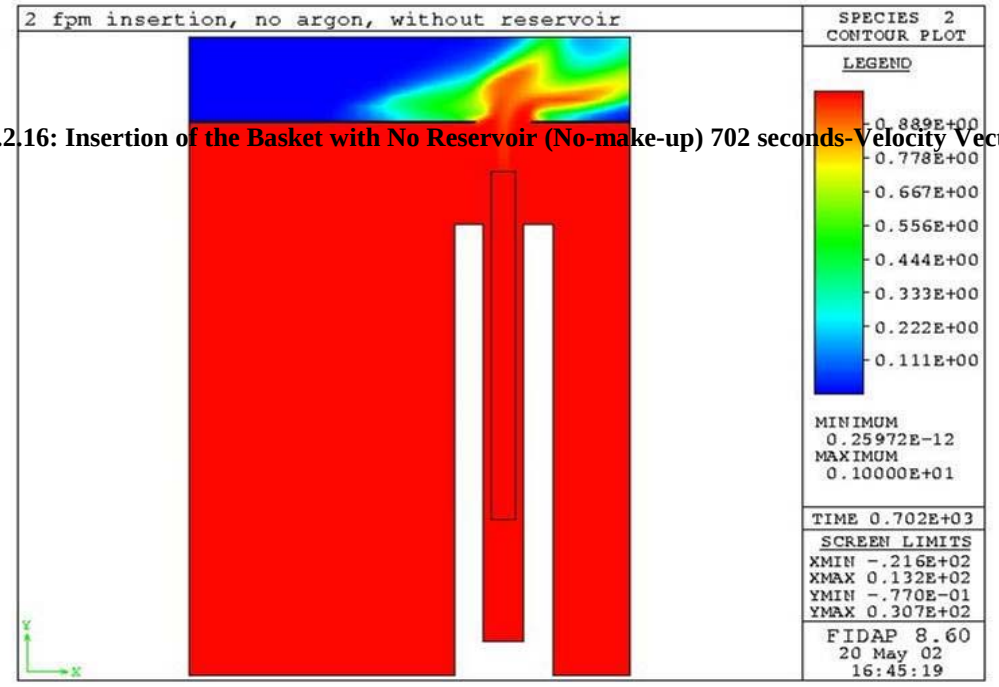

Figure 4.2.16: Insertion of the Basket with No Reservoir (No-make-up) 702 seconds-Velocity Vector.

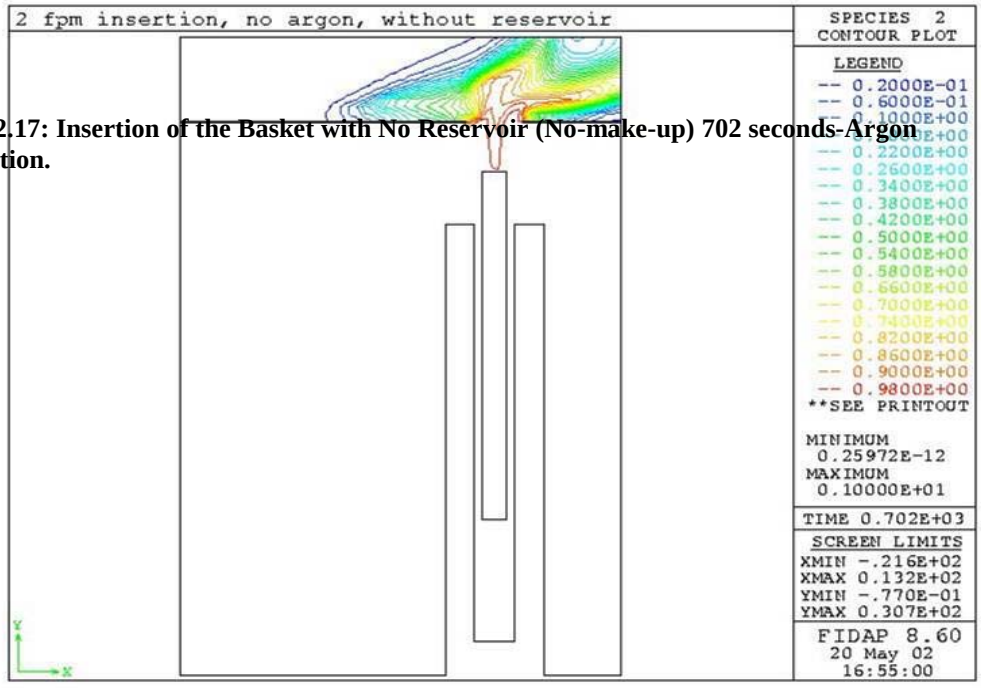

Figure 4.2.17: Insertion of the Basket with No Reservoir (No-make-up) 702 seconds-Argon concentration.

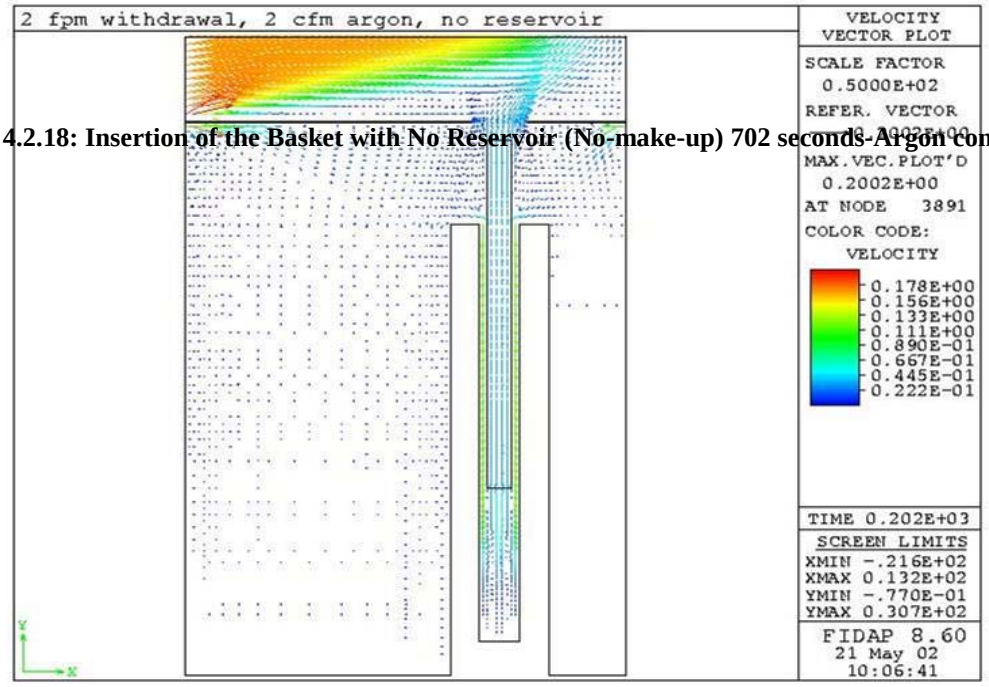

Figure 4.2.18: Insertion of the Basket with No Reservoir (No-make-up) 702 seconds-Argon contour.

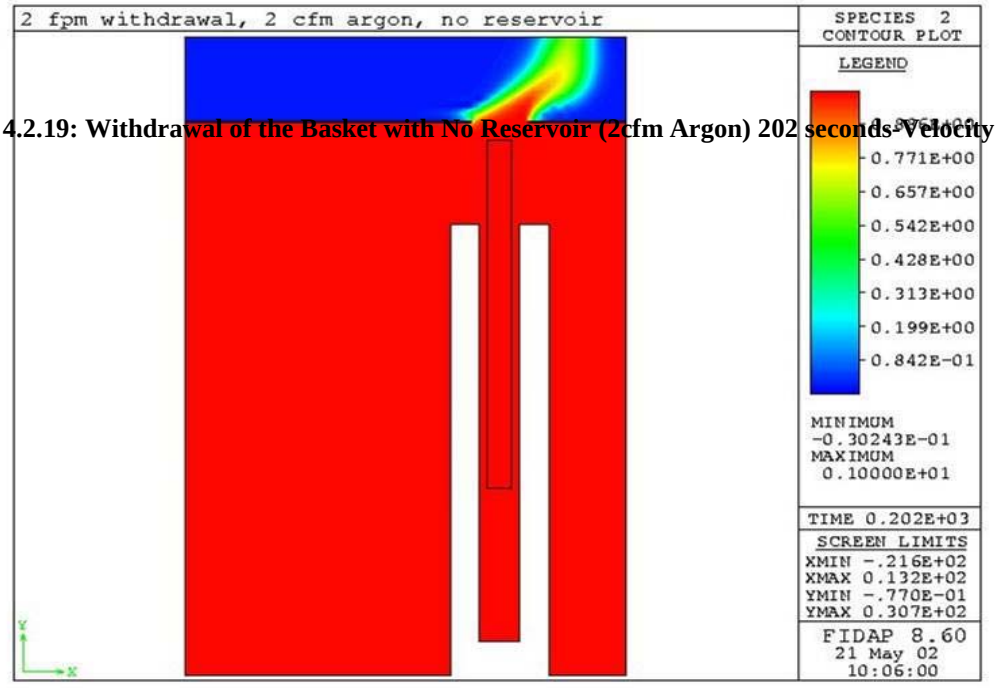

Figure 4.2.19: Withdrawal of the Basket with No Reservoir (2cfm Argon) 202 seconds-Velocity Vector.

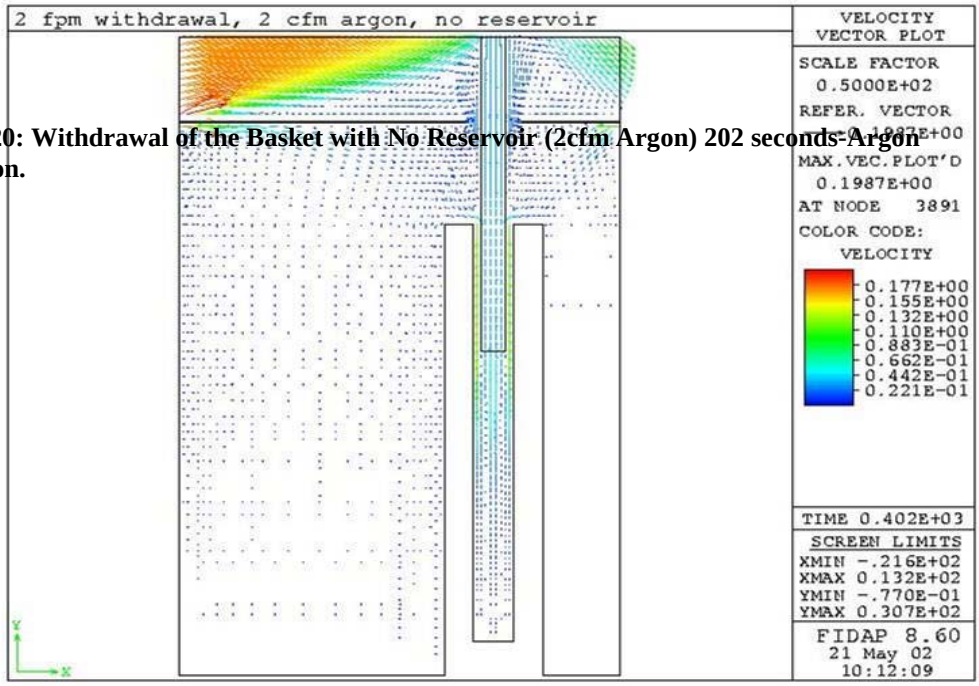

Figure 4.2.20: Withdrawal of the Basket with No Reservoir (2cfm Argon) 202 seconds-Argon concentration.

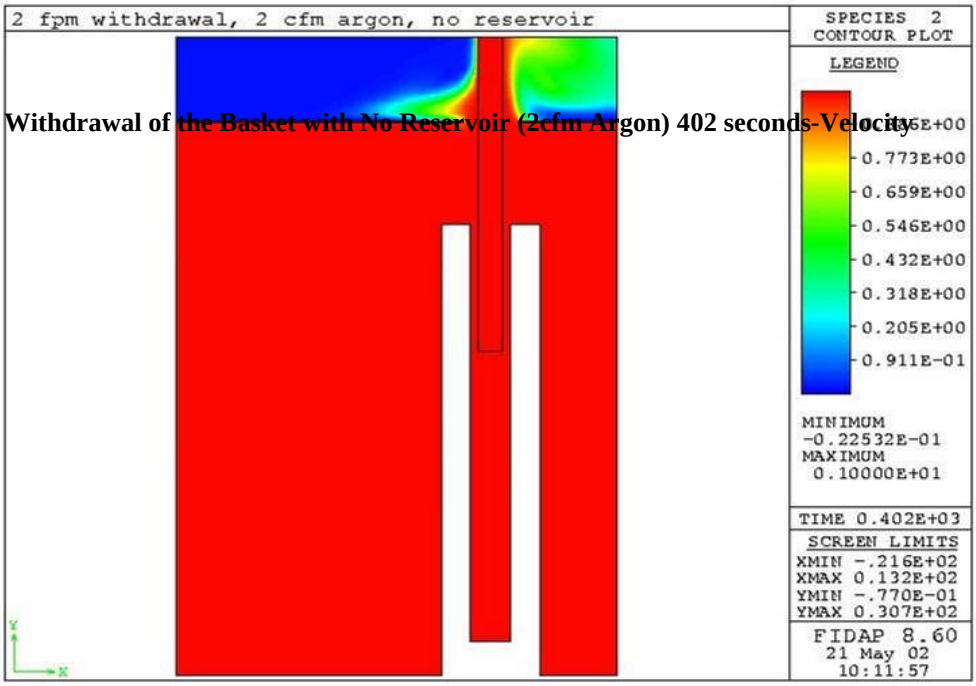

Figure 4.2.21: Withdrawal of the Basket with No Reservoir (2cfm Argon) 402 seconds-Velocity Vector.

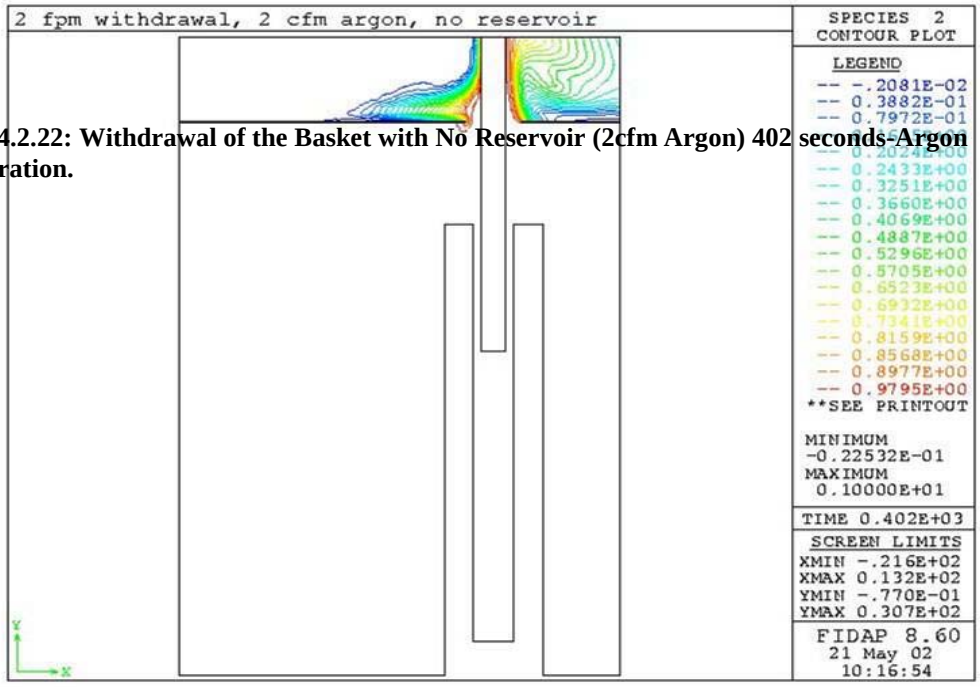

Figure 4.2.22: Withdrawal of the Basket with No Reservoir (2cfm Argon) 402 seconds-Argon concentration.

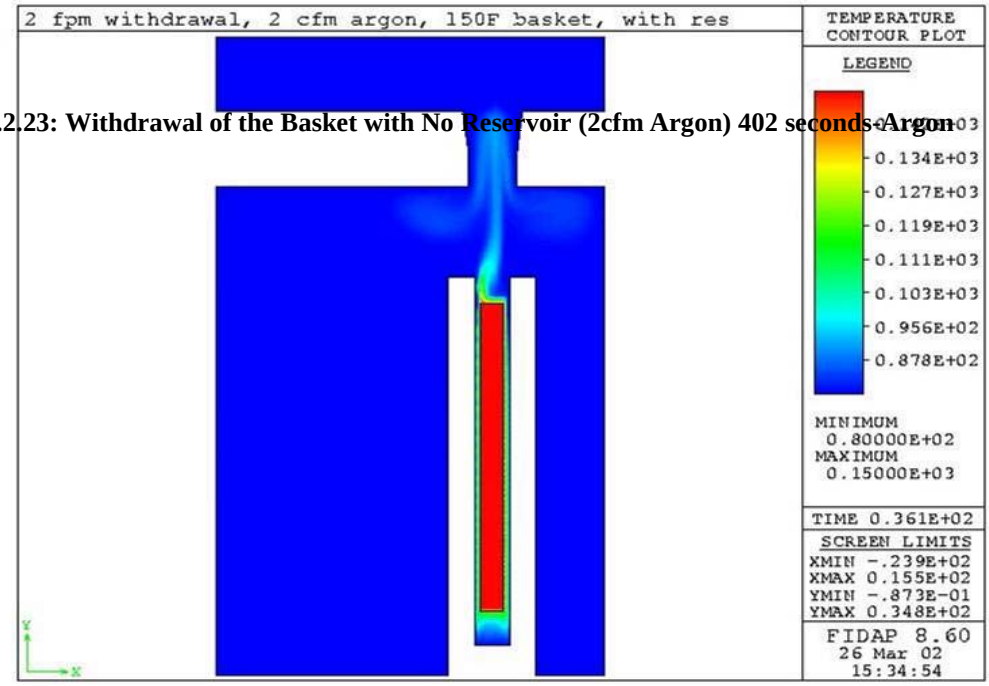

Figure 4.2.23: Withdrawal of the Basket with No Reservoir (2cfm Argon) 402 seconds-Argon contour.

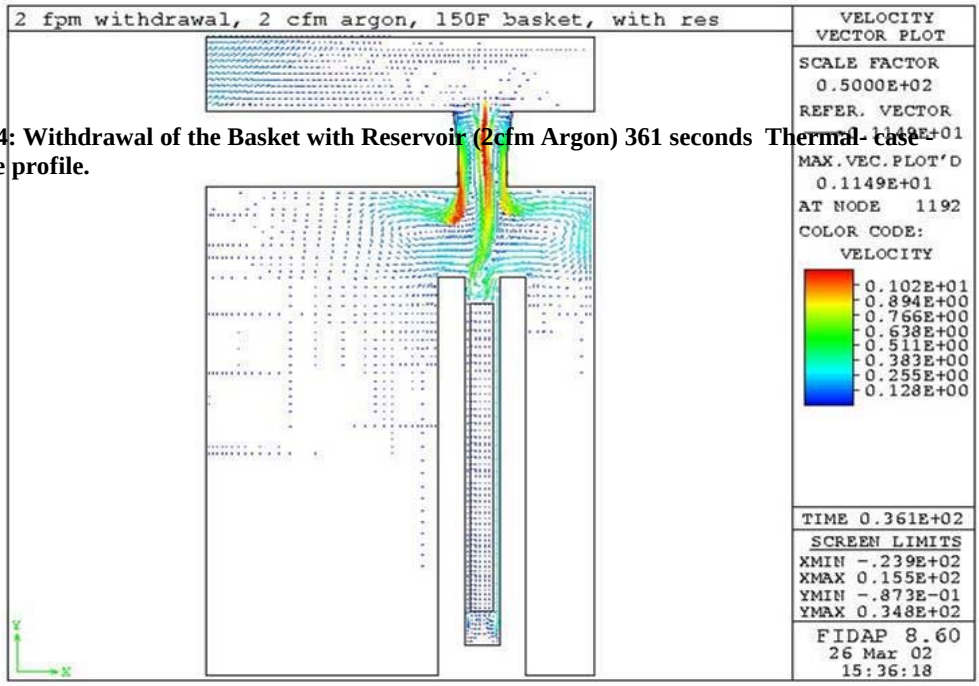

Figure 4.2.24: Withdrawal of the Basket with Reservoir (2cfm Argon) 361 seconds Thermal- case - Temperature profile.

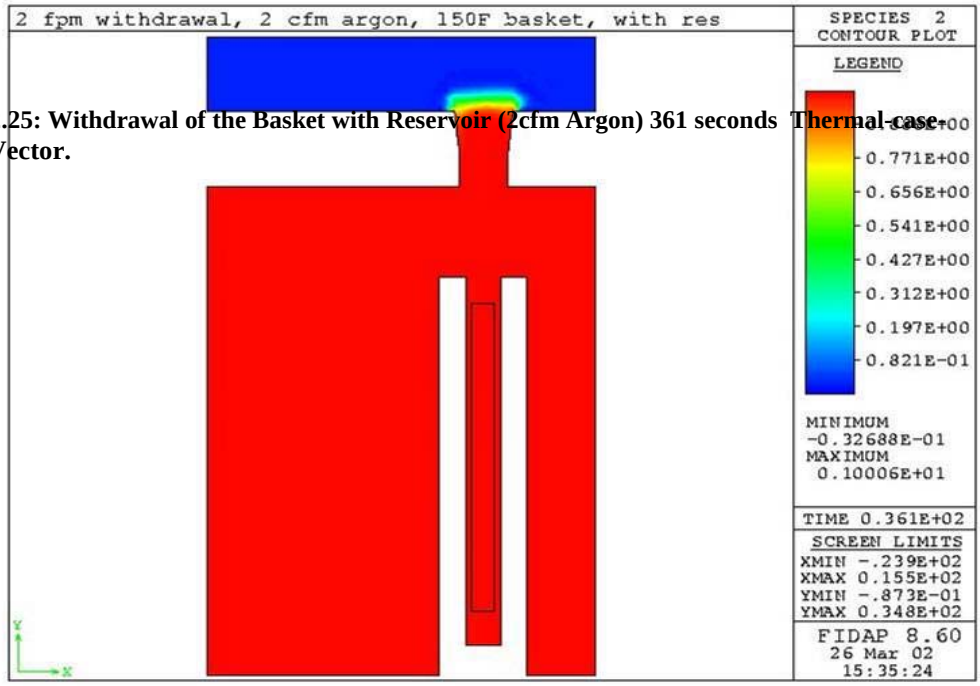

Figure 4.2.25: Withdrawal of the Basket with Reservoir (2cfm Argon) 361 seconds Thermal-case - Velocity Vector.

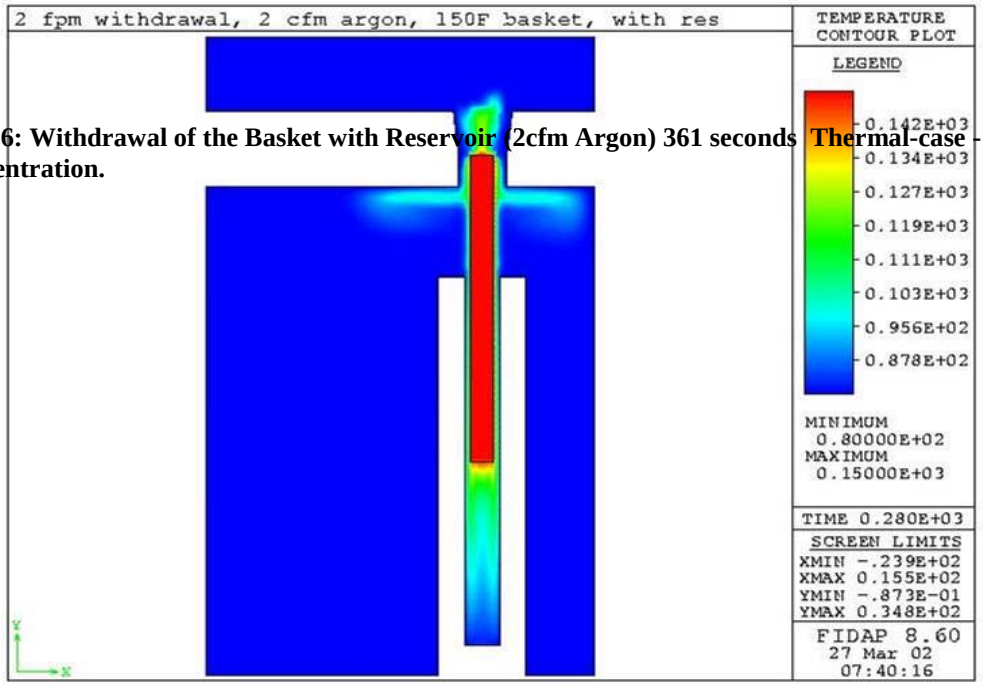

Figure 4.2.26: Withdrawal of the Basket with Reservoir (2cfm Argon) 361 seconds Thermal-case - Argon concentration.

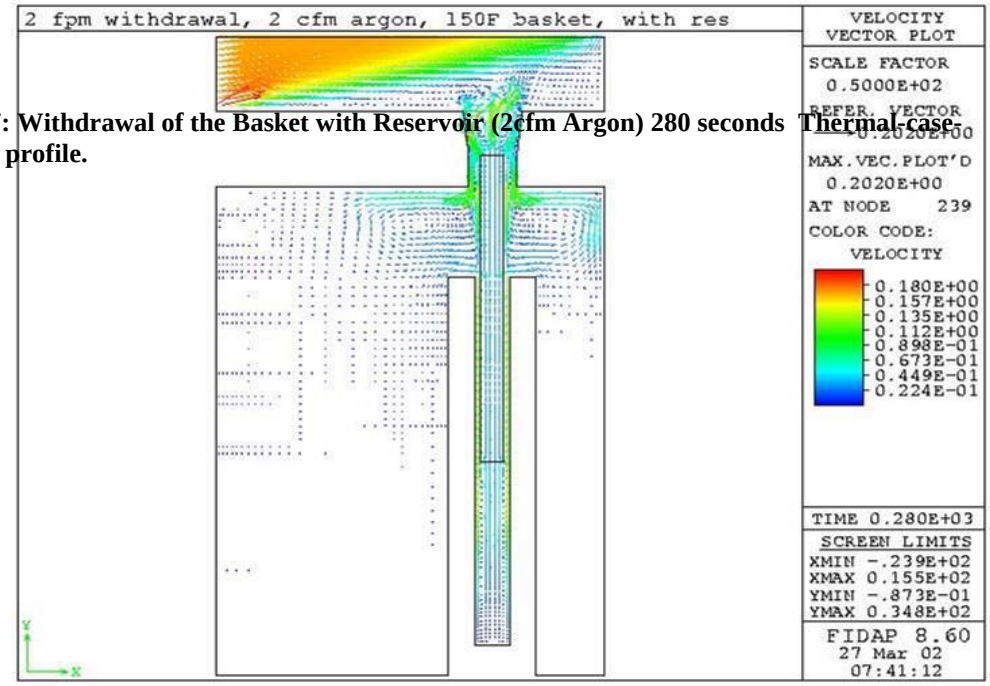

Figure 4.2.27: Withdrawal of the Basket with Reservoir (2cfm Argon) 280 seconds Thermal-case- Temperature profile.

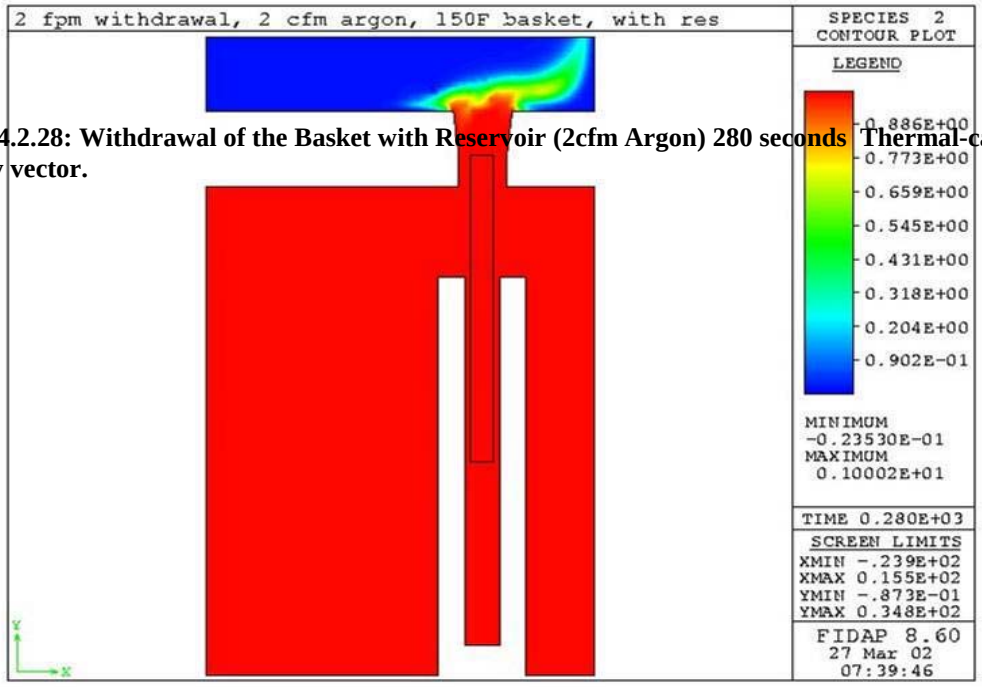

Figure 4.2.28: Withdrawal of the Basket with Reservoir (2cfm Argon) 280 seconds Thermal-case Velocity vector.

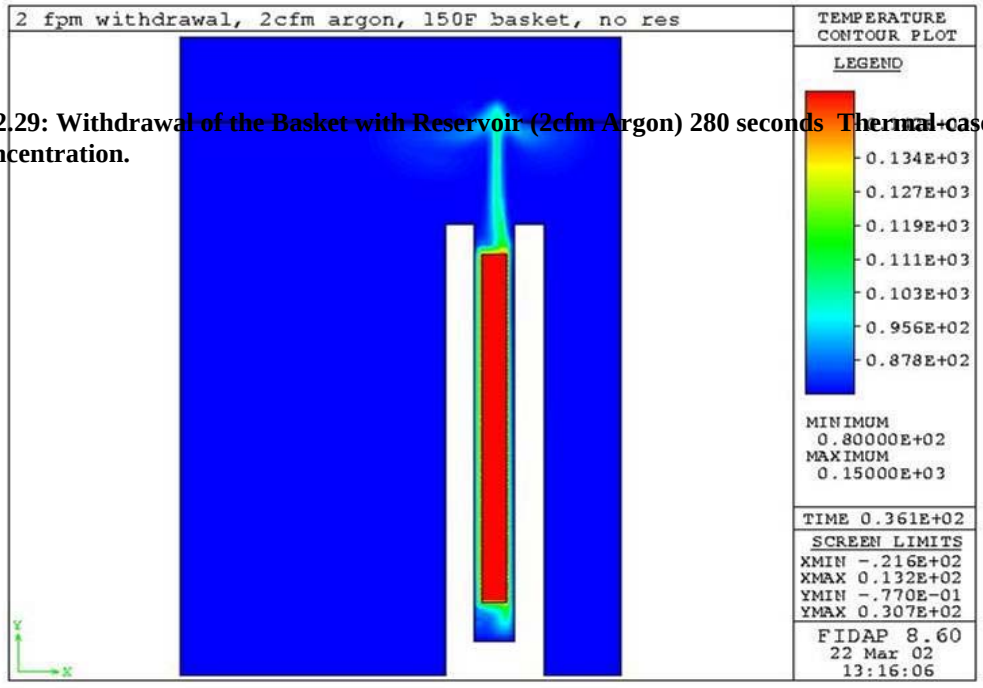

Figure 4.2.29: Withdrawal of the Basket with Reservoir (2cfm Argon) 280 seconds Thermal-case - Argon concentration.

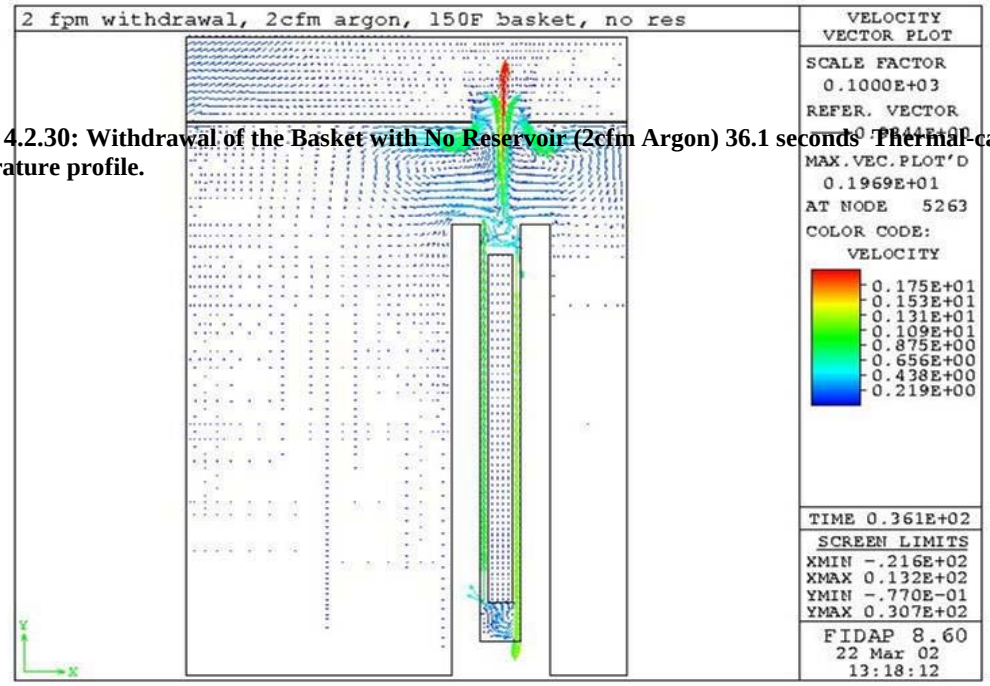

Figure 4.2.30: Withdrawal of the Basket with No Reservoir (2cfm Argon) 36.1 seconds Thermal-case – Temperature profile.

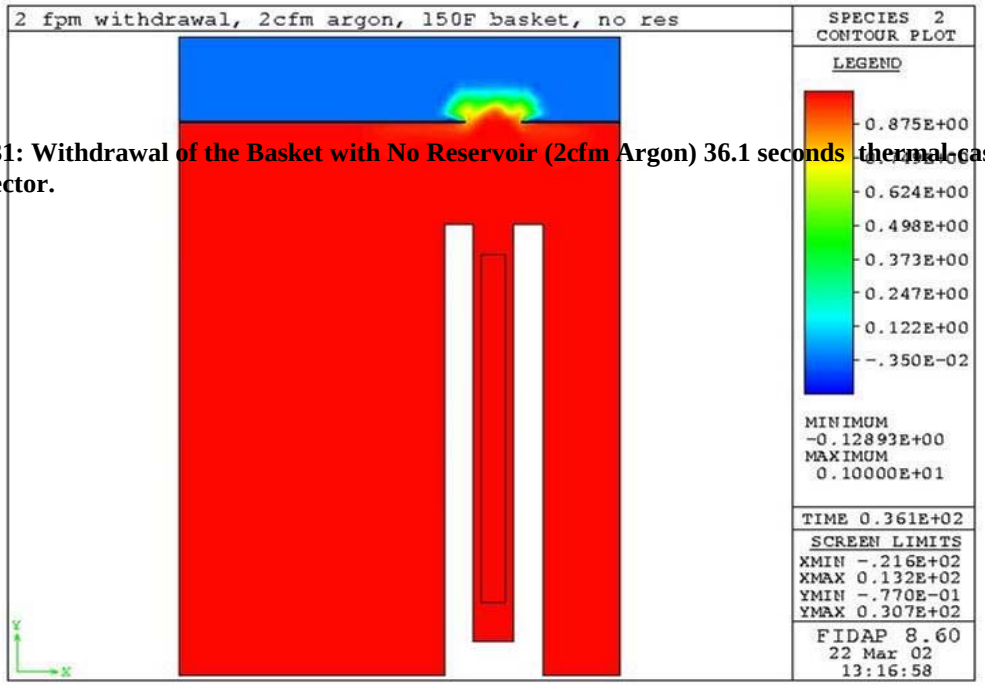

Figure 4.2.31: Withdrawal of the Basket with No Reservoir (2cfm Argon) 36.1 seconds thermal-case -Velocity Vector.

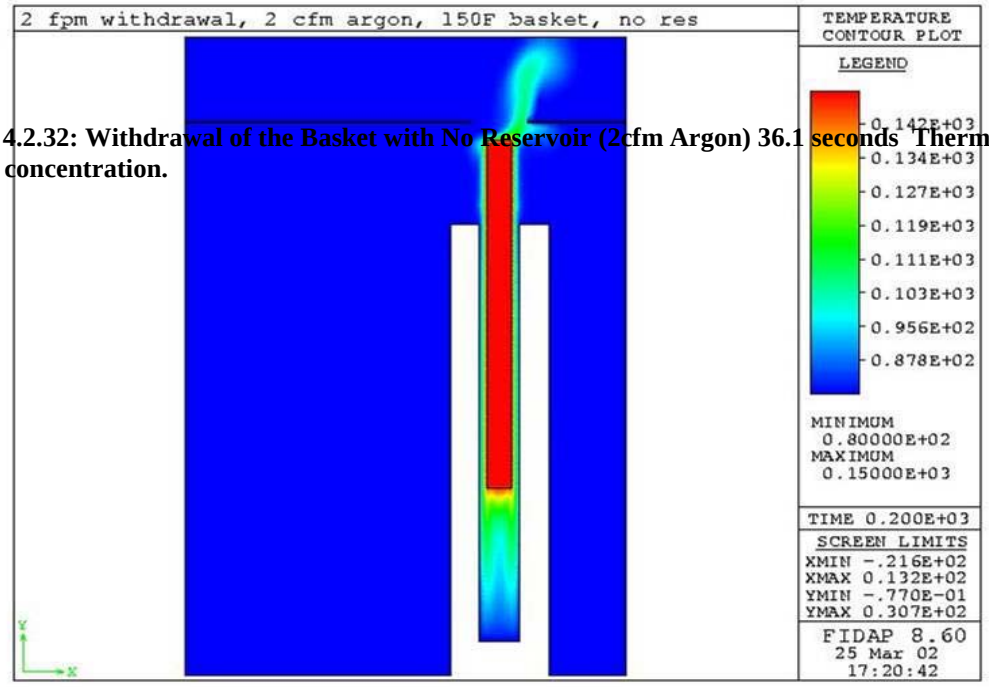

Figure 4.2.32: Withdrawal of the Basket with No Reservoir (2cfm Argon) 36.1 seconds Thermal-case -Argon concentration.

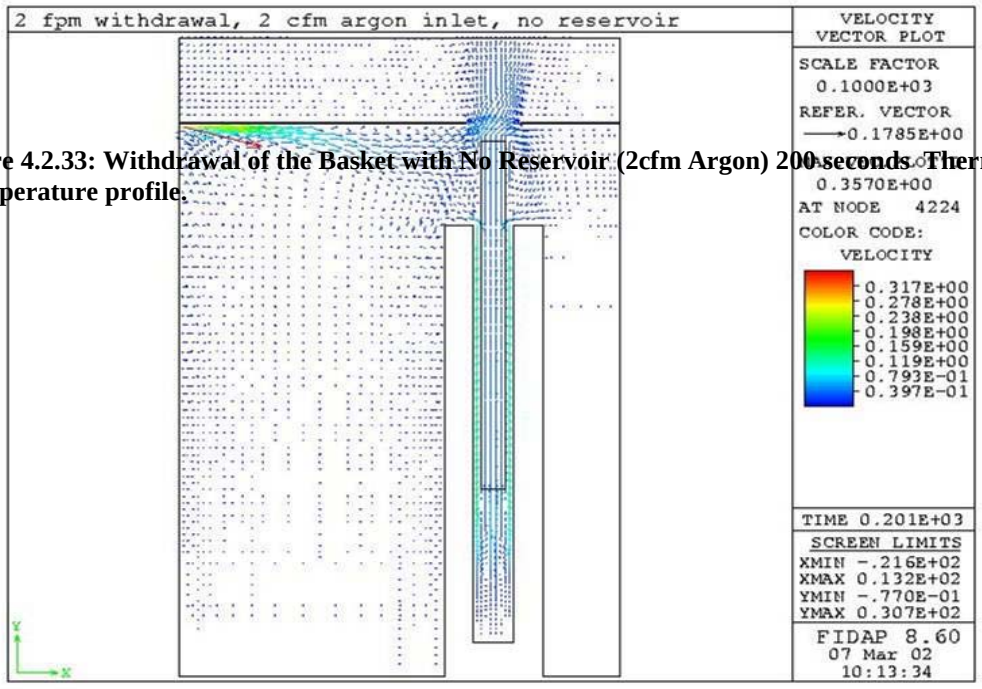

Figure 4.2.33: Withdrawal of the Basket with No Reservoir (2cfm Argon) 200 seconds Thermal-case –Temperature profile.

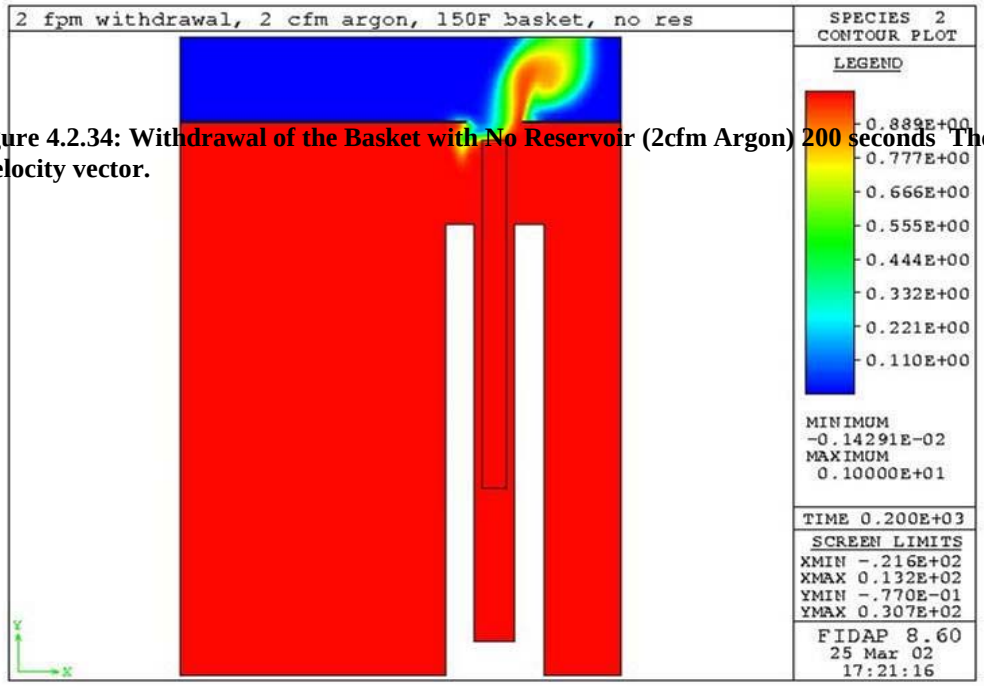

Figure 4.2.34: Withdrawal of the Basket with No Reservoir (2cfm Argon) 200 seconds Thermal-case –Velocity vector.

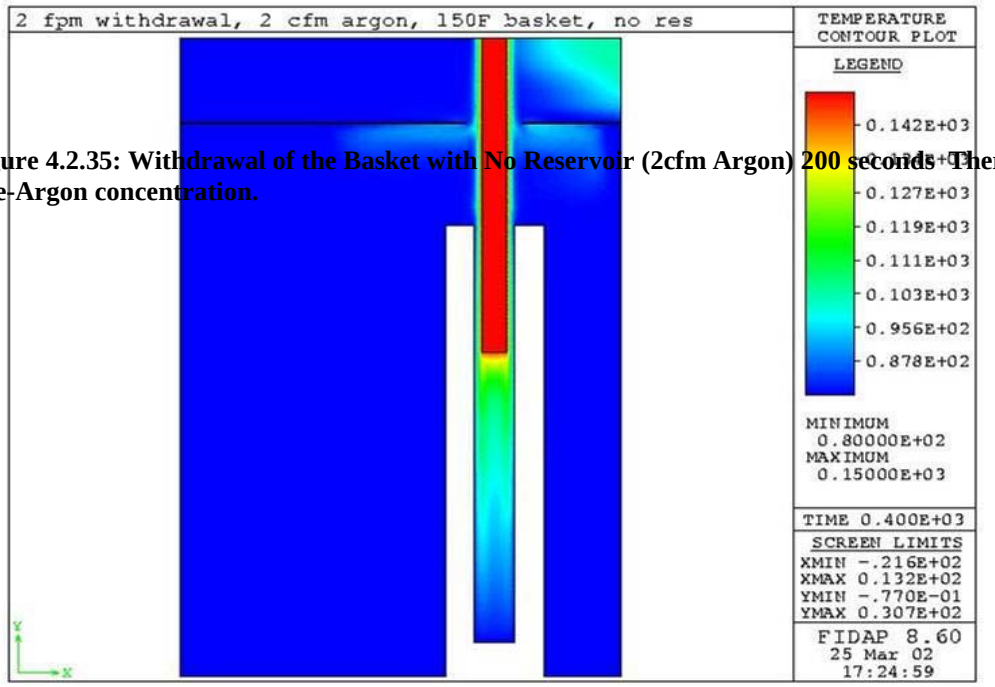

Figure 4.2.35: Withdrawal of the Basket with No Reservoir (2cfm Argon) 200 seconds Thermal-case-Argon concentration.

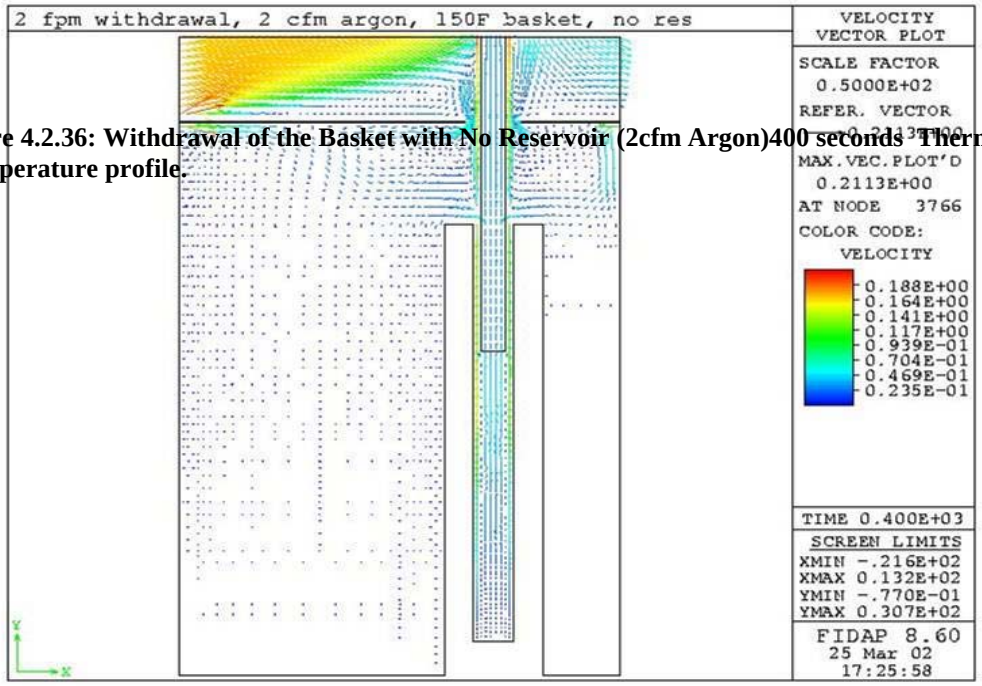

Figure 4.2.36: Withdrawal of the Basket with No Reservoir (2cfm Argon)400 seconds -Thermal-case –Temperature profile.

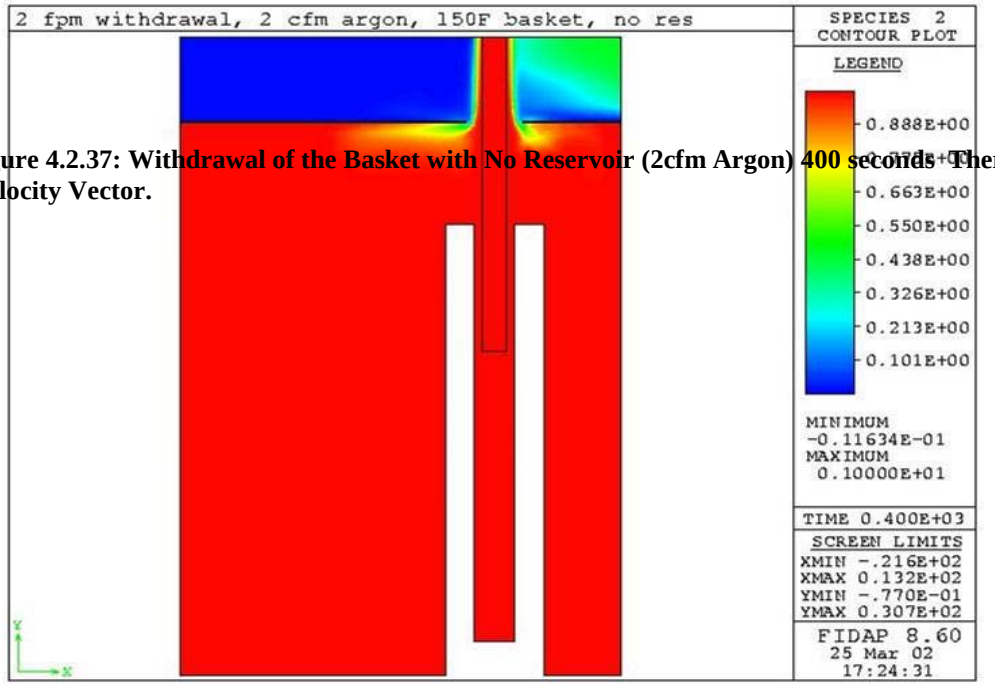

Figure 4.2.37: Withdrawal of the Basket with No Reservoir (2cfm Argon) 400 seconds -Thermal-case -Velocity Vector.

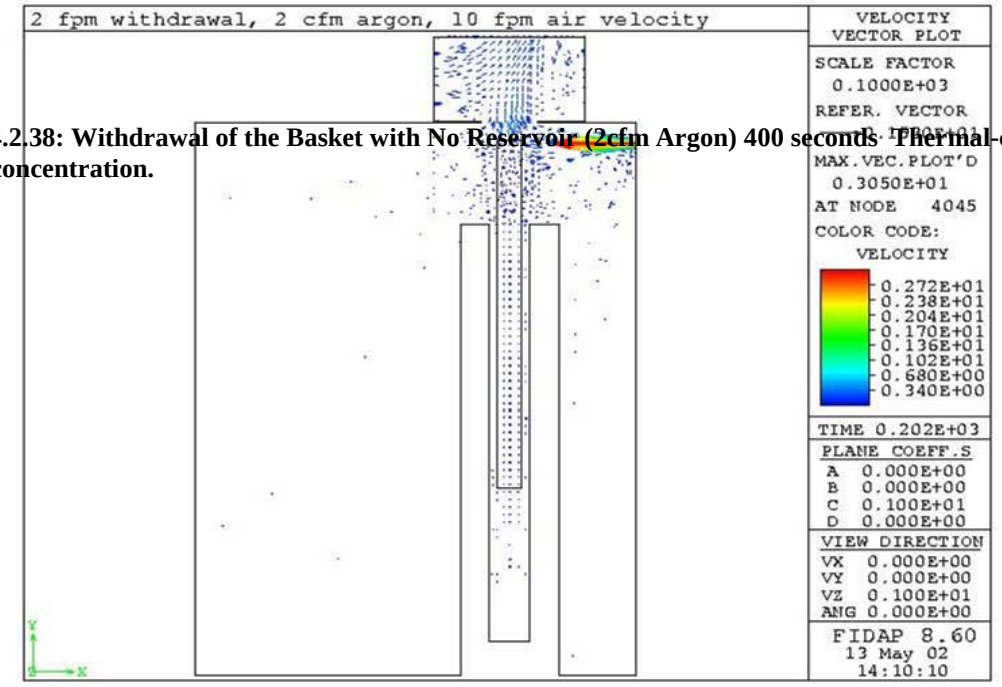

Figure 4.2.38: Withdrawal of the Basket with No Reservoir (2cfm Argon) 400 seconds -Thermal-case -Argon concentration.

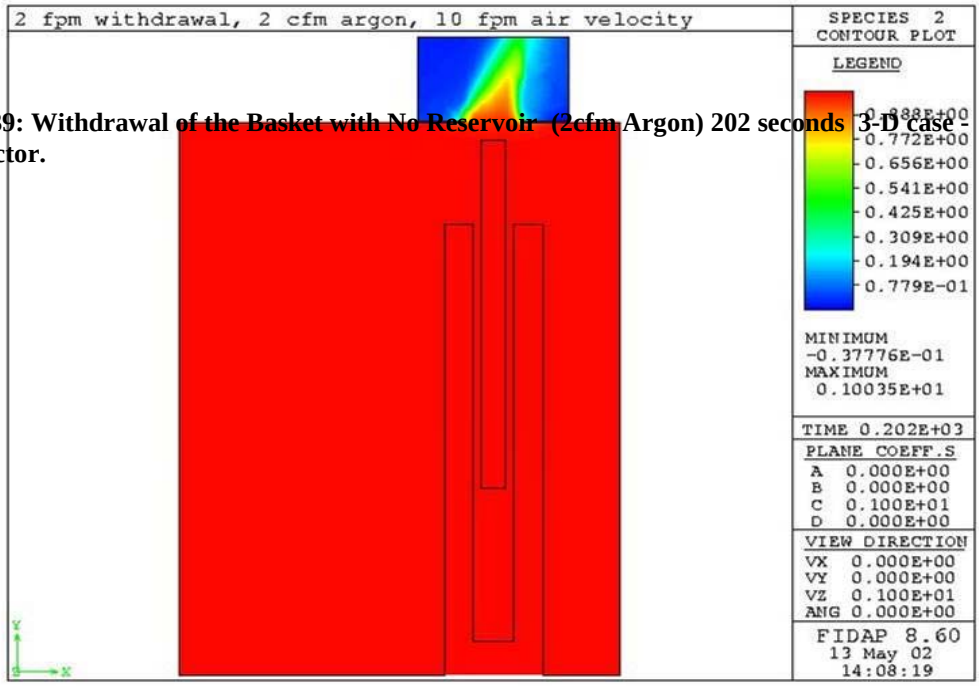

Figure 4.2.39: Withdrawal of the Basket with No Reservoir (2cfm Argon) 202 seconds -3-D case - Velocity Vector.

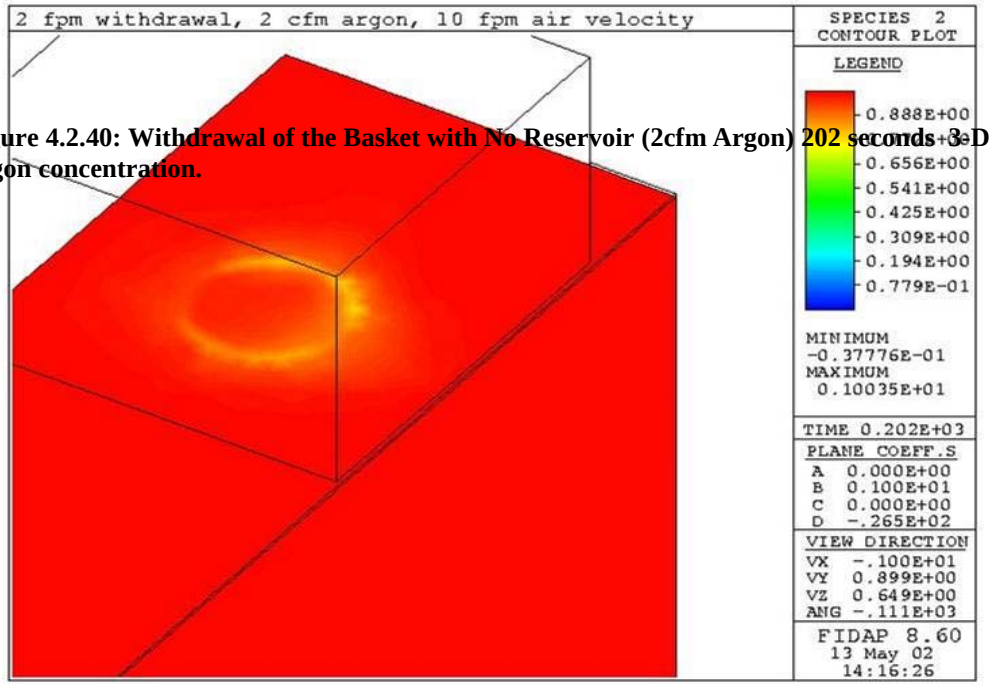

Figure 4.2.40: Withdrawal of the Basket with No Reservoir (2cfm Argon) 202 seconds 3-D case- Argon concentration.

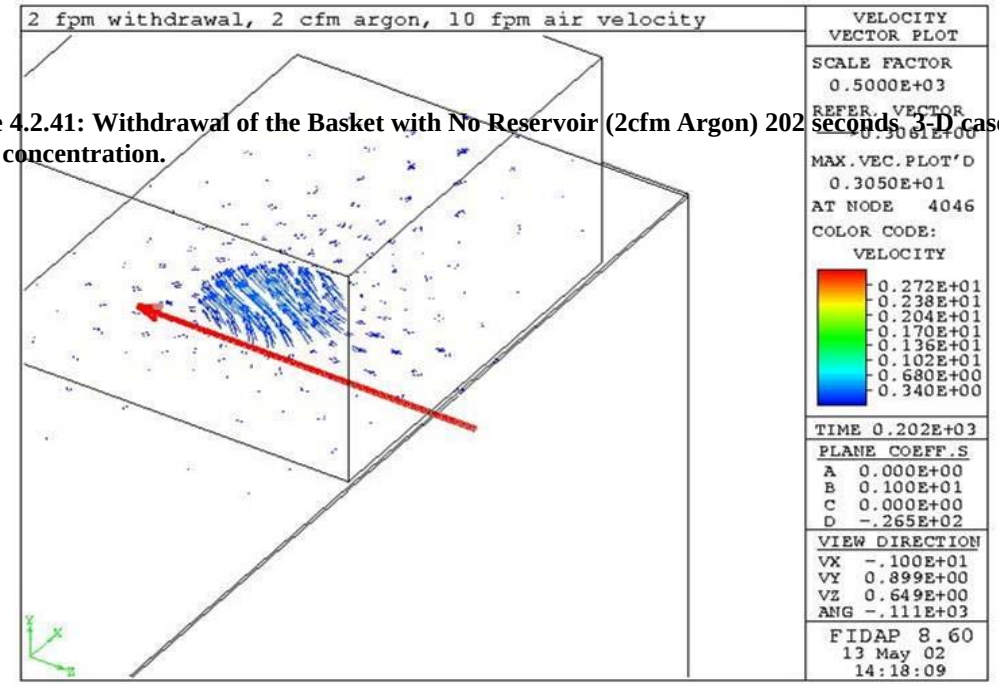

Figure 4.2.41: Withdrawal of the Basket with No Reservoir (2cfm Argon) 202 seconds 3-D case- Argon concentration.

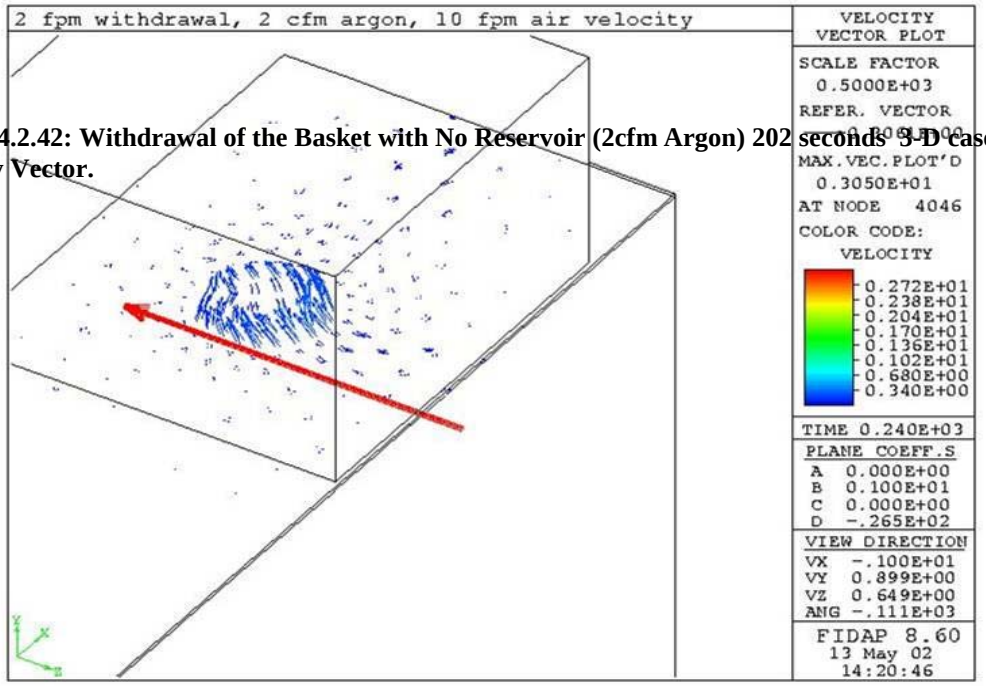

Figure 4.2.42: Withdrawal of the Basket with No Reservoir (2cfm Argon) 202 seconds 3-D case-Velocity Vector.

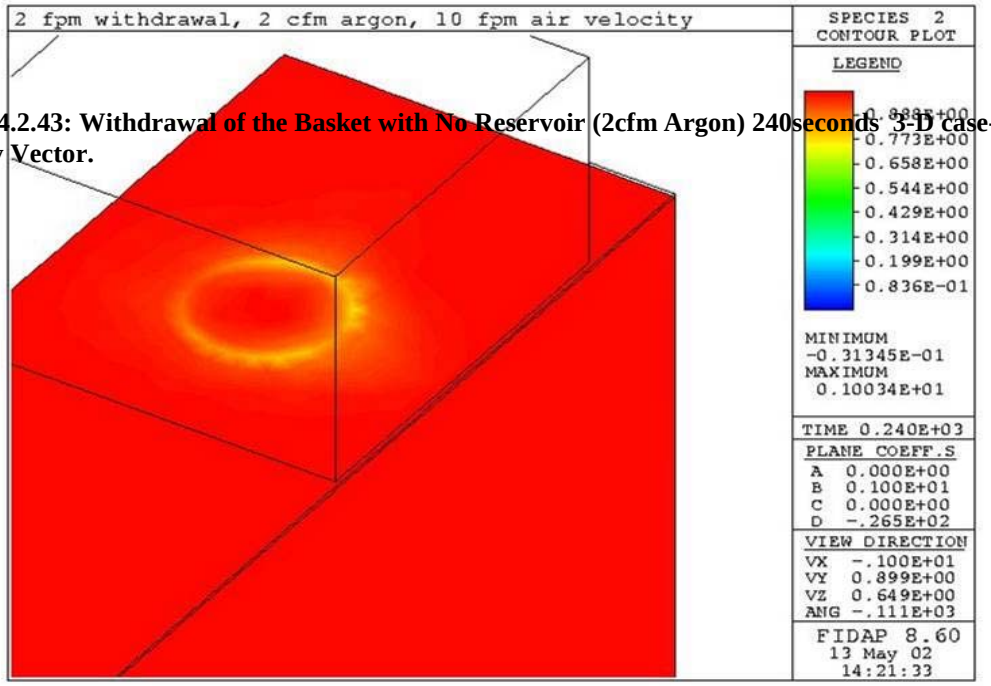

Figure 4.2.43: Withdrawal of the Basket with No Reservoir (2cfm Argon) 240seconds 3-D case-Velocity Vector.

Figure 4.2.44: Withdrawal of the Basket with No Reservoir (2cfm Argon) 240 seconds 3-D case-Argon concentration

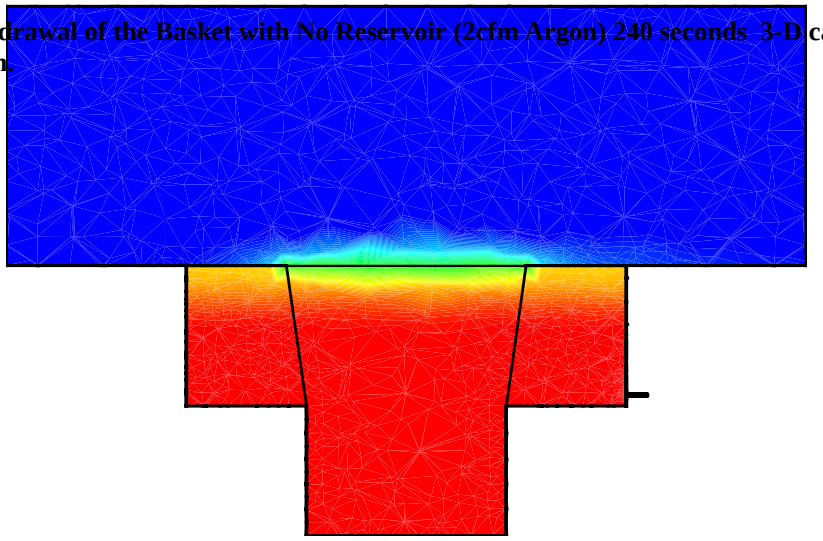

Figure 4.2.45: Reservoir Filling after 7687 secs (air 10 ft/m, argon 2.0 cfm).

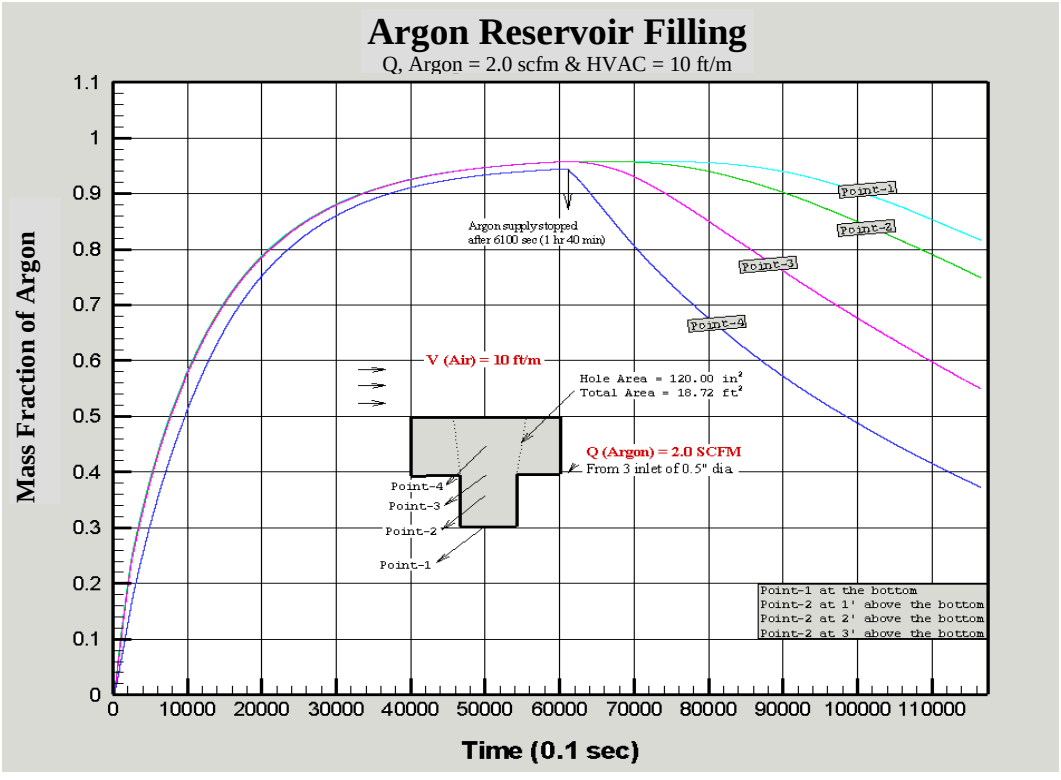

Figure 4.2.46: Filling the Argon Reservoir while HVAC air is Blowing across the Reservoir.

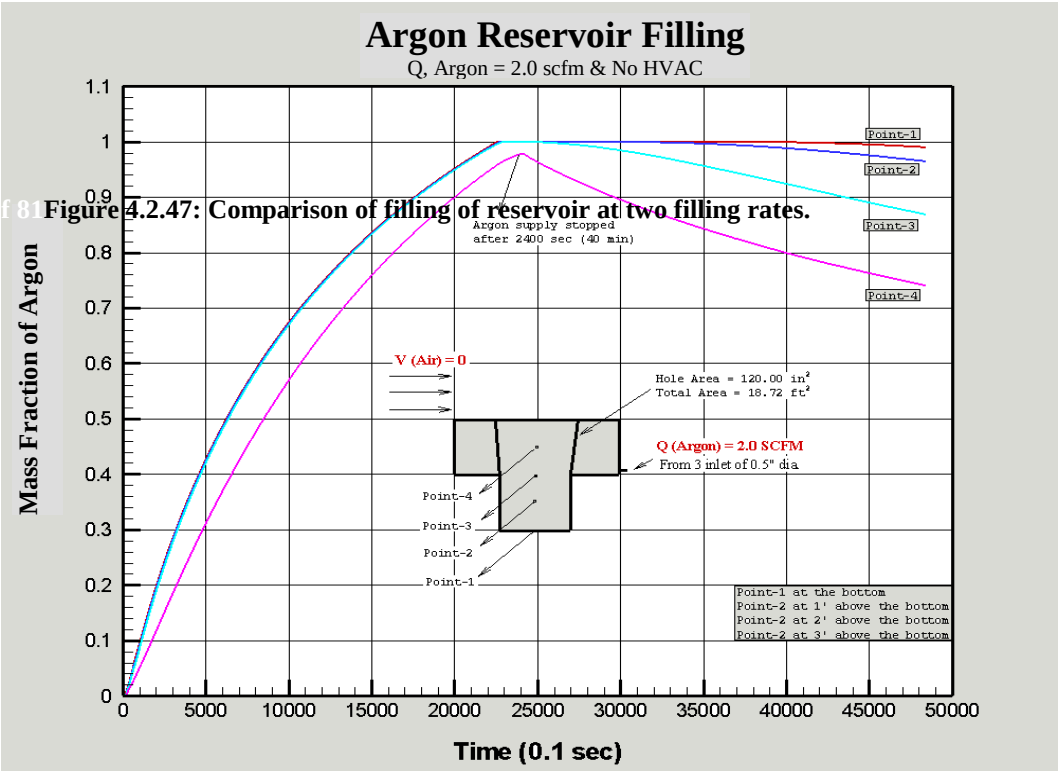

Figure 4.2.47: Comparison of filling of reservoir at two filling rates.

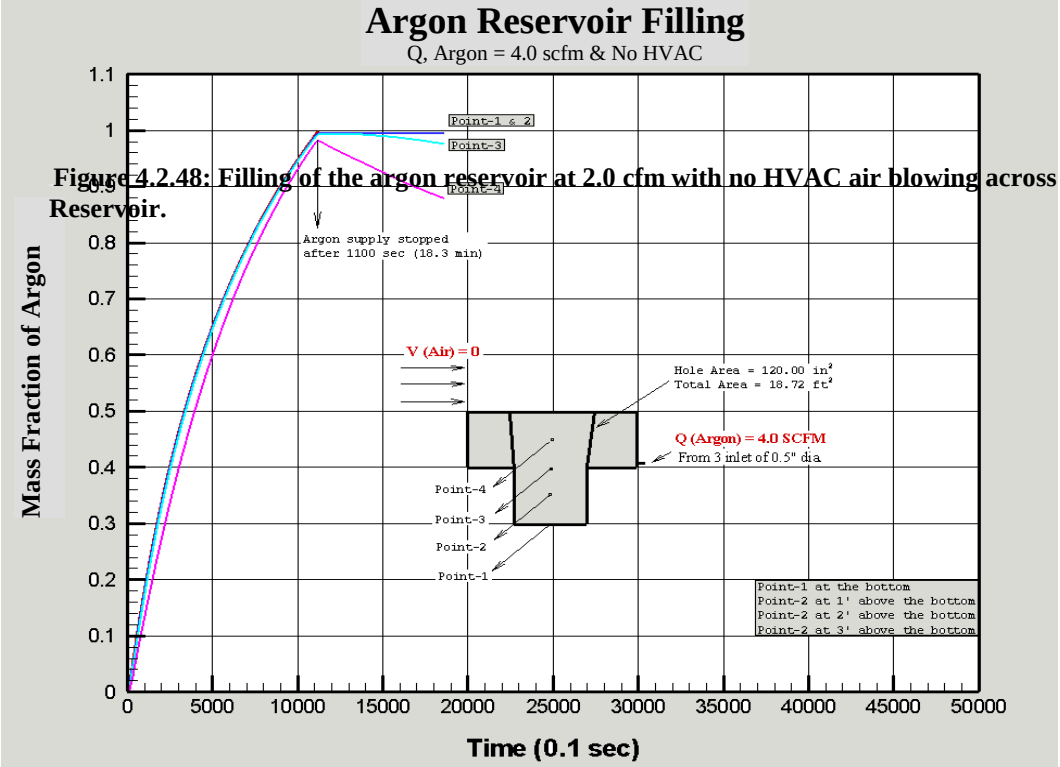

Figure 4.2.48: Filling of the argon reservoir at 2.0 cfm with no HVAC air blowing across the Reservoir.

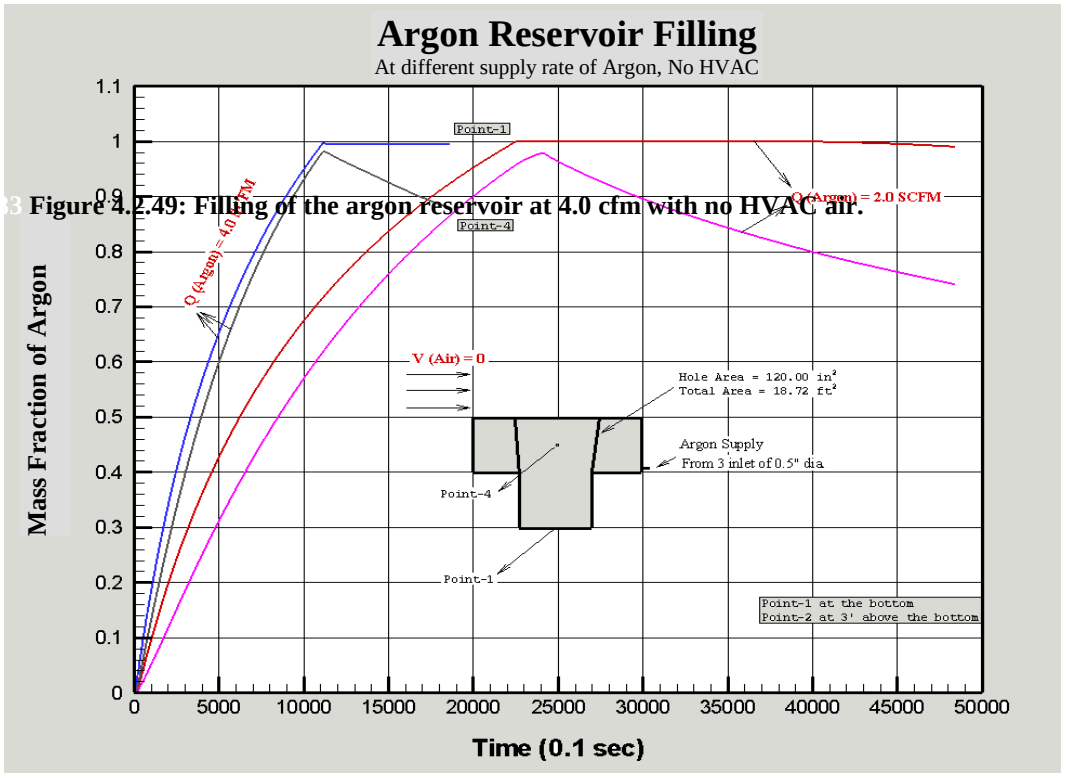

Figure 4.2.49: Filling of the argon reservoir at 4.0 cfm with no HVAC air.

Figure 4.2.50: Comparison of the Filling time for two different flow rates with no HVAC air.

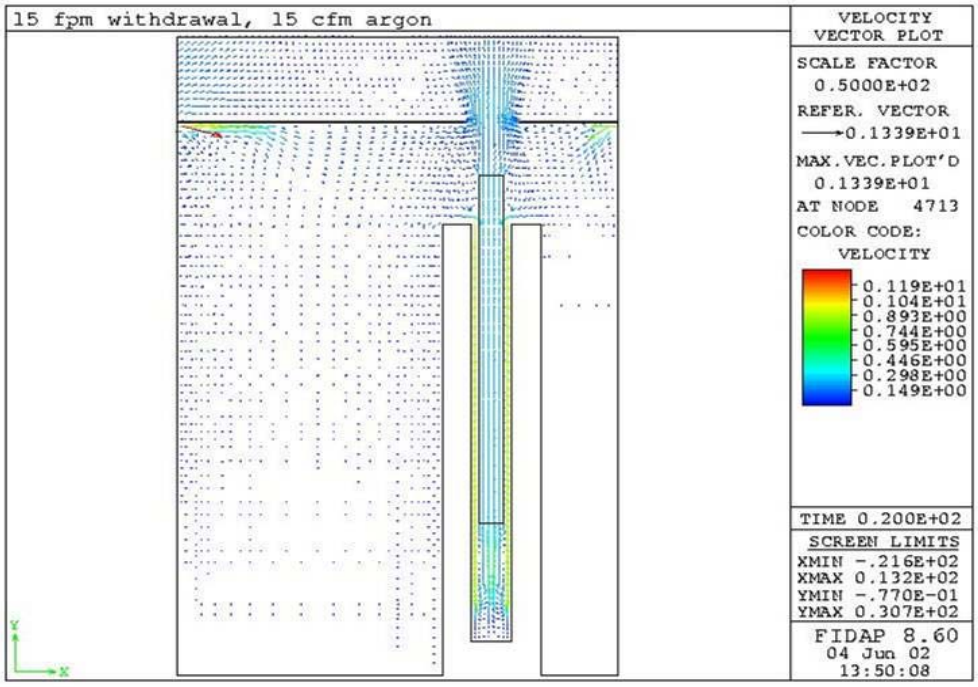

Figure 4.2.51: Velocity vectors at 20 seconds for 15 ft/min withdrawal-Velocity vector.

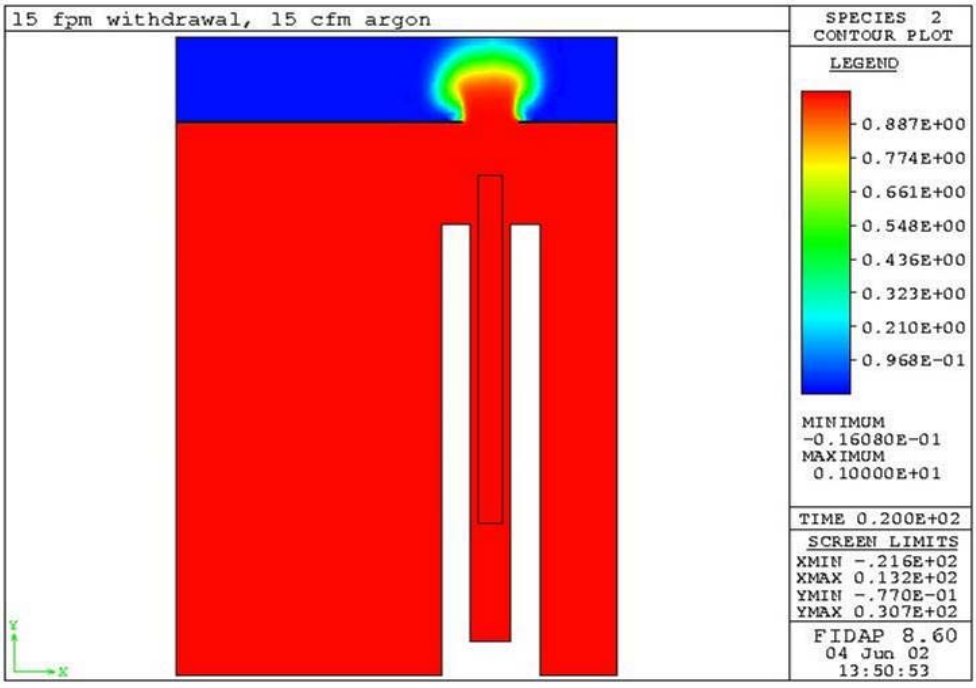

Figure 4.2.52: Species concentration at 20 seconds for 15 ft/min withdrawal-Argon concentration.

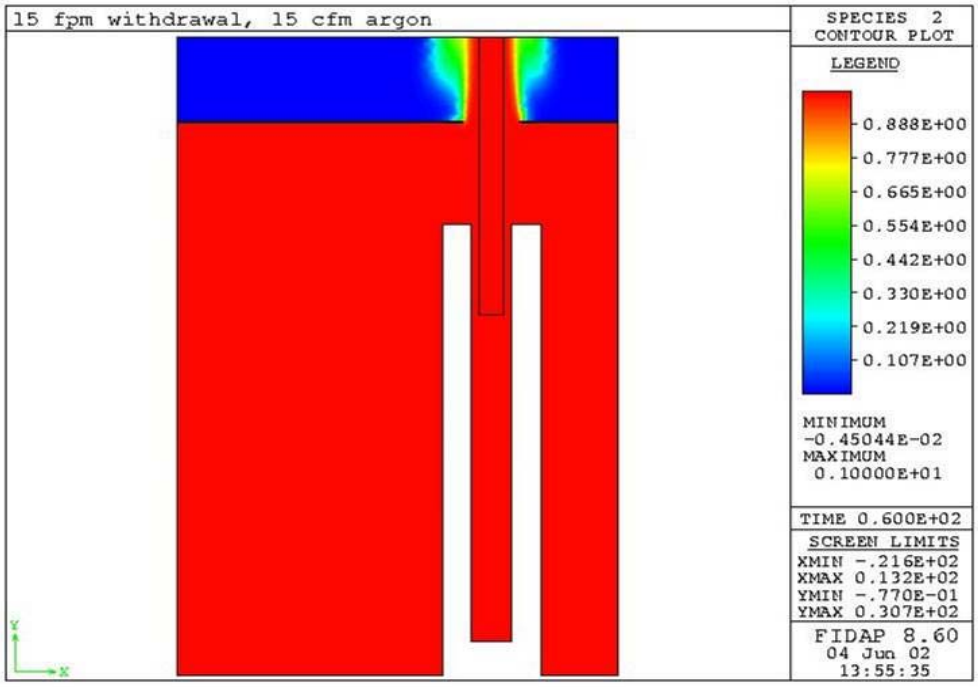

Figure 4.2.53: Species concentration at 60 seconds for 15 ft/min withdrawal-Argon concentration.

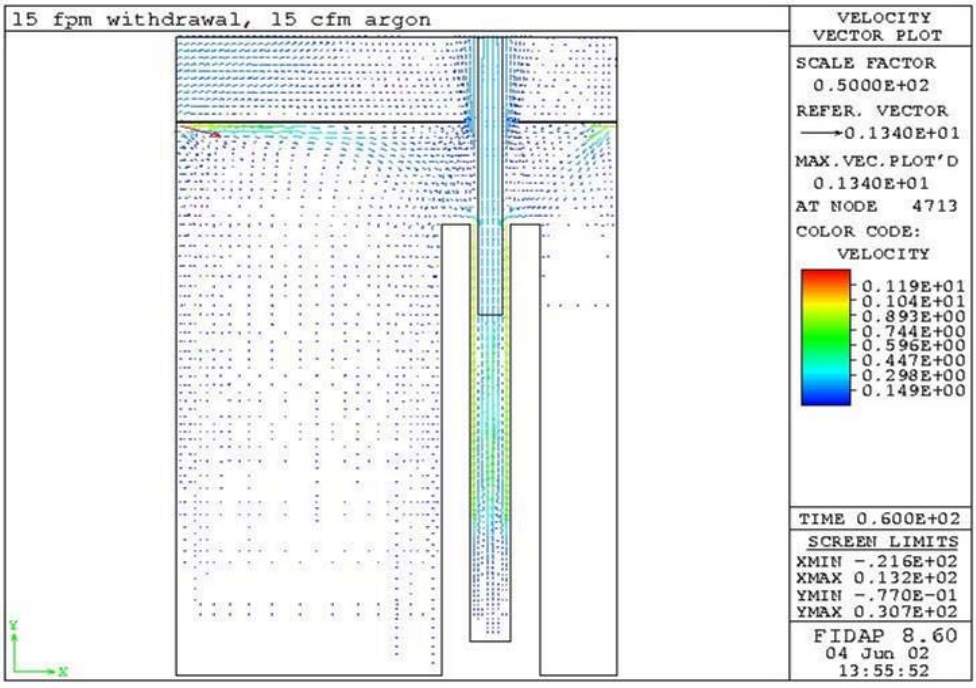

Figure 4.2.54: Velocity vectors at 60 seconds for 15 ft/min withdrawal-Velocity vector.

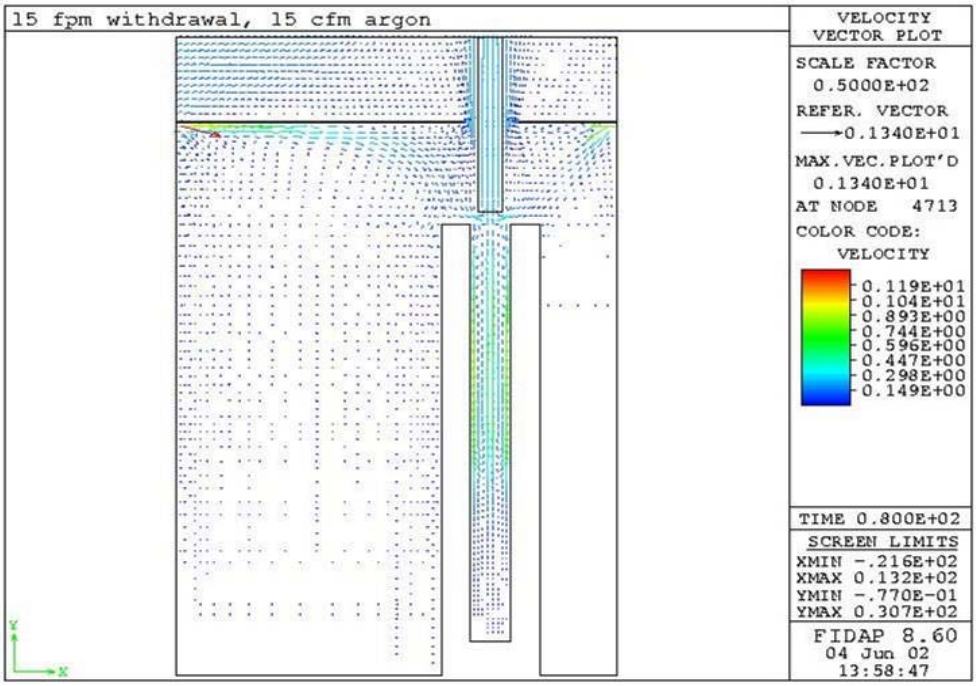

Figure 4.2.55: Velocity vectors at 80 seconds for 15 ft/min withdrawal-Velocity vector.

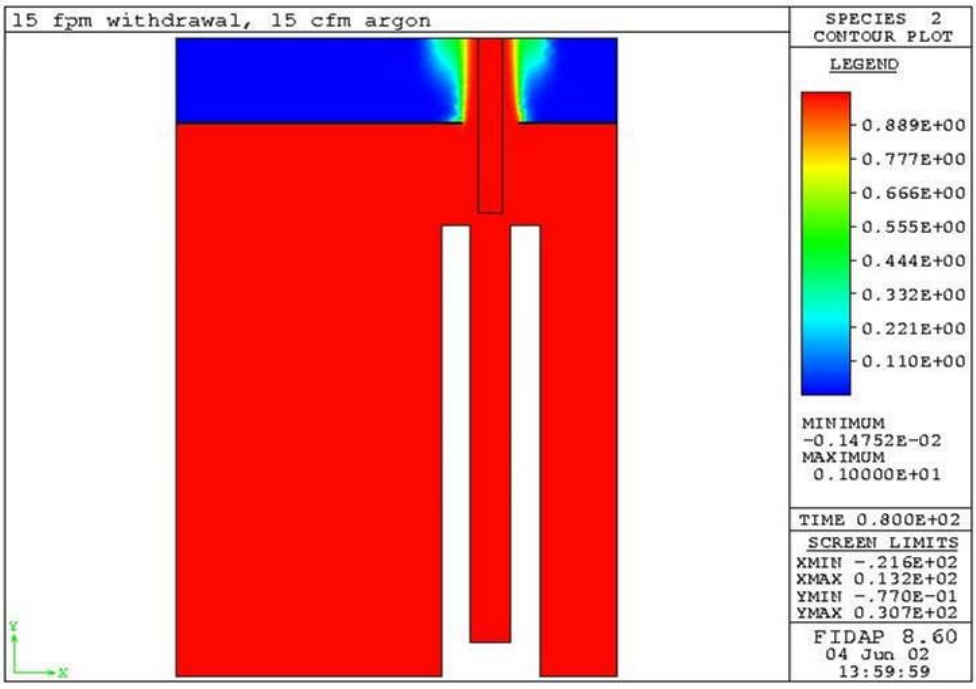

Figure 4.2.56: Species concentration at 20 seconds for 15 ft/min withdrawal-Argon concentration.

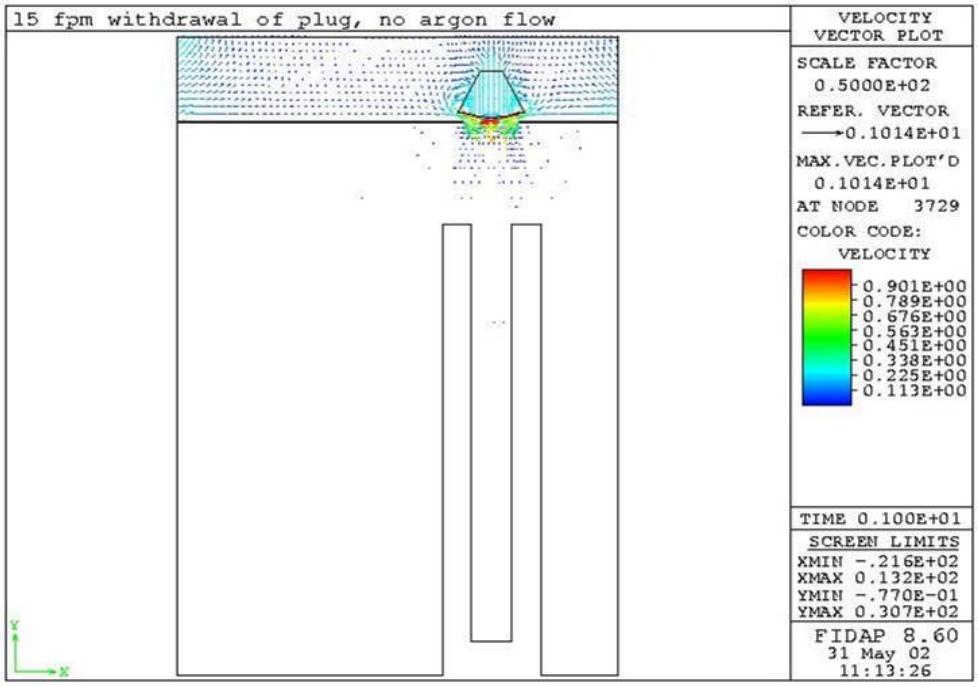

Figure 4.2.57: Velocity vectors during the lifting of the plug at 15 ft/min (1.0 seconds) -Velocity vector.

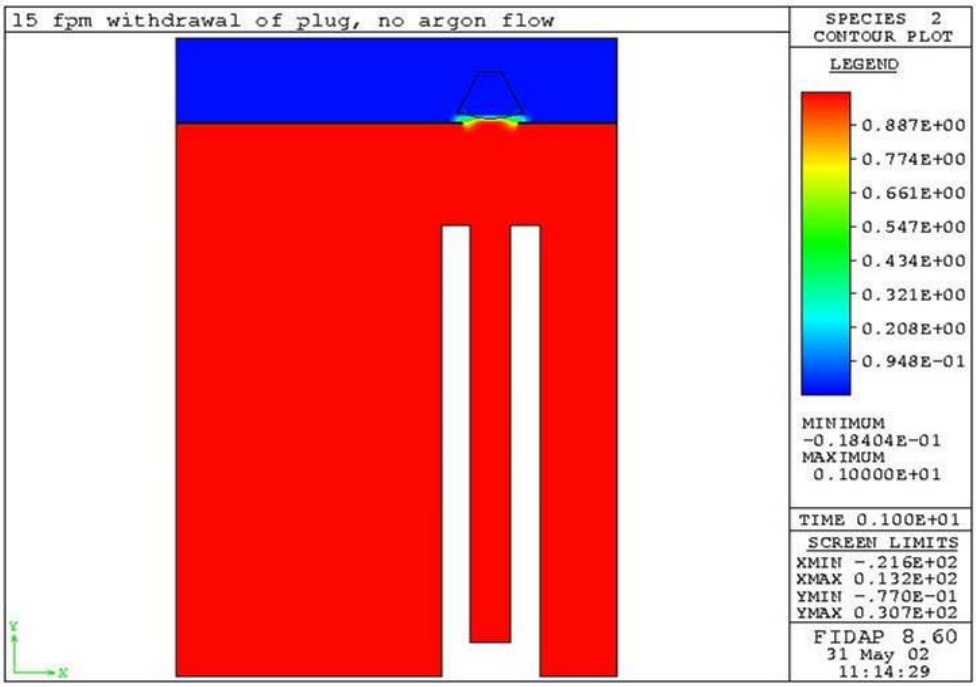

Figure 4.2.58: Species concentration during the lifting of the plug at 15 ft/min (1.0 seconds) -Argon concentration.

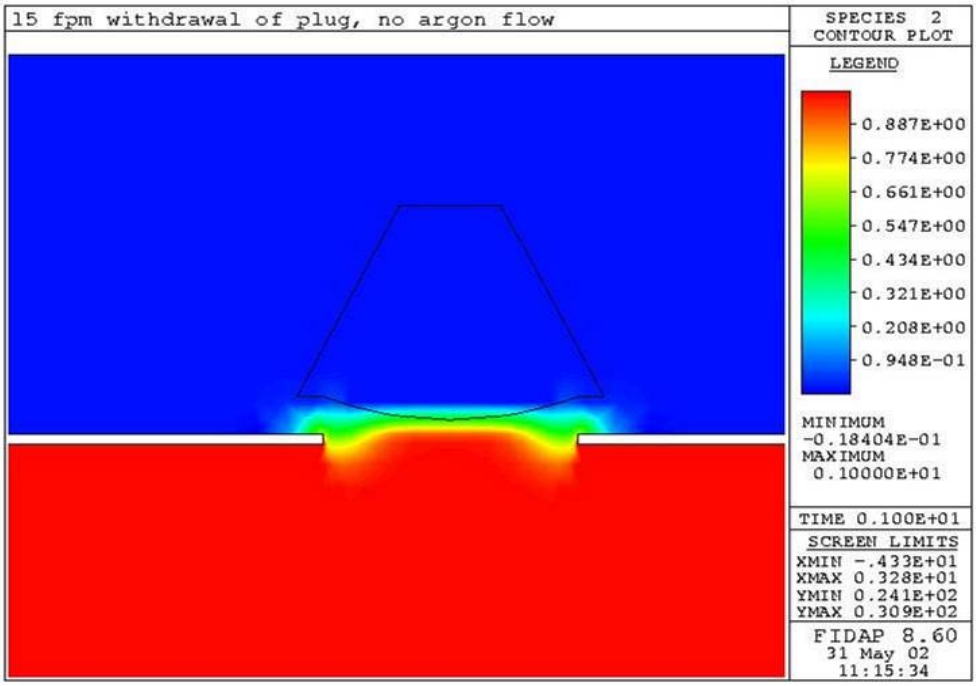

Figure 4.2.59: Species concentration during the lifting of the plug at 15 ft/min (1.0 seconds) -Argon concentration.

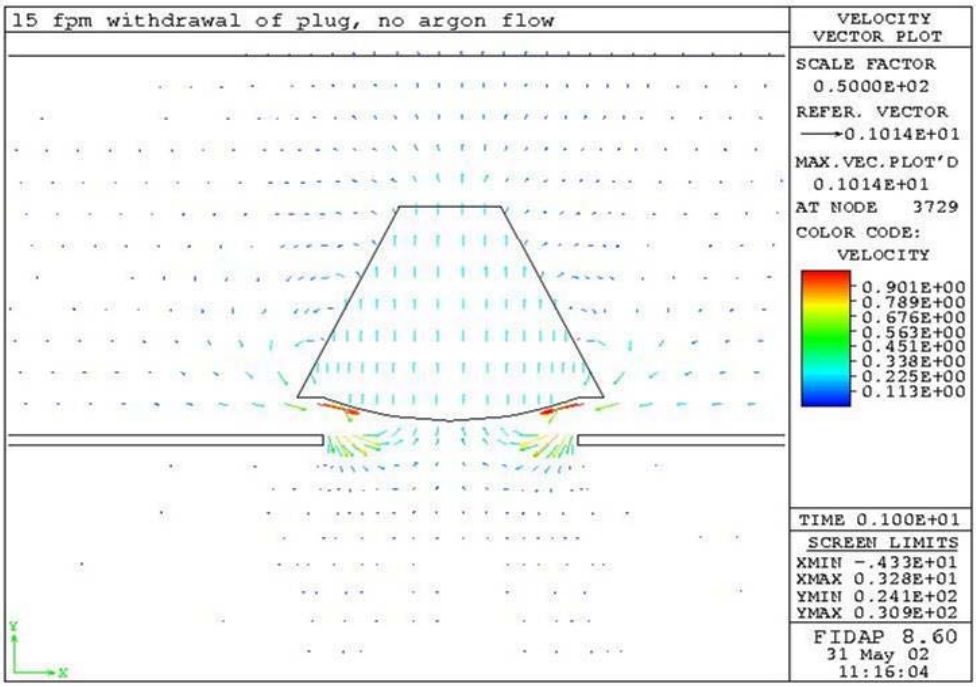

Figure 4.2.60: Velocity vectors during the lifting of the plug at 15 ft/min (1.0 seconds) -Velocity vector.

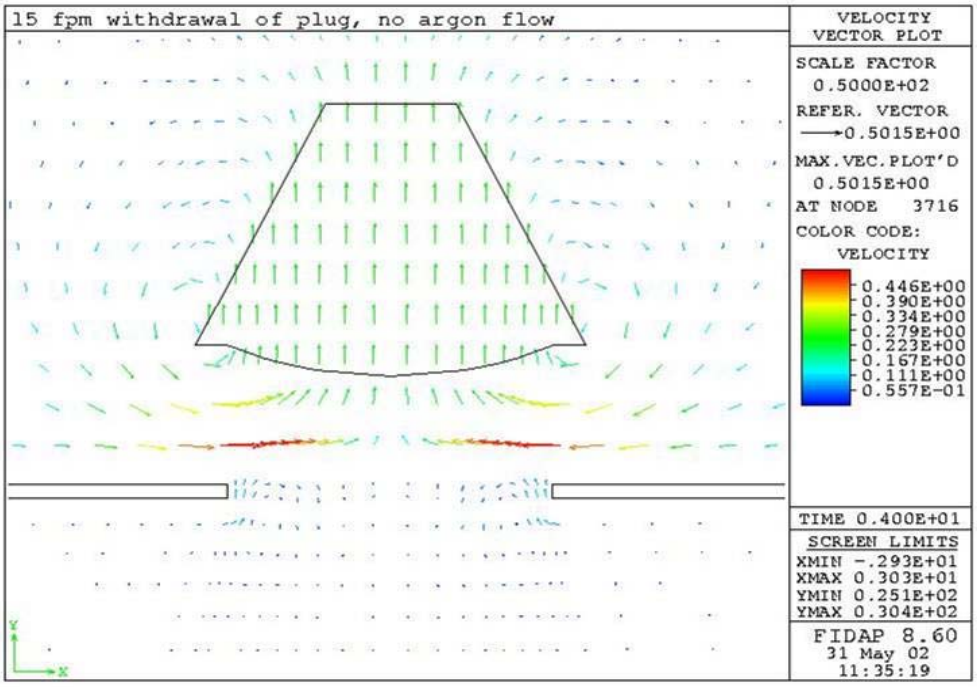

Figure 4.2.61: Velocity vectors during the lifting of the plug at 15 ft/min (10.0 seconds) -Velocity vector.

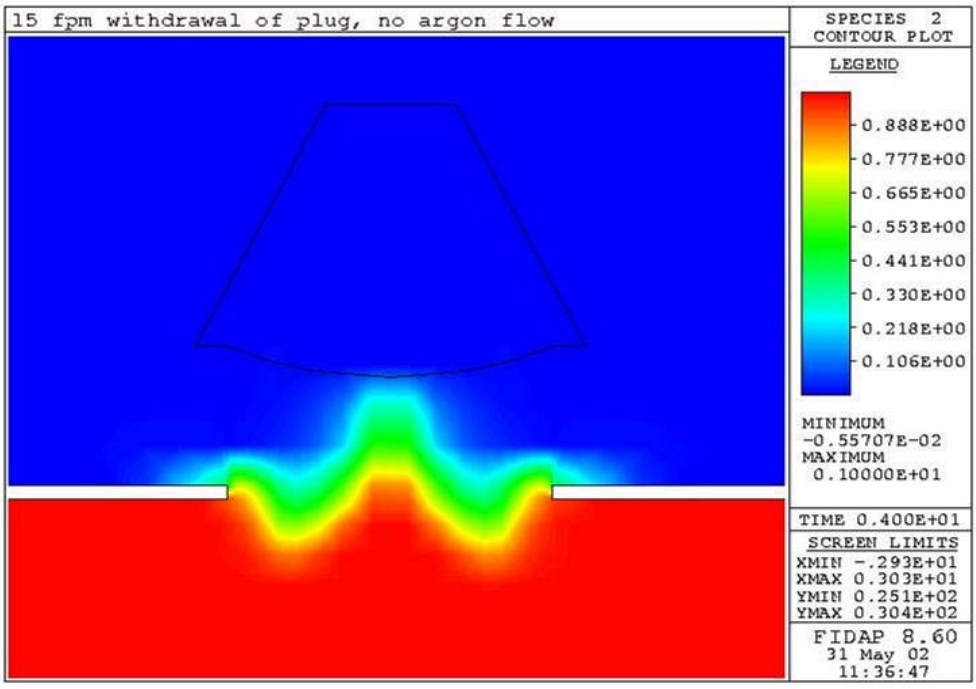

Figure 4.2.62: Species concentration during the lifting of the plug at 15 ft/min (10.0 seconds) -Argon concentration.

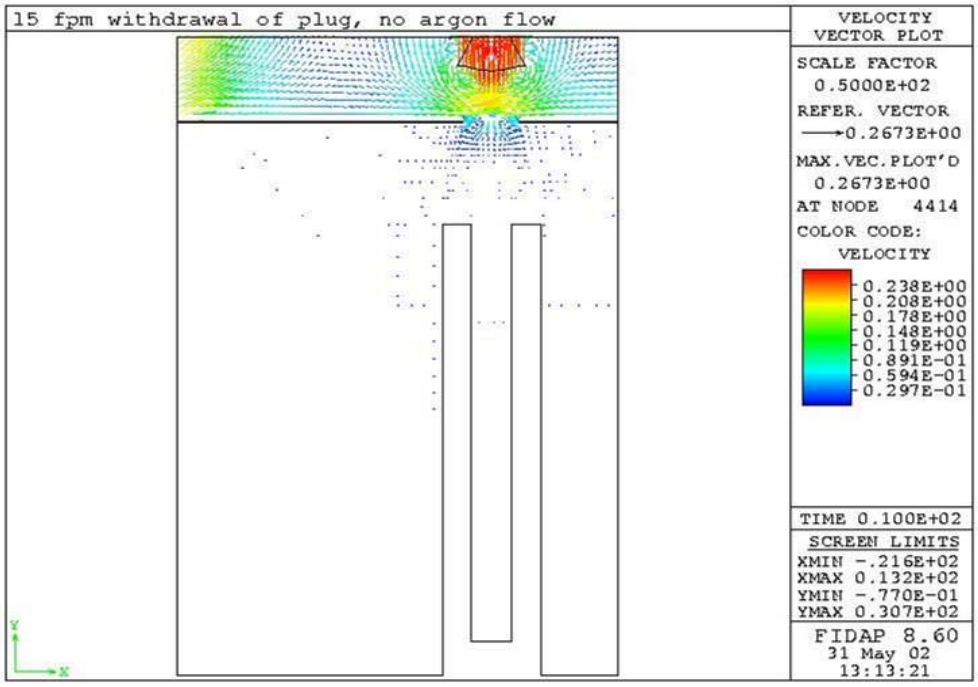

Figure 4.2.63: Velocity vectors during the lifting of the plug at 15 ft/min (10.0 seconds) -Velocity vector.

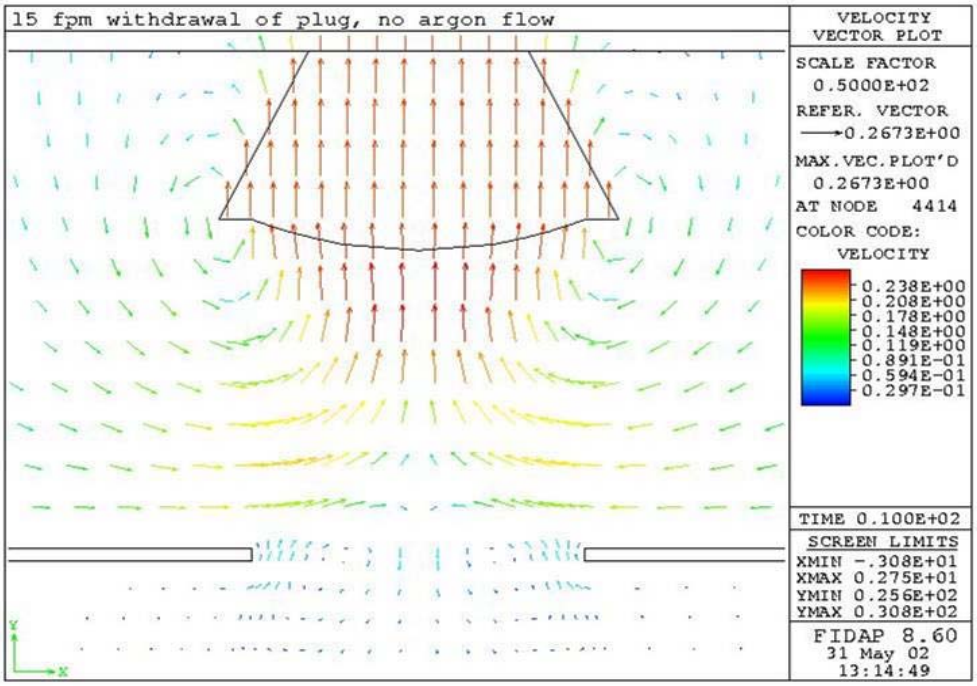

Figure 4.2.64: Velocity vectors during the lifting of the plug at 15 ft/min (10.0 seconds) -Velocity vector.

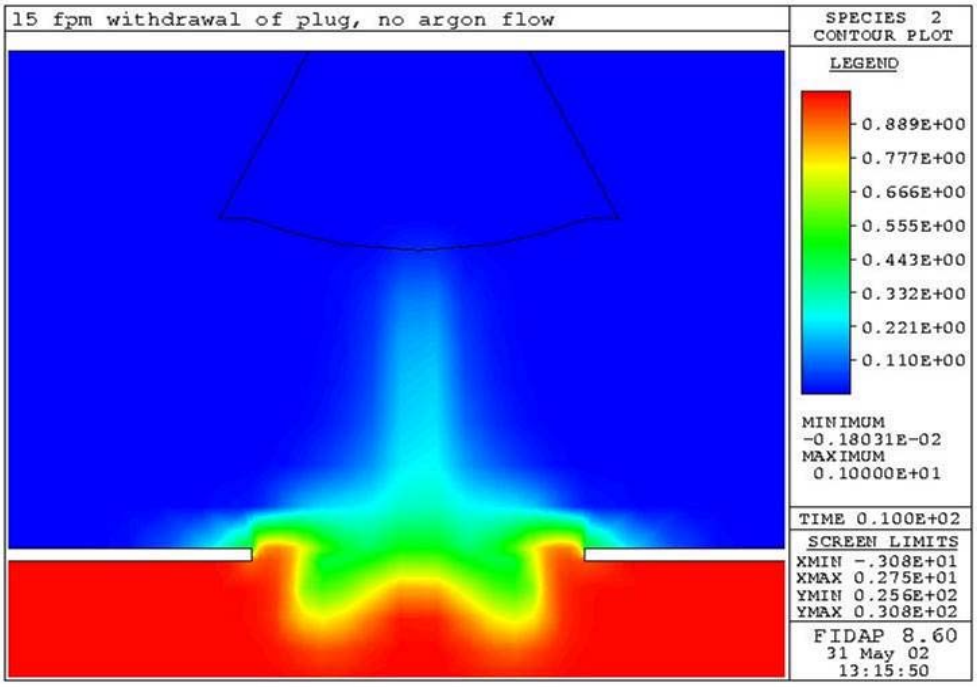

Figure 4.2.65: Species concentration during the lifting of the plug at 15 ft/min (1.0 seconds) -Argon concentration.

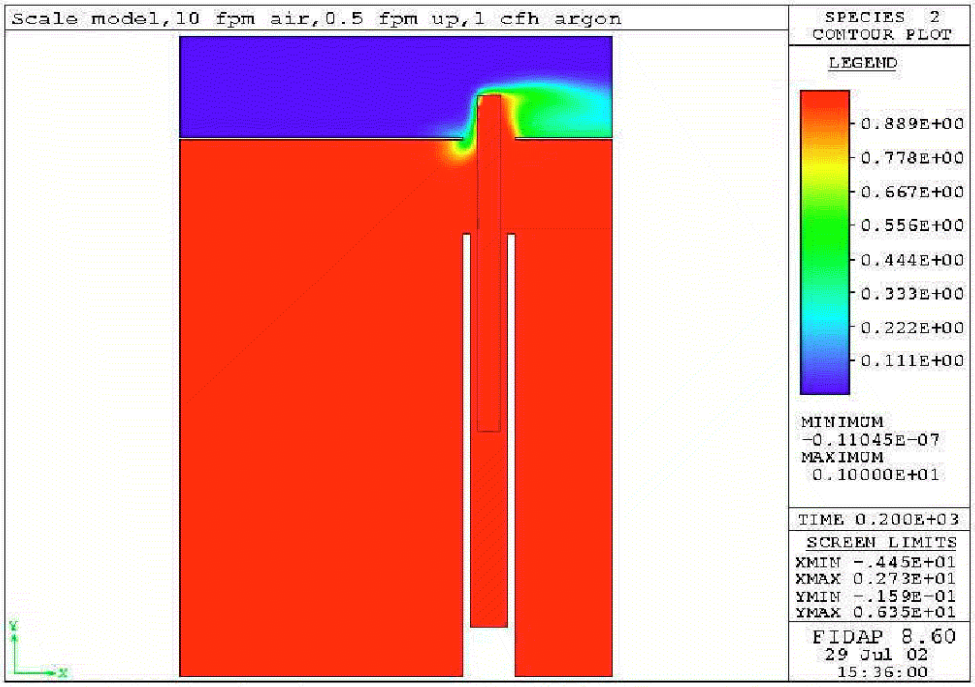

Figure 4.2.66: Computational results for the model with 1 cfh argon make-up and 0.5 ft/min withdrawal with 10 ft/min HVAC air-Argon concentration.

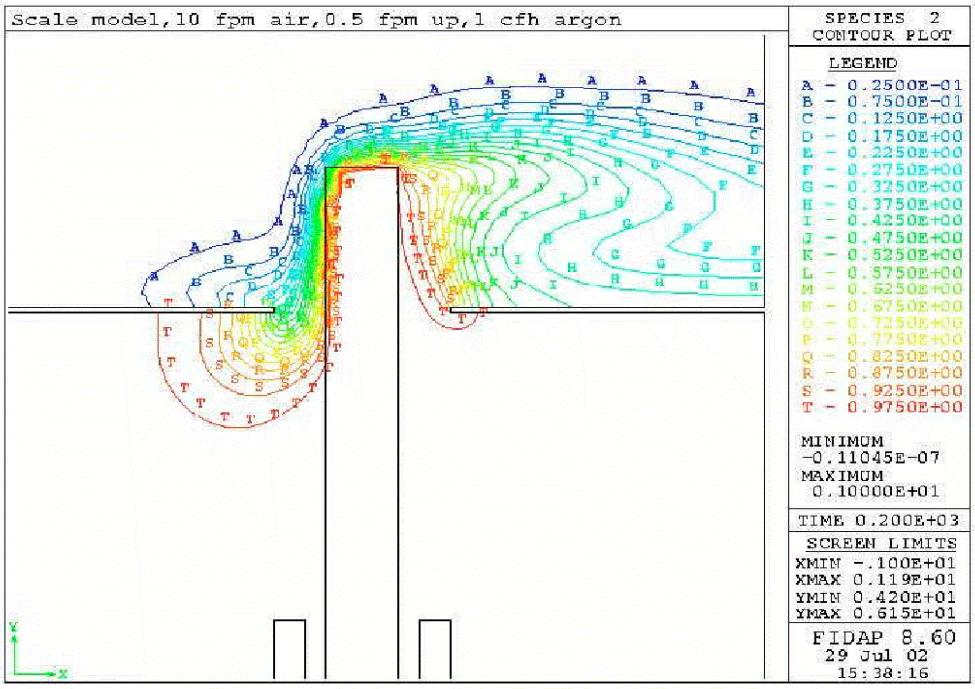

Figure 4.2.67: Computational results for the model with 1 cfh argon make-up and 0.5 ft/min withdrawal with 10 ft/min HVAC air-Argon contour.

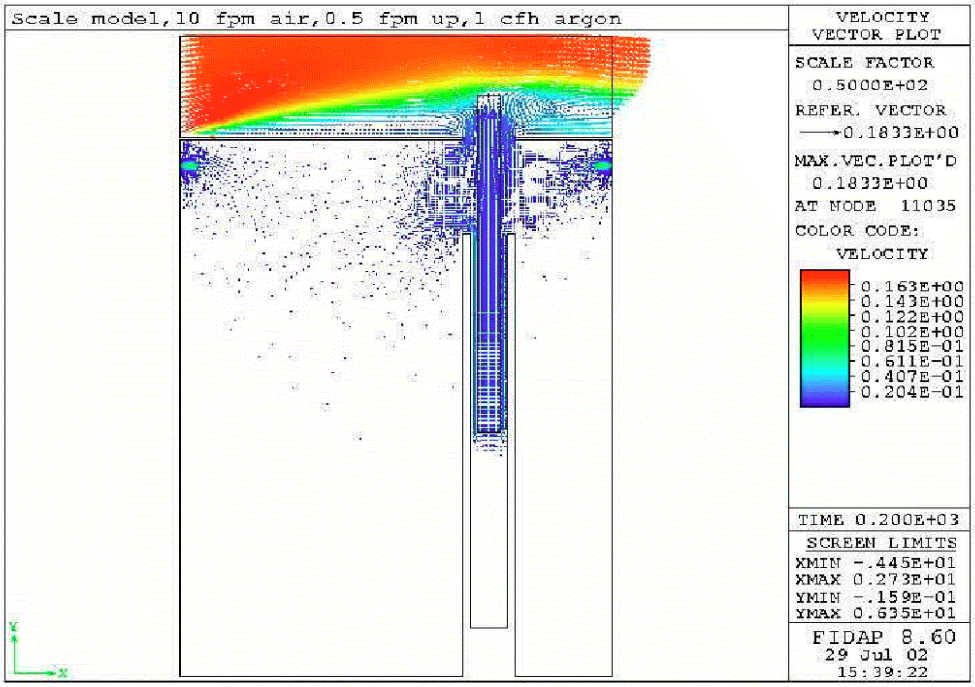

Figure 4.2.68: Computational results for the model with 1 cfh argon make-up and 0.5 ft/min withdrawal with 10 ft/min HVAC air-Velocity vector.

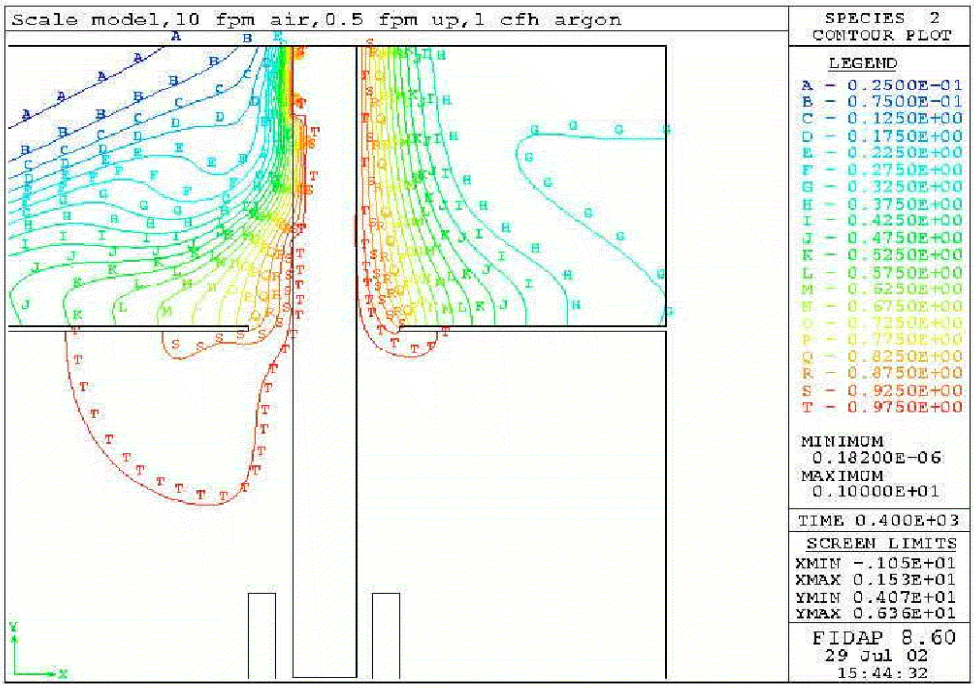

Figure 4.2.69: Computational results for the model with 1 cfh argon make-up and 0.5 ft/min withdrawal with 10 ft/min HVAC air- Argon contour.

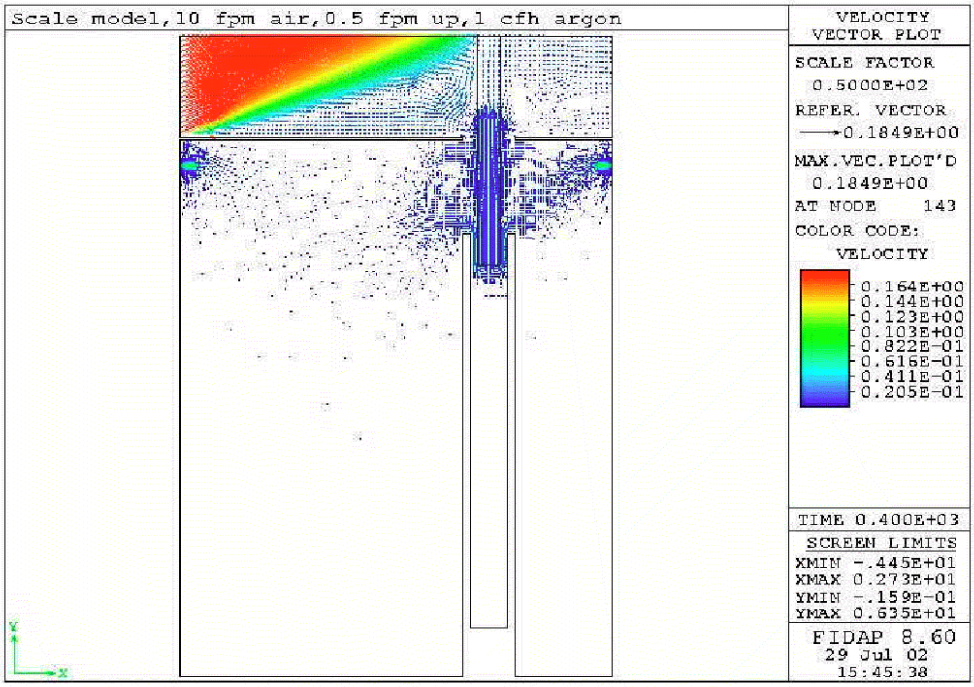

Figure 4.2.70: Computational results for the model with 1 cfh argon make-up and 0.5 ft/min withdrawal with 10 ft/min HVAC air-Velocity vector.

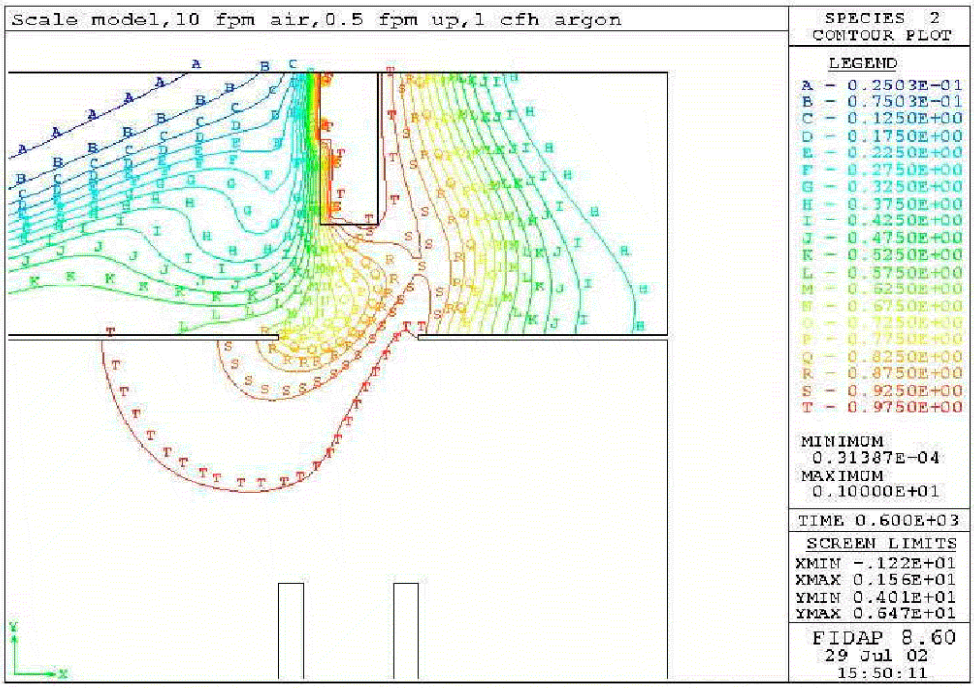

Figure 4.2.71: Computational results for the model with 1 cfh argon make-up and 0.5 ft/min withdrawal with 10 ft/min HVAC air- Argon contour.

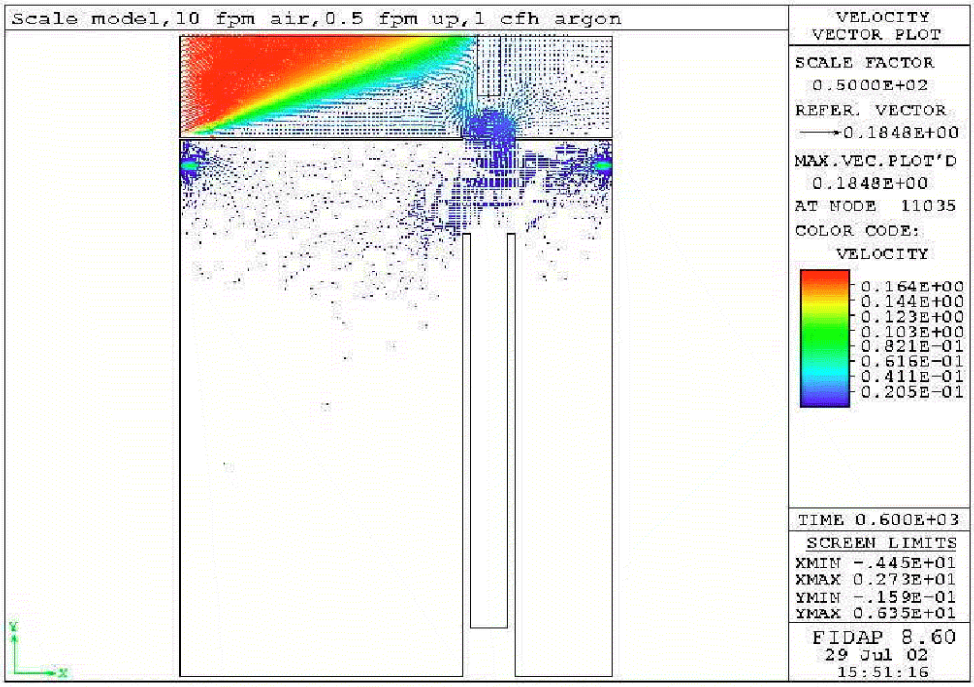

Figure 4.2.72: Computational results for the model with 1 cfh argon make-up and 0.5 ft/min withdrawal with 10 ft/min HVAC air-Velocity vector.

Chapter 5 : Conclusions & Recommendations

Computational and experimental investigations were carried out to study the ingress of air into the furnace module during the withdrawal and insertion of the extraction basket. These studies were performed for two different cases: (a) With Argon Reservoir (AR) and (b) Without the Argon Reservoir. Several parameters were studied. Computational results were validated with experimental results. Based on the experimental and computational results the following conclusions were drawn.

The argon reservoir will effectively prevent air from entering the furnace module only if there is a continuous supply of make-up argon during the basket withdrawal process. Without a continuous supply of make-up argon the AR is not effective. If the volume flow rate of make-up argon is the same as the withdrawal volume flow rate then the AR will allow a negligible amount of air ingress.

The filling process of the AR is time consuming, and requires considerably more argon than its volume being filled. Since the withdrawal and insertion are batch processes, before each withdrawal or insertion process the reservoir has to be filled up. Also, it was found computationally that if the filled reservoir is left alone (note that the reservoir has porous inner wall), the reservoir looses argon due to diffusion of argon into the room air. Therefore, once filled the AR has to have a continuous supply of make-up argon.

One case study confirmed that the 2-D computational studies provided results that agree with 3-D simulations. Also, for all the cases studied, tests of variable grid sizes showed grid-independence of the performed computation.

The computational studies and experimental studies predicted similar trends and the results were of the same order of magnitude. In general, the computational studies predicted lower oxygen/air infiltration than was indicated by experimental studies.

It was determined that when there is HVAC room air flow, the ingress of air into the furnace module is greater than if there was no HVAC air flow, both with and without an argon reservoir. This was consistent with both experimental and numerical calculations. The increased rate due to HVAC air flow is about 50%. Nevertheless, the amount of air ingress was less than 3% for all the isothermal cases.

For all the isothermal cases, faster withdrawal rates resulted in lower infiltration of oxygen/air, provided the make-up argon flow rate was nominal (i.e. equal to the volumetric withdrawal rate) or more. This result is intuitive since a faster withdrawal rate translates into shorter duration of the gate opening, therefore less time for diffusive and convective transport.

For thermal cases experimentally determined ingress of oxygen was much higher. For the cases when the retort surface temperature was 150^{o}F, the maximum infiltration of oxygen was about 1%, (at withdrawal speed of 2.5 ft/min) with nominal make-up argon, which translates to about 5% air ingress. However, for the same retort temperature if the withdrawal rate is 14 ft/min the infiltration of air is only 0.7%. Therefore, based on this finding, it is recommended that the basket not be withdrawn when the retort is at an elevated temperature. If it is absolutely necessary to withdraw it then it should be done at faster crane speed.

For delta-T cases, where the entire furnace module gas is at a higher temperature (delta-T = 50^{o}F) experimentally determined ingress of oxygen was even higher. For the cases when the retort surface temperature was 150^{o}F, at a withdrawal rate of 2.5 ft/min and nominal argon make-up, the maximum infiltration was 3% oxygen or about 14.3% air. Experiments were not performed for this case with faster crane speed. Again, it is recommended that the basket not be withdrawn when the furnace module gas is at an elevated temperature. If it is absolutely necessary to withdraw it, then it should be done at faster crane speed.

Computational and experimental studies for cases where no argon reservoir is used, indicated that during the withdrawal of the extraction basket, if make-up argon was injected into the furnace module, then less than 1% oxygen (less than 3% air) infiltrates into the furnace module. The rate of optimum make-up argon required was determined to be equal to the volume withdrawal rate. Similarly, during the insertion process, it was determined that the infiltrated oxygen was much less than 1% without make-up argon. Although, the amount of infiltrated oxygen was slightly more than with the AR, the oxygen infiltration without the AR was found to meet the design requirements for the furnace module. As a result it is concluded that the furnace module will operate well below the design requirement (<3% of O_2 infiltration) without the argon reservoir, provided make-up argon is supplied to the furnace module.

Bibliography

1. Heung L.K. “Tritium Transport Vessel Using Depleted Uranium.” Fusion Technology Vol: 28 (3): 1385-1390 Part 2, 1995.

2. Chen D.G. , Jia M.M., Li B.X., Lu QM, and Xie H.S, Hou W. “Argon Diffusion From Biotite At High-Temperature And Pressure.” Science In China Series B-Chemistry Life Sciences & Earth Sciences Vol: 38 (2): 221-227, 1995.

3. Murphy A.B. “Transport-Coefficients Of Air, Argon-Air, Nitrogen-Air, And Oxygen-Air Plasmas.” Plasma Chemistry And Plasma Processing Vol: 15 (2): 279-307, 1995.

4. Partridge J.F., and Mukhopadhyay S.K. “The Permeability Behavior Of Various Gases Through Automotive Airbag Fabrics” Journal Of The Textile Institute Vol: 91 (3): 397-409 Part 1 2000.

5. Fumizawa M. “Discharge Of A Laminar Argon Jet Into Stagnant Air.” KERNTECHNIK Vol: 58 (5): 269-272, 1993.

6. Egoshi N., Kusuno T., and Kawakami H. “Mass Transfer In Binary Distillation Of Nitrogen-Oxygen And Argon-Oxygen Systems In A Wetted-Wall Column” Journal Of Chemical Engineering Of Japan Vol: 30 (1): 7-12, 1997.

7. Gunes H. “Low-order dynamical models of thermal convection in high-aspect ratio enclosures.” Fluid Dynamics Research Vol: 30 (1): 1-29, 2002.

8. Dragojlovic Z., Kaminski D.A., and Ryoo J. “Tuning of a fuzzy rule set for controlling convergence of a CFD solver in turbulent flow.” International Journal Of Heat And Mass Transfer. Vol: 44 (20): 3811-3822, 2001.

9. Davidson P.A. “Similarities In The Structure Of Swirling And Buoyancy-Driven Flows.” Journal Of Fluid Mechanics. Vol: 252: 357-382, 1993.

10. Kazmierczak M., and Chinoda Z. “Buoyancy-Driven Flow In An Enclosure With Time-Periodic Boundary-Conditions.” International Journal Of Heat And Mass Transfer. Vol: 35 (6): 1507-1518, 1992.

11. Shahraki F. “Modeling Of Buoyancy-Driven Flow And Heat Transfer For Air In A Horizontal Annulus: Effects Of Vertical Eccentricity And Temperature-Dependent Properties.” Numerical Heat Transfer Part A-Applications. Vol: 42 (6): 603-621, 2002.

12. Moshkin N.P. “Numerical Model To Study Natural Convection In A Rectangular Enclosure Filled With Two Immiscible Fluids.” International Journal Of Heat And Fluid Flow. Vol: 23 (3): 373-379, 2002.

13. Papanicolaou E., and Belessiotis V. “Transient Natural Convection In A Cylindrical Enclosure At High Rayleigh Numbers.” International Journal Of Heat And Mass Transfer Vol: 45 (7): 1425-1444, 2002.

14. Khanafer K., and Vafai K. “Buoyancy-Driven Flow And Heat Transfer In Open-Ended Enclosures: Elimination Of The Extended Boundaries.” International Journal Of Heat And Mass Transfer. Vol: 43 (22): 4087-4100, 2000.

15. Li Y.H., Chu T.C. and Lin T.F. “Numerical Simulation Of Flow Pattern Formation In A Bottom Heated Cylindrical Fluid Layer.” Numerical Heat Transfer Part A-Applications. Vol: 30 (5): 459-476, 1996.

16. Khan J.A., and Yao G.F. “Comparison Of Natural-Convection Of Water And Air In A Partitioned Rectangular Enclosure.” International Journal Of Heat And Mass Transfer. Vol: 36 (12): 3107-3117, 1993.

17. Fiegley C.E., Bennett J.S., Lee E., and Khan J.A. “Improving the use of Mixing Factors for Dilution Ventilation Design.” Applied Occupational and Environmental Hygiene. Vol: 17(5): 333-343, 2002.

18. Bennett J.S., Fiegley C.E., Khan J.A., and Hosni M.H. “Comparison of Mathematical Models for Exposure Assessment With Computational Fluid Dynamic Simulation.” Applied Occupational and Environmental Hygiene. Vol: 15(1): 131-144, 2000.

19. Sherman M.H.. “Tarcer Gas Techniques For Measuring Ventilation in a Single Zone.” Building and Environment. Vol: 25(4): 365-374, 1990.

20. Furtaw E.J., Pandian M.D., Nelson D.R., Behar J.V. “Modeling Indoor Air Concentrations Near Emission Sources in Imperfectly Mixed Rooms.” Air & Waste Manage. Assoc. Vol: 46: 861-868, 1996.

21. Nicas Mark. “Estimating Exposure Intensity in an Imperfectly Mixed Room. American.” Industrial Hygiene Association Journal. Vol: 57: 542-550, 1996.

22. Waters J.R., and Simons M.W. “The Evaluation of Contaminant Concentrations and Air Flows in a Multizone Model of a Building.” Building And Environment. Vol: 22 (4): 305-315 1987.

23. Fiegley C.E., Bennett J.S., Khan J.A. and Lee E., “Performance of Deterministic Workplace Exposure Assessment Models for Various Contaminant Source, Air Inlet, and Exhaust Locations.” American Industrial Hygiene Association Journal. Vol: 63: 402-412, 2002.

24. Nicas Mark, and Jayjock M. “Uncertainty in Exposure Estimates Made by Modeling Versus Monitoring.” American Industrial Hygiene Association Journal. Vol: 63(3): 275-283, 2002.

25. Dunham M.L., Bullock W.H., and Oestenstad R.K. “A Practical Approach to Exposure Assessment Programs in the Private Sector: A Partial Ventilation Study of a Qualitative Chemical Exposure Assessment Model.” Applied Occupational and Environmental Hygiene. Vol: 16(2): 257-262, 2001.

26. Lee E., Fiegley C.E., and Khan J.A. “An Investigation of Air-Inlet Velocity in Simulating the Dispersion of Indoor Contaminants via Computational Fluid Dynamics.” On Process.

Appendix

Table A.1: Properties of air at normal temperature and pressure**.**

Density:	1.225	kg/m^3
Specific Heat, C_p	1006.30	j/kg-k
Thermal Conductivity, K	0.0242	w/m-k
Viscosity	1.79 E-05	kg/m-s
Molecular Weight	28.97	kg/kgmol

Table A.2: Properties of argon at normal temperature and pressure.

Density:	1.623	kg/m^3
Specific Heat, C_p	520.64	j/kg-k
Thermal Conductivity, K	0.0158	w/m-k
Viscosity	2.125 E-05	kg/m-s
Molecular Weight	39.95	kg/kgmol